

**MODELING AND CONTROL STRATEGIES FOR
RADIANT FLOOR HEATING SYSTEMS**

Song Chun Li

A thesis in

Department of Building, Civil and Environmental Engineering

Presented in Partial Fulfilment of the Requirements

for the Degree of Master of Applied Science at

Concordia University

Montreal, Quebec, Canada

August 2010

© Song Chun Li



Library and Archives
Canada

Published Heritage
Branch

395 Wellington Street
Ottawa ON K1A 0N4
Canada

Bibliothèque et
Archives Canada

Direction du
Patrimoine de l'édition

395, rue Wellington
Ottawa ON K1A 0N4
Canada

Your file *Votre référence*
ISBN: 978-0-494-71059-3
Our file *Notre référence*
ISBN: 978-0-494-71059-3

NOTICE:

The author has granted a non-exclusive license allowing Library and Archives Canada to reproduce, publish, archive, preserve, conserve, communicate to the public by telecommunication or on the Internet, loan, distribute and sell theses worldwide, for commercial or non-commercial purposes, in microform, paper, electronic and/or any other formats.

The author retains copyright ownership and moral rights in this thesis. Neither the thesis nor substantial extracts from it may be printed or otherwise reproduced without the author's permission.

AVIS:

L'auteur a accordé une licence non exclusive permettant à la Bibliothèque et Archives Canada de reproduire, publier, archiver, sauvegarder, conserver, transmettre au public par télécommunication ou par l'Internet, prêter, distribuer et vendre des thèses partout dans le monde, à des fins commerciales ou autres, sur support microforme, papier, électronique et/ou autres formats.

L'auteur conserve la propriété du droit d'auteur et des droits moraux qui protègent cette thèse. Ni la thèse ni des extraits substantiels de celle-ci ne doivent être imprimés ou autrement reproduits sans son autorisation.

In compliance with the Canadian Privacy Act some supporting forms may have been removed from this thesis.

While these forms may be included in the document page count, their removal does not represent any loss of content from the thesis.

Conformément à la loi canadienne sur la protection de la vie privée, quelques formulaires secondaires ont été enlevés de cette thèse.

Bien que ces formulaires aient inclus dans la pagination, il n'y aura aucun contenu manquant.


Canada

ABSTRACT

Modeling and Control Strategies for Radiant Floor Heating Systems

Song Chun Li

A dynamic model of a radiant floor heating (RFH) system which predicts the dynamic response of RFH system has been developed. The overall model consists of a boiler, an embedded tube floor slab and building enclosure. The overall model was described by nonlinear differential equations, which were programmed and solved using in MATLAB.

The RFH system model has been applied to both a single zone and a multi-zone RFH system. The predicted dynamic responses of the model under several operating conditions were studied. Also, a zonal model of RFH system was developed to study the air temperature distribution in the zone.

Three different control strategies for improving the performance of RFH systems were explored. These are: (i) a conventional PI control, (ii) a predictive control and (iii) an optimal control.

The simulation results show that PI control strategy is an efficient control strategy for RFH system from the point of view of temperature regulation.

The simulation results also show that the predictive PI control maintains zone air temperature close to the set-point better than the conventional PI control. Besides, the

predictive PI control strategy saves 10~15% energy, compared to the conventional PI control strategy. In addition, the simulation results also show that the optimal PI control strategy could slightly improve both the zone air temperature regulation and energy efficiency, compared to the predictive PI control. Since the predictive control strategy is simple and easy to implement, it is considered as a good candidate strategy for RFH systems.

ACKNOWLEDGEMENTS

I would like to express my sincere gratitude to my supervisor, Dr. M. Zaheer-Uddin, for his initiating this study, his invaluable guidance, his suggestions, encouragement and financial support in all phases of this research work.

Special thanks are given to my colleagues, especially Lianzhong Li and Ming Nin, for their helpful discussions and constructive suggestions in my study. My sincere appreciations also go to the staff in BCEE Department.

I would like to dedicate and express my appreciation for this thesis to my wife, Fangli CAO, and my parents for their patience, understanding, encouragement and support during my whole studies.

TABLE OF CONTENTS

List of Figures.....	xi
List of Tables.....	xv
Nomenclature.....	xvi
Abbreviations.....	xxiv
Greek Letters.....	xxv

Chapter 1 Introduction	1
1.1 Introduction.....	1
Chapter 2 Literature Review.....	5
2.1 A review of RFH system models.....	5
2.2 A review of control strategies for RFH systems.....	9
2.3 Experimental studies.....	14
2.4 Summary.....	16
2.5 Objectives of the thesis.....	17
Chapter 3 Dynamic Model of RFH System.....	18
3.1 Introduction.....	18
3.2 The formulation of radiant floor heating (RFH) system.....	19
3.2.1 Wall model.....	20
3.2.2 Floor slab model.....	22
3.2.3 Zone model.....	34
3.2.4 Boiler model.....	38
3.3 Overall RFH system model.....	40
3.4 Open loop simulations of single zone RFH system.....	41

3.4.1 Simulation results of the single zone model under design condition.....	42
3.5 Zonal model of single zone RFH system.....	46
3.5.1 The formulation of the zonal model.....	47
3.5.2 Simulation results of the zonal model.....	59
3.5.3 Open-loop test of the zonal model.....	63
3.5.4 Summary.....	63
3.6 Open loop simulation of multi-zone RFH system.....	64
3.6.1 Nodes in the multi-zone RFH system.....	65
3.6.2 Simulation results of multi-zone model under design condition.....	67
3.7 Summary.....	70
Chapter 4 Control Strategies for RFH System.....	71
4.1 Introduction	71
4.2 The impact of load disturbances on the single zone RFH system.....	71
4.3 Closed loop PI control responses of the single zone RFH system.....	74
4.4 Closed-loop PI control responses of the multi-zone RFH system.....	78
4.5 PI control of multi-zone RFH system under simulated operating condition.....	83
4.6 Impact of one zone to the other zones under conventional PI control.....	86

4.7 Summary.....	88
Chapter 5 Predictive PI Control strategy for RFH System.....	90
5.1 Introduction.....	90
5.2 Predictive PI control strategy.....	91
5.3 Predictive PI control strategy on the single zone.....	93
5.3.1 Comparison between the conventional PI control strategy and the predictive PI control strategy.....	95
5.4 Predictive PI control of the multi-zone RFH system.....	96
5.5 Comparison between the conventional PI control and the predictive PI control strategy for the multi-zone RFH system.....	101
5.6 Predictive PI control of multi-zone RFH system subject to multiple disturbances.....	102
5.7 Predictive PI control strategy of multi-zone RFH system: the impact of one zone on the other zones.....	104
5.8 Summary.....	106
Chapter 6 Optimal Operation of PI Control Strategy for RFH System.....	108
6.1 Introduction.....	108

6.2 Formulation of the optimization problem for RFH system.....	108
6.2.1 Determination of the optimized set-point of boiler water temperature.....	108
6.2.2 Performance of the single zone RFH system under optimal PI control....	110
6.3 Comparison between conventional, predictive and optimal control.....	112
6.4 Summary.....	113
Chapter 7 Conclusions, contributions and Recommendations for Future Research.....	115
7.1 Conclusions and contributions.....	115
7.1.1 Modelling RFH system.....	115
7.1.2 Control strategies for RFH system.....	116
7.2 Recommendations for future research.....	117
Reference.....	118

List of Figures

Figure 3.2.1 Single zone RFH system.....	19
Figure 3.2.2 Structure of external and internal wall.....	20
Figure 3.2.3 Plan view of the embedded tube.....	22
Figure 3.2.4 Structure of floor slab.....	23
Figure 3.2.5 Heat transfer model in slab.....	25
Figure 3.2.6 Nodes mesh in floor slab	26
Figure 3.4.1 Elevation view and floor plan view of the single room with RFH system....	41
Figure 3.4.2 Predicted zone air temperature and ceiling surface temperature.....	42
Figure 3.4.3 Predicted external wall temperature and water temperature.....	43
Figure 3.4.4 Surface temperature distribution.....	44
Figure 3.4.5 Open loop test of single zone RFH system.....	46
Figure 3.5.1 Vertical interface of mass transfer between cells.....	48
Figure 3.5.2 Horizontal interface of mass transfer between cells.....	49
Figure 3.5.3 9 cells in the single room.....	50

Figure 3.5.4 Simulation results of air mass transfer rate in each cell.....	60
Figure 3.5.5 Mass transfer rate and direction in the boundary layers.....	61
Figure 3.5.6 Simulation results of air temperature in each cell.....	61
Figure 3.5.7 Cell temperature under steady state.....	62
Figure 3.6.1 Plan view of the 4-zone apartment with RFH system.....	65
Figure 3.6.2 Simulation results of multi-zone model under design condition.....	68
Figure 3.6.3 Open-loop test of the multi-zone model.....	69
Figure 4.2.1 Predicted outdoor air temperature.....	73
Figure 4.2.2 Predicted zone air temperature under predicted outside air temperature.....	73
Figure 4.3.1 Control inputs for single zone RHF system.....	75
Figure 4.3.2 PI controller block diagram with zone air temperature feedback.....	75
Figure 4.3.3 PI controller block diagram with boiler water temperature feedback.....	76
Figure 4.3.4 Validation of the constant gain values of PI controllers for single zone RFH system.....	77
Figure 4.4.1 Control inputs for multi-zone RHF system.....	78
Figure 4.4.2 Validation of the constant gain values of PI controllers for multi-zone RFH system.....	80

Figure 4.4.3 Simulation results of multi-zone under conventional PI control.....	82
Figure 4.5.1 Incident Solar Radiation.....	83
Figure 4.5.2 Internal heat gain.....	83
Figure 4.5.3 Simulation results of multi-zone RFH system under conventional PI control with multiple disturbances.....	85
Figure 4.6.1 Simulation results of multi-zone on energy saving mode.....	88
Figure 5.3.1 Predicted boiler water temperature set-point and outdoor air temperature.....	93
Figure 5.3.2 Predictive PI control responses of single zone RFH system.....	94
Figure 5.4.2 Validation of the constant gain values of PI controllers for multi-zone RFH system under predictive PI control strategy.....	98
Figure 5.4.3 Simulation results of multi-zone under predictive PI control.....	100
Figure 5.6.1 Simulation results of multi-zone RFH system under conventional PI control with multiple disturbances.....	103
Figure 5.7.1 The performance of multi-zone RFH system with predictive PI control under energy saving mode.....	106
Figure 6.2.1 Optimization of the open loop test single zone RFH system.....	110

Figure 6.2.2 Validation of the constant gain values of PI controllers for single
zone RFH system under optimal PI control strategy.....111

Figure 6.2.3 Responses of single zone under optimal PI control strategy.....112

List of Tables

Table 3.2.1 Properties of Construction Materials.....	24
Table 3.2.2 Symbols in the equations 3.2.1-3.2.20.....	34
Table 3.4.1 Open loop test of single zone RFH system model.....	45
Table 3.5.1 Open loop runs of air temperature in each cell.....	63
Table 3.6.1 Simulation results of open loop test of multi-zone RFH system.....	69
Table 5.3.1 Comparison between conventional PI control and predictive PI control for single zone RFH system.....	96
Table 5.5.1 Comparison between conventional PI control and predictive PI control for the multi-zone RFH system.....	101
Table 6.3.1 Comparison among the 3 PI control strategy for single zone with RFH....	113

Nomenclatures

ACH	air change rate per hour (time/h)
A_f	area of ceiling (m^2)
A_{sw} / A_{nw}	area of south/north direction external wall (m^2)
Cd_v	discharge coefficient
CF	cloud factor
c_{air}	specific heat of air ($J/Kg^{\circ}C$)
C_{air}	thermal capacity of air in the air layer ($J/^{\circ}C$)
C_b	thermal capacity of boiler ($J/^{\circ}C$)
C_{blos} / C_{blon}	thermal capacity of block layer in south/north direction external wall ($J/^{\circ}C$)
C_{cems} / C_{cenn}	thermal capacity of cemmol layer in south/north direction external wall ($J/^{\circ}C$)
C_{crt}	thermal capacity of concrete underneath the tube ($J/^{\circ}C$)
C_{gyp}	thermal capacity of gypsum layer of ceiling ($J/^{\circ}C$)
C_{gyps} / C_{gypn}	thermal capacity of gypsum layer of south/north external wall ($J/^{\circ}C$)
C_{inss} / C_{insn}	thermal capacity of insulation layer in south/north direction layer ($J/^{\circ}C$)
C_{mor}	thermal capacity of the mortar in mortar layer ($J/^{\circ}C$)
C_{morp}	thermal capacity of the mortar above tube ($J/^{\circ}C$)
c_w	specific heat of water ($J/Kg^{\circ}C$)

C_w	thermal capacity of water in the tube (J/°C)
C_{wd}	thermal capacity of wood (J/°C)
C_{wdp}	thermal capacity of the wood right above the tube (J/°C)
C_{wmor}	thermal capacity of mortar in the tube layer (J/°C)
C_z	thermal capacity of the zone air of the heated space (J/°C)
C_{zi}	thermal capacity of air in cell i (J/°C)
D_o	outer diameter of embedded tube (m)
eb	efficiency of the boiler
E_1	error between set-point of zone air temperature and real time zone air temperature (°C)
E_2	error between set-point of boiler water temperature and real time boiler water temperature (°C)
F_{i-en}	angle factor between i^{th} wood surface node and enclosure
g	gravitational acceleration (m/s ²)
H	height of heated space (m)
H_{crt}	height of concrete layer (m)
h_i	heat transfer coefficient of interior surface film (w/m ² *°C)
H_{insp}	thickness of insulation layer (m)
h_{it}	convective heat transfer coefficient between water and tube surface (w/m ² *°C)

H_{mor}	height of mortar layer (m)
HV	specific heat of natural gas (J/Kg)
H_{wd}	height of wood layer (m)
I_c	solar radiation intensity (w/m^2)
k_i	integrate gain of PI controller
k_{ins}	conductivity of insulation material ($w/m^*°C$)
k_p	proportional gain of PI controller
L	length of each tube (m)
L_p	length of pipe from boiler to the radiant floor zone (m)
m_{AB}	mass transfer rate from zone A to zone B (Kg/s)
$m_{f\max}$	maximum mass flow rate of natural gas (Kg/s)
m_{wd}	water mass flow rate under design condition (Kg/s)
P	pressure (Pa)
q_{conv}	convective heat transfer from the wood surface (w)
$Q_{flrsuri}$	convective heat transfer rate from floor surface to zone i (w)
Q_{ij}	energy transfer from zone i to j because of air movement (w)
Q_{inf}	the rate of heat loss due to infiltration (w)
Q_{inf_nh}	heat loss rate of unheated zone by infiltration (w)
Q_{int}	internal heat generation (w/m^2)

Q_{int_nh}	internal heat gain of unheated zone (w)
Q_{loss}	heat transfer between the zone air and interior surfaces, except for floor surface (w)
Q_{nh_o}	heat transfer rate from unheated zone to outside by conduction (w)
q_{pconv}	convective heat transfer from the wood surface right above the tube (w)
q_{prad}	radiative heat transfer from the wood surface right above the tube (w)
q_{pre}	predicted heat transfer rate (w)
q_{rad}	radiative heat transfer from the wood surface (w)
q_{radi}	radiative heat transfer between i^{th} wood surface node and enclosure (w)
$Q_{rad,conv}$	total radiative and convective heat transfer from floor slab surface (w)
q_{sol}	solar radiation gain (w/m^2)
Q_{sols}	solar radiation gain from south direction window (w)
Q_{solsw}	solar radiation gain of south direction external wall (w)
Q_{z1}	heat transfer rate from room 1 to unheated area (w)
Q_{z2}	heat transfer rate from room 2 to unheated area (w)
Q_{z3}	heat transfer rate from living room to unheated area (w)
Q_{z4}	heat transfer rate from Master room to unheated area (w)
Q_{zirad}	radiative heat to zone i (w)
R	perfect gas constant (Pa/Kg*K)

R_p	thermal resistance of tube wall ($m^2 \cdot ^\circ C / w$)
SF	shading factor
t	time (s)
T_b	boiler water temperature ($^\circ C$)
T_{blos} / T_{blon}	temperature of block layer in south/north direction external wall ($^\circ C$)
T_{bset}	set-point of boiler water temperature ($^\circ C$)
T_{ceil}	temperature of ceiling ($^\circ C$)
T_{ceilsf}	ceiling surface temperature ($^\circ C$)
T_{cems} / T_{cemn}	temperature of cemmol layer in south/noth direction external wall ($^\circ C$)
T_{doorsf}	surface temperature of door ($^\circ C$)
T_{en}	average enclosure interior surfaces temperature ($^\circ C$)
T_{flr}	temperature of floor slab ($^\circ C$)
T_{flrsf}	temperature of floor slab surface ($^\circ C$)
T_{gypts} / T_{gypn}	temperature of gypsum layer in south/north direction external wall ($^\circ C$)
T_{inss} / T_{insn}	temperature of insulation layer in south/north direction external wall ($^\circ C$)
T_o	outside air temperature ($^\circ C$)
T_r	temperature of the water returned from the radiant floor ($^\circ C$)
T_{rb}	temperature of the water return to boiler ($^\circ C$)

T_{sp}	temperature of the water supplied to the radiant floor (°C)
T_{swsf} / T_{nwsf}	temperature of interior surface of south/north external wall (°C)
T_{tbsf}	temperature of embedded tube surface (°C)
T_{wi}	temperature of internal wall (°C)
T_{winsf}	surface temperature of window (°C)
T_{wisf}	internal surface temperature of internal wall (°C)
T_{wo}	temperature of external wall (°C)
T_z	zone air temperature of heated space (°C)
T_{z1}	zone air temperature of room 1 (°C)
T_{z2}	zone air temperature of room 2 (°C)
T_{z3}	zone air temperature of living room (°C)
T_{z4}	zone air temperature of Master room (°C)
T_{zh}	air temperature of heating area (°C)
T_{znh}	zone air temperature of unheated zone (°C)
T_{zset}	set-point of zone air temperature (°C)
$U_{air, gyp}$	heat transfer coefficient between the air and gypsum of ceiling (w/m ² *°C)
$U_{blo, ins}$	heat transfer coefficient between block layer and insulation layer (w/m ² *°C)
$U_{blo, o}$	heat transfer coefficient between block layer and outside air (w/m ² *°C)

$U_{crt,air}$	heat transfer coefficient between concrete and the air in air layer ($w/m^2*^{\circ}C$)
$U_{crt,crt}$	heat transfer coefficient between concrete and concrete ($w/m^2*^{\circ}C$)
$U_{cem,gyf}$	heat transfer coefficient between cemmol layer and gypsum layer ($w/m^2*^{\circ}C$)
U_f	control signal of gas combustion rate
$U_{gyp,ceilsf}$	heat transfer coefficient between gypsum layer and ceiling surface ($w/m^2*^{\circ}C$)
$U_{ins,gyf}$	heat transfer coefficient between insulation layer and gypsum layer ($w/m^2*^{\circ}C$)
$U_{mor,wd}$	heat transfer coefficient between the mortar in mortar layer and the wood ($w/m^2*^{\circ}C$)
$U_{mor,mor}$	heat transfer coefficient between mortar and mortar in mortar layer ($w/m^2*^{\circ}C$)
U_p	heat transfer coefficient of the tube, including the insulation layer ($w/m^2*^{\circ}C$)
U_w	water flow rate control signal, 0~1
$U_{w,crt}$	heat transfer coefficient between water and concrete in unit length ($w/m*^{\circ}C$)
$U_{w,mor}$	heat transfer coefficient between water and mortar in the tube layer in unit length ($w/m*^{\circ}C$)
$U_{wd,wd}$	heat transfer coefficient between wood and wood $w/m^2*^{\circ}C$)
$U_{wd,wdsf}$	heat transfer coefficient between wood and wood surface ($w/m^2*^{\circ}C$)

$U_{wmor,crt}$ heat transfer coefficient between the mortar in tube layer and concrete
($w/m^2*^{\circ}C$)

$U_{wmor,mor}$ heat transfer coefficient between the mortar in tube layer and the mortar in
mortar layer ($w/m^2*^{\circ}C$)

W pitch between two embedded tubes (m)

Abbreviations

C_1, C_2, C_3, C_4, C_5 controllers

z_1 zone 1

z_2 zone 2

z_3 zone 3

z_4 zone 4

Greek Letters

τ	the transmittance of the glass
θ	change ratio of outdoor air temperature
η	proportional factor
ρ	density of zone air (kg/m^3)
$\rho_{o_{air}}$	density of outside air (kg/m^3)
σ	Stefan-Boltzmann constant value of radiation ($\text{W/m}^2 \cdot \text{K}^4$)
ν	viscosity of zone air (m^2/s)
μ	dynamic viscosity of water ($\text{kg/m} \cdot \text{s}$)
ε	emissivity of surface

CHAPTER 1

Introduction

1.1 Introduction

Heating is necessary when the outdoor air temperature falls below the buildings' balance point temperature. The concept of radiant heating is centuries old. Around 100 B.C., Koreans let the smoke, generated by burning wood when cooking, exhaust upwards in the wall like a chimney and/or through the floor. In this way, the wall/floor is warmed up by the hot smoke and also the mass of the wall/floor was used as a thermal storage. As the heating techniques improved, radiant heating replaced the original heating method gradually, resulting in a cleaner and safer heating system. The radiant panel, embedded in floor/wall could be heated by electrical power, so that it could continuously release heat to the heated spaces. The operation of this heating system is convenient and it is easy to control. Another popular radiant heating system is a hydronic radiant floor heating system, in which water is the heat transport medium. This kind of RFH system could make use of the large thermal capacity of the floor slab to deliver uniform heat.

Among the several heating systems available for space heating, the radiant floor heating (RFH) systems offer several benefits.

In the space where the radiant floor heating system is applied, more than half of the thermal energy emitted is in the form of radiant heat, and the rest is convective heat, which could directly transfer to the occupied zone at the floor level. The radiant heat exchange happens between the warm surfaces and the surrounding surfaces, occupants

and objects inside the space. The surrounding surfaces or objects, which have lower temperature, would receive more radiative heat. Therefore, a relatively uniform thermal environment is established. Experimental measurements show that the temperature variation inside the space is negligible [15] (1995). Also, Inard's [19] (1996) zonal model results show that an almost perfect isothermy of the inside air volume could be achieved by floor heating system.

Besides, the water flow rate in RFH system is very low, and pump is always far away from the heating spaces, which results in no noise generation in the heating space.

In addition, the pipes are embedded inside the floor slab, which not only do not occupy any living space, but also there is no requirement of cleaning. Since the air movement in the space with a RFH system is low, it results in less transportation of dust, compared to other heating systems. In other words, floor heating could reduce the factorable living conditions for house dust mites [33] (2002).

According to reference [17], the thermal environment supplied by a RFH system is much closer to the ideal heating curve of human, compared to conventional heating systems, which are baseboard heating and air-conditioning systems. The RFH system could also prevent cold corners. That is to say, the RFH system could create a better thermal comfort space.

Finally, but not the least, much of the interest in RHF system stems from the claim of reduced energy consumption and use of low intensity energy sources. It is suggested in reference [4] that energy cost reductions of up to 30% are possible. In reference [33] (2002), Olesen concluded that the required operative temperature could be obtained at a

lower indoor air temperature in a radiant floor heating system, which reduces ventilation heat loss. And also, the low water temperature used in RFH system, which increases the efficiency of heat generators, is the other reason of energy saving. Besides, several studies about the different heating systems, conducted by reference [14] (1978), reference [21] (1979), and reference [31] (1980) show that heated floor systems had 10% to 40% lower energy consumption in poorly insulated buildings, and about 10% less energy consumption in well insulated buildings, compared to other heating systems.

Since RFH system is able to offer various advantages presented above, during the last two decades, RFH system applications have increased significantly. In Germany, Austria and Denmark, 30% to 50% of new residential buildings apply floor heating as the heating method to warm up the living spaces. In Korea, about 90% of residential buildings are heated by RFH system. Meanwhile, in Europe, RFH system is also widely used in commercial and industrial applications [33] (2002).

In order to achieve the advantages, such as energy saving and thermal comfort, one area which still requires further research concerns the development of improved control strategies for operating RFH systems. Before applying any control strategies to RFH system to see the control performance of the system, an efficient model should be developed. Based on the literature reviews presented in the next chapter, a dynamic model of single zone and multi-zone RFH system will be developed, and then the model will be used to explore improved control strategies for operating the RFH system. The thesis is organized as follows:

- 1) In Chapter 2, literature review is presented.

- 2) In Chapter 3, the RFH system model for a single zone and a multi-zone is developed and the simulation results are presented.
- 3) Base case control strategies using PI control are presented in Chapter 4.
- 4) A predictive control strategy is developed and applied for the single zone and the multi-zone RFH system. The simulation results are presented in Chapter 5 to show the advantages of the predictive control strategy compared to the base case PI control strategy.
- 5) An optimal control strategy is presented and compared with the predictive and base case PI control strategies in Chapter 6.
- 6) Conclusions are given in Chapter 7.

CHAPTER 2

Literature Review

The literature survey is organized into three sub-sections:

- 1) Studies about modelling of RFH systems,
- 2) Control strategies for RFH systems,
- 3) Experimental study of RFH systems.

2.1 A review of RFH system models

The steady state technique has been widely used for the thermal comfort and energy consumption analysis of RFH systems. Hogan and Blackwell [16] (1986) used a numerical model, which emphasized the steady-state performance of floor heating panels, to evaluate the ASHRAE design recommendations for a single radiant floor heating panel. The simulation result shows that the ASHRAE design recommendations are conservative, resulting from that the downward and edgewise heat loss and the panel thermal resistance are overestimated.

Miriél, Serres and Trombe [30] (2002) developed a TRANSYS model for the ceiling panel heating system. The simulation results reveal that ceiling panel could be used as the heating system for buildings with good thermal insulation. However, the power of panel is limited; therefore, the heating load of the space should be low.

In order to demonstrate the advantage, such as energy saving, of RFH system, Strand and Pedersen [41] (1997) implemented a radiant heating and cooling model, which

combined radiative and convective heat transfer from the radiant system, and the resulting thermal environment, into an integrated building energy analysis program. The model utilises a derivative of conduction transfer functions that includes the effects of embedded sources or sinks to accurately account for the transient heat conduction in the radiant system. The program predicts energy consumption of a RFH system and a conventional forced-air system that provide equal levels of thermal comfort. The simulation results show that there is a small increase in heating load due to slightly higher surface temperatures (less than 0.1°C) in RFH system, but the conventional system had a higher mean air temperature (more than 5°C higher on an average) and thus higher infiltration/ventilation air heat loss. That is to say, the radiant system was slightly more energy efficient than the conventional system while providing comparable thermal comfort.

Since steady state analysis model can not show the dynamic response of RFH system, more and more dynamic models of RFH system are developed. Zhang [48] (2001) developed a one-dimensional dynamic model which includes the interactions between boiler, floor slab and a single zone. The floor slab is divided into 3 layers and the temperature in each layer is regarded as uniform. By using the logarithmic-mean-temperature-difference method, it is shown that the model predictions are in general agreement with the experimental data.

Laouadi (2004) [20] combined a one-dimensional numerical model of the energy simulation software with a two-dimensional analytical model which predicts the contact surface temperature of the circuit-tubing and the adjacent medium. It was found that the model predictions compared very well with the results from a full two-dimensional

numerical model. In addition, it was concluded that the thermal capacity of the system was significantly oversized when one dimensional model was used.

Ho, Hayes and Wood [15] (1995) developed a two-dimensional model for a heating panel. The model coupled the hot circulating water, heat conduction and heat accumulation in the panel to an enclosure, which is able to predict both steady temperature profiles and transient responses. It was concluded that the effect of the heat retention in the structure should be considered when modelling the dynamic response of the living spaces.

Campo and Amon [5] (2005) developed a two-dimensional ground-coupled floor heating model. He concluded that using the average concrete temperature can not fully account for dynamical and absolute values of the heat consumption. He pointed out that the model of floor construction and the room model should be combined to analyse the dynamic response of floor heating system.

Chapman and Zhang [6] (1996) developed a three-dimensional mathematical model, which combines room air and wall energy balance, radiation mathematical model, and conduction and convection models, to calculate the mass-averaged room air temperature and the wall surface temperature distribution under the steady state. They recommended that the effect of air-movement should be incorporated into the analysis model, and the model should be modified to include transient effects in order to accurately identify the benefits of set-back thermostats and the transient response of radiative, convective and hybrid heating system.

Good and Ugursal [13] (2005) developed an In-Floor Radiant Heating model, which confirmed some of the benefits of RFH system, such as its ability to provide an even temperature profile.

Steinman, Kalisperis and Summers [39] (1989) proposed a new method to improve the accuracy of the mean radiant temperature (MRT) method which does not account for an enclosed environment's surface-to-surface exact angle. Strand and Pedersen [41] (2002) improved the simulation model for radiant systems, based on the research about MRT method done by Liesen and Pedersen [24] (1997), which mainly focus on interior radiant exchange algorithm. In the model, they proposed a new calculation method for view factor, which is regarded as more accurate than the various MRT-based methods. Assuming internal wall surfaces do not have thermal capacity, no dynamic equation for their thermal storage was written. In reference [42] (1980), a new algorithm for radiant energy interchange in room was developed.

In the last ten years, solar energy's utilization, and combination of solar-collector system and RFH system are studied. Athienitis [3] (1994) proposed a transient approach to solve an explicit nonlinear difference network model and predict the performance of a RFH system with high solar gain.

Recently, a large number of researchers have studied the influence of design parameters on the performance of RFH system. In order to model the impact of floor construction and foundation on the performance of RFH system, Weitzmann [43] (2005) developed a two-dimensional dynamic model of the heat losses and temperature in a slab on grade floor with floor heating. It is found that the foundation has a large influence on

the energy consumption of the buildings heated by floor heating, which is also found by reference [5] (2005). Besides, in reference [37] (2006), they summarized that most important design parameters for RFH system are type and thickness of the cover of the floor slab, compared to the type, diameter and number of the embedded pipes.

The skin temperature of the human body is still one of the most reliable indices of thermal sensation. Song [38] (2005) studied the buttocks skin responses to contact with the floor covering materials used in the ONDOL under floor heating system. It was concluded that the floor finishing materials do affect the surface temperature of the floor slab. If the floor is finished with wood instead of mortar in mild seasons, heating will not be required because wood has low conductivity and low specific heat. Therefore, floor covering materials should be taken into consideration in floor heating system designs.

2.2 A review of control strategies for RFH systems

Because the relationship between heat output and supply water temperature is linear function in the supply water temperature control method in which the flow rate is constant, it is desirable for the supply water temperature to be controlled according to the variation in the outdoor temperature [1] (1953). Zhang [48] (2001) also considered the utilization of water temperature modulation as opposed to flow rate modulation as an effective control strategy.

Olesen [33] (2002) studied three control methods, which are time of operation, intermittent operation of circulation pump and supply water temperature control, by dynamic computer simulations. It was concluded that the best thermal comfort and

energy performance is obtained by controlling the water temperature as a function of outside air temperature, compared to the other two control strategies.

MacCluer [28] (1991) developed an analytical model to show the performance of control method, in which the temperature of supply water to radiant floor is proportional to outdoor air temperature, for RFH system. The simulation results revealed that modifying outdoor reset by inhibiting circulation during periods of overheating is warranted. Besides, by using mixing valve, decreasing or increasing the zone reset slope and the system controlled by indoor temperature feedback, the system performance can be improved, but it may let the system become unstable during high loads. However, MacCluer stated that, with careful design and installation, offset modulation, which supplies the zone with water at a temperature proportional to outside air temperature except that the intercept is modified in proportion to inside air temperature, could achieve modest performance improvements, without danger of instabilities.

Gibbs [12] (1994) conducted a study of three control strategies, which are pulse-width-modulated zone valves with constant temperature boiler, outdoor reset with indoor temperature feedback and outdoor reset plus pulse-width-modulated zone valves, on multi-zone RFH systems. He concluded that the combination of outdoor reset control plus indoor temperature feedback with pulse width modulated zone control could best regulate the room air and floor surface temperatures. Meanwhile, he proposed that the control algorithms could be improved through addition of integral plus derivative functions and/or predictive algorithms to remove offset error and provide faster response to normal load changes.

From what is stated above, it may be concluded that supply water temperature control may have a significant importance on the control performance of RFH systems, compared to water flow rate control. However, it is undeniable that both the supply water temperature and water flow rate influence the heat transfer to the zone in RFH system, and the combination of the two control parameters may have a better performance than any one of them. Therefore, a lot of models have been built to explore the performance of the RFH system when both supply water temperature and water flow rate are controlled, and it was proved that the control strategy of the combination of water temperature control and flow rate regulation gave better control.

Leigh [22] (1994) did a comparative study of proportional flux-modulation and various types of temperature-modulation approaches for RFH system control. He concluded that the proportional flux-modulation control, in which the heat flow rate sent to the floor slab as a function of thermostat error from the set-point was controlled (a thermostat with a heat anticipator), for RFH system, has favourable performance, compared to various types of temperature modulation, which are temperature modulation via mixing valve without/with indoor feedback, and temperature modulation via flow inhibition without/with indoor feedback. Besides, MacCluer [25~28] (1989, 1990, 1991) has also suggested that improved control of RFH systems was possible while using a flux modulation control strategy rather than temperature modulation.

Cho and Zaheer-uddin [10] (2003) explored a predictive control strategy as a means of improving the energy efficiency of intermittently heated RFH system. By determining the total length of time in hours per day that the heat must be supplied and then reasonably distributing the heating period over the day according to the prediction of outdoor air

temperature, the energy savings could reach 10% to 12% in cold winter, compared to conventional on/off control strategy. Moreover, the energy saving is higher in mild winter. The simulation results in reference [46] (2002) showed that the temperature regulation of RFH systems could be significantly improved, when the multi-stage on/off control was used, compared to the conventional on/off control. However, in this kind of predictive control, the prediction of outside air temperature was required and the most important consideration was the accuracy of predicting the outdoor reset curves. Any inaccuracies in the reset curves would give rise to the excessive overshoot or poor tracking. On the other hand, it was possible to use the anticipatory thermostat mentioned in reference [25] (1989) to achieve good regulation.

On/off control has many advantages, such as simple control strategy and low initial cost. However, it also has some disadvantages. Chun [11] (1999), used SERI-RES to do a comparative analysis between intermittent heating mode and continuous heating mode of RFH system. The simulation results revealed that a relatively large temperature swings occurred in the case of intermittent heating with solar heat gains. By contrast, the continuous heating system was able to avoid those undesirable temperature fluctuations and was more energy efficient over the intermittent heating mode.

Chen [7] (2002) studied the performance of three controllers, which were generalised predictive control (GPC), on/off and PI controller, applied in RFH system with large thermal lag. The results demonstrated that the GPC controller was superior to the other two in every aspect. It had the fastest response to changes in set-point and eliminates on-off cycling.

In order to mitigate the disadvantages of conventional on/off control strategy, Zaheer-uddin [46] (2002) applied an augmented control strategy to RFH system. The simulation results showed that the augmented control offered faster response and smaller variation in zone air temperature, compared to proportional control.

By employing two control inputs in RFH system, such as combustion rate of natural gas and water flow rate, Zaheer-uddin [45] (1997) explored an optimal operation of RFH system with control input constraints. The most important part was to seek an optimal operating sequence for combustion rate of natural gas and water flow rate, the two control inputs, which would minimize the energy consumption. Then, using suitably tuned PI controllers, the RFH system could achieve the acceptable performance with the minimum energy consumption.

Finally, one aspect which should be paid attention to is that almost all the control strategies mentioned above were only applied to single zone RFH system. Studies on control strategies for multi-zone RFH system are lacking. In an extensive study performed as basis for the new German energy code for buildings [33] (2002), it was showed that 15% -30% of energy could be saved by using an individual room control in multi-zone RFH systems, compared to a central control system. Rhee [35] (2010) also concluded that individual room control was highly recommended because it could ensure thermal comfort and energy saving more successfully than that of central control. What's more, adopting hydronic balancing could maximise the performance of individual room control in multi-zone RFH systems.

2.3 Experimental studies

Olesen [32] (1994) conducted a comparative experimental study of performance of radiant floor-heating system with tubes embedded in a concrete floor, floor heating system with a low thermal mass, and a wall panel heating system with a radiator at an outside wall. Changes in outside air temperature, solar radiation gain and internal heat generation from lights and people were considered. The experiment results showed that the indoor thermal environment could be controlled within recommended limits in all the three kind of systems. Meanwhile, the energy consumption of the three heating systems was within 5% of each other.

Ryu [36] (2004) did an experimental study of the performance of various control strategies, such as supply water temperature control and outdoor reset plus on/off bang-bang control, in RFH system. From the simulation results, it could be clearly seen that the supply water temperature control was better than the water flow rate control, because the former control strategy was able to supply a stable room temperature and floor surface temperature. Besides, outdoor reset methods to on/off bang-bang control could decrease the fluctuation of average room air temperature. Moreover, by applying pulse-width modulation to on/off bang-bang control, the stability of room temperature and floor surface temperature was improved.

Cho and Zaheer-uddin [8] (1997) conducted an experimental study to consider the performance of the two-parameter on-off control in RFH system. It was concluded that on-off control using room air temperature was cost-effective control strategy, but it resulted in big variation in room air temperature. On the other hand, on-off control using

slab temperature as a control signal results in a good room temperature regulation, but it may not be satisfactory for different heating load scenarios that could emerge over a heating season. Proportional plus integral (PI) control showed the best performance, but it was expensive. However, two-parameter on-off control, in which both room air temperature and slab temperature were taken as control signal, and priority was given to air temperature, had the performance close to PI control. Also, it was simple and cost-effective.

The experimental study mentioned above demonstrated that two-parameter on/off control had a much better performance than the conventional on/off control in RFH systems. Cho and Zaheer-uddin [9] (1999) did the other experimental study based on the two-parameter on/off control and named the new control strategy as two parameter switch control (TPSC), in which the valve was operated in on/off control mode for the first period of time based on the feedback signals received from slab temperature sensor, and during the next period of time, the indoor air temperature signals from the thermostat control the valve. The results revealed that that better temperature regulation could be achieved when switching interval was less than 40 minutes.

In order to confirm the energy savings in predictive control for intermittently operated RFH systems, compared to the conventional control, Cho, S.H. & Zaheer-uddin [10] (2003) conducted an experiment. The experiment results showed that the energy savings of 14.6% on a cold day, 24.13% on a mild day and 35.4% on a warm day when the system was operated under predictive control.

Integrated solar and RFH system were studied by some researchers. The experiment results from reference [34] (2009) showed that a solar assisted water source heat pump for RFH system (SWHP-RFH) with hot pipe vacuum tube solar collector as heating source and radiant floor as terminal device gave acceptable performance. Moreover, Zhang and Pate [47] (1988) monitored the performance of radiant panels connected to solar collectors installed in a test house in the US. It was reported that 74.9% of heating load could be contributed by solar.

2.4 Summary

From the literature review, the following issues are identified.

- 1) All the models focus on single zone RFH system and very little attention is paid to the simulation of multi-zone RFH system.
- 2) It is instructive to study the temperature distribution of floor slab and air temperature in the zone to get a better idea of the range of temperature variation.
- 3) The available models mainly focus on the convective, conductive and radiative heat exchange at zone level. They ignore the model for boiler, heat loss from the water to the ground, which is part of system level modeling. The operation of boiler has important impact on the performance of RFH system. To this end, dynamic model of multi-zone RFH system needs to be developed for control analysis.

- 4) Most control strategies presented in the literature are either on-off or PI control with reset actions. There is a need to develop simple and efficient predictive control algorithm which is suitable for practical implementation.

2.5 Objectives of the thesis

This thesis will focus on solving the problems identified above concerning modelling and control strategies of RFH system. Therefore, the major objectives of this thesis include the following:

- 1) Develop dynamic models of single and multi-zone RFH systems to accurately predict the dynamic responses. Also, the models should be useful for control analysis.
- 2) Develop a zonal model of RFH system to study the air temperature distribution in the zone and the variation in the floor slab surface temperature.
- 3) Design a simple and effective predictive control strategy for operating RFH system efficiently and check the control performance of single zone and multi-zone RFH systems under typical operating conditions.
- 4) Optimize the RFH system to improve energy efficiency. Conduct simulation study and compare the performance of predictive control, optimal control with the conventional PI control strategy.

CHAPTER 3

Dynamic Model of RFH System

3.1 Introduction

In this chapter, a dynamic model for RFH system will be developed. Since in RFH system, the zone air temperature, the floor slab surface temperature, water temperature and slab temperature are the most important parameters, the model will focus on calculating and analysing those temperatures. Firstly, the physical system will be described. Then the dynamic model of each component, including zone air, enclosure structure, floor slab and boiler will be built. Thirdly, all of the component models will be integrated to build dynamic models of a single and multi-zone RFH system. Finally, open loop simulation results will be presented to study the dynamic responses of the RFH systems. Also, air temperature distribution in the zone will be studied by developing a zonal model of RFH system.

Since water delivers heat to the floor slab when it flows inside the tubes in the floor slab, the water temperature decreases in the water flow direction. As a result, it is important to track the temperature of the flow water to accurately predict the temperature of the floor slab. Therefore, the model given in reference [45] (1997) will be used as a basis to develop a model for simulating the temperature of the water nodes. Although a lot of dynamic equations are needed in the model, it could accurately predict the flow water temperature and circuit tube-mortar contact surface temperature, which are required to compute the supply water temperature from boiler to maintain the zone air temperature at set-point, and the temperature distribution in floor slab and floor slab

surface temperature distribution. In a RFH system, the floor slab surface temperature distribution not only affects the zone air temperature distribution, but also has impact on occupants' thermal comfort. For this reason, it is necessary to develop a model, which could show the floor slab surface temperature distribution. According to the surface temperature distribution, some measurements may be taken to improve the performance of RFH systems. For example, from the surface temperature distribution, we could directly know the area where occupants stay may result in bad thermal comfort while sitting on the floor directly, according to the theory stated in reference [38] (2005).

3.2. The formulation of single zone radiant floor heating (RFH) system model

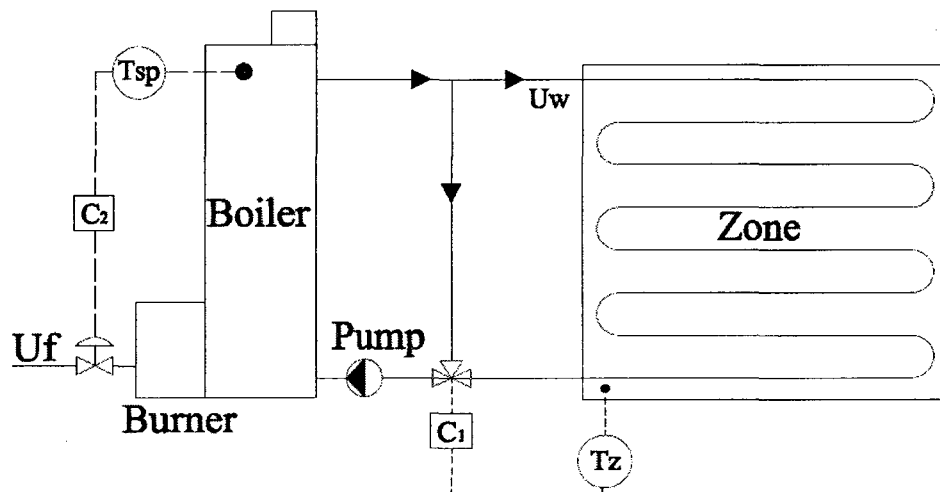


Figure 3.2.1 Single zone RFH system

As shown in Figure 3.2.1, a complete RFH system consists of an environment enclosure, floor slab, piping network, a hot water boiler, circulating pump and a control system. A dynamic model for the RFH system should incorporate all aspects of heat transfer mechanisms, including conduction, convection, radiation and thermal storage.

Besides, the dynamic model will be formulated by applying the energy balance principle on each of the components, which are walls of the enclosure, flow water and connecting mortar, construction layers of slab, interior surfaces, and a gas-burning boiler. Each component will be modeled individually based on its own physical arrangement by applying energy balance technique. The resulting time dependent differential equations will be solved using finite numerical techniques.

It is noted here that the design parameters of RFH system presented in this thesis were chosen from reference [45] which corresponds to a typical RFH system in South Korea.

3.2.1 Wall Model

A typical outside wall and internal wall structure are shown in Figure 3.2.2. The properties of the materials are listed in Table 3.2.1.

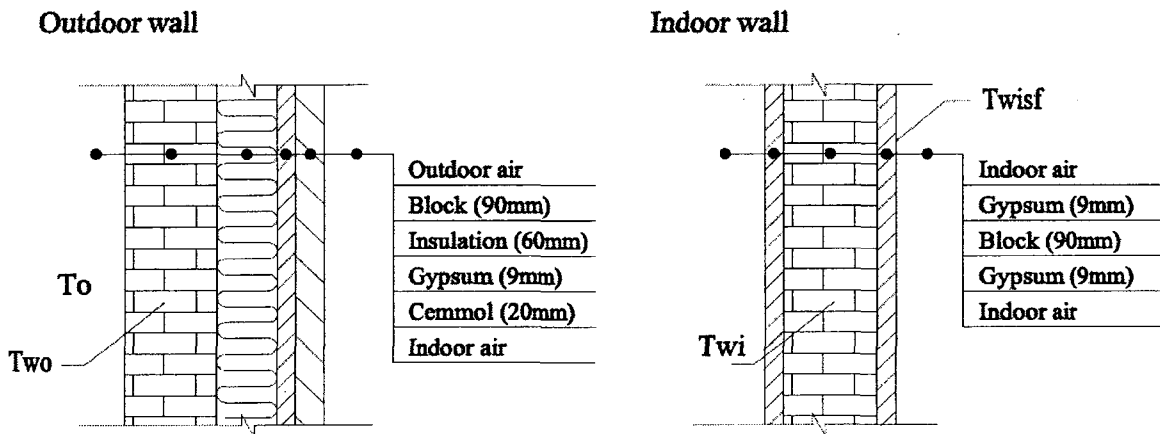


Figure 3.2.2 Structure of external and internal wall

In order to simplify the model, the temperature in each construction layer in the wall is regarded as uniform. Therefore, the heat transfer process in the wall can be simply considered as one-dimensional problem and there are 4 nodes in the south direction

external wall and 4 nodes in north direction wall, resulting from the solar radiation gain in the south direction wall. Based on the energy conservation law at each node, the temperature dynamic equation for each layer can be expressed as:

Nodes in south wall:

$$\frac{dT_{blos}}{dt} = C_{blos}^{-1} [U_{blo,ins} A_{sw} (T_{inss} - T_{blos}) - U_{blo,o} A_{sw} (T_{blos} - T_o) + Q_{solsw}] \quad (3.2.1)$$

$$\frac{dT_{inss}}{dt} = C_{inss}^{-1} [U_{ins,gyp} A_{sw} (T_{gyps} - T_{inss}) - U_{blo,ins} A_{sw} (T_{inss} - T_{blos})] \quad (3.2.2)$$

$$\frac{dT_{gyps}}{dt} = C_{gyps}^{-1} [U_{cem,gyp} A_{sw} (T_{cems} - T_{gyps}) - U_{ins,gyp} A_{sw} (T_{gyps} - T_{inss})] \quad (3.2.3)$$

$$\frac{dT_{cems}}{dt} = C_{cems}^{-1} [U_{cemsf,cem} A_{sw} (T_{swsf} - T_{cems}) - U_{cem,gyp} A_{sw} (T_{cems} - T_{gyps})] \quad (3.2.4)$$

Nodes in north wall:

$$\frac{dT_{blon}}{dt} = C_{blon}^{-1} [U_{blo,ins} A_{nw} (T_{insn} - T_{blon}) - U_{blo,o} A_{nw} (T_{blon} - T_o)] \quad (3.2.5)$$

$$\frac{dT_{insn}}{dt} = C_{insn}^{-1} [U_{ins,gyp} A_{nw} (T_{gypn} - T_{insn}) - U_{blo,ins} A_{nw} (T_{insn} - T_{blon})] \quad (3.2.6)$$

$$\frac{dT_{gypn}}{dt} = C_{gypn}^{-1} [U_{cem,gyp} A_{nw} (T_{cemn} - T_{gypn}) - U_{ins,gyp} A_{nw} (T_{gypn} - T_{insn})] \quad (3.2.7)$$

$$\frac{dT_{cemn}}{dt} = C_{cemn}^{-1} [U_{cemsf,cem} A_{nw} (T_{nwsf} - T_{cemn}) - U_{cem,gyp} A_{nw} (T_{cemn} - T_{gypn})] \quad (3.2.8)$$

where Q_{solsw} is the solar radiation gain of south direction wall which is given in equation 3.2.26. The temperature nodes are defined in the following.

$T_{blon}, T_{inss}, T_{gyps}, T_{cems}$ is the temperature of block layer, cement layer, insulation layer and gypsum layer in south direction wall respectively, °C.

$T_{blon}, T_{inss}, T_{gyps}, T_{cems}$ is the temperature of block layer, cement layer, insulation layer and gypsum layer in north direction wall respectively, °C.

T_{swsf}, T_{nwsf} is the interior surface temperature of south direction wall and north direction wall respectively, °C.

3.2.2 Floor Slab Model

A hydronic radiant floor typically consists of a serpentine pipe shown in Figure 3.2.3. Hot water inside the tubes transfers heat to the tube wall by convection due to the temperature difference. The tube wall transfers the heat to the contacted floor slab medium by conduction both vertically and horizontally.

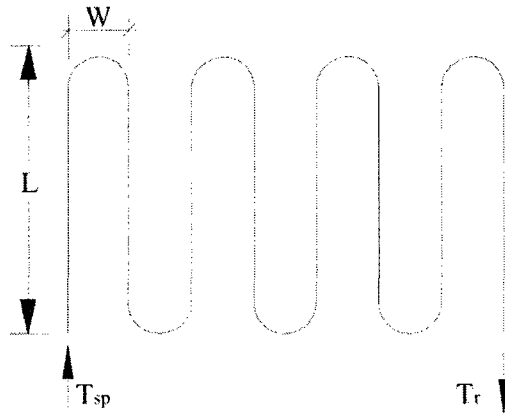


Figure 3.2.3 Plan view of embedded tube

A typical floor slab with 6 layers, which are shown in Figure 3.2.4, was considered.

The tubes are embedded at the bottom of the mortar layer.

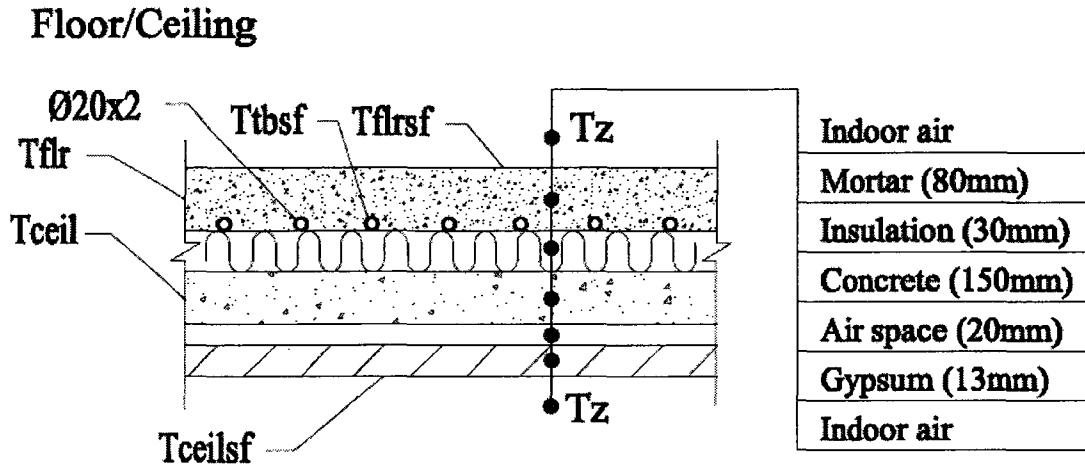


Figure 3.2.4 Structure of floor slab

The properties of the materials and the heat transfer coefficients of each material are listed in the Table 3.2.1, according to reference [18].

Material	Conductivity $w/(m \cdot K)$	Capacity $J/(Kg \cdot ^\circ C)$	Density Kg/m^3
Block	$K_{blo} = 1.4$	$c_{blo} = 836$	$d_{blo} = 2242$
Insulation	$K_{ins} = 0.033$	$c_{ins} = 840$	$d_{ins} = 30$
Gypsum	$K_{gyp} = 0.18$	$c_{gyp} = 270$	$d_{gyp} = 910$
Cemmol	$K_{cem} = 1.4$	$c_{cem} = 836$	$d_{cem} = 2000$
Wood	$K_{wd} = 0.17$	$c_{wd} = 2510$	$d_{wd} = 700$
Mortar	$K_{mor} = 1.4$	$c_{mor} = 836$	$d_{mor} = 2000$
Concrete	$K_{crt} = 1.4$	$c_{crt} = 836$	$d_{crt} = 2242$

Air Space	Resistance: $R_{air} = 0.17 \text{ m}^2 \cdot \text{K}/\text{w}$
Interior surface film conductance: $h_i = 8.72 \text{ w}/(\text{m}^2 \cdot ^\circ\text{C})$	
External surface film conductance (South Korea) $h_o = 27.9 \text{ w}/(\text{m}^2 \cdot ^\circ\text{C})$	

Table 3.2.1 Properties of Construction Materials

As shown in Figure 3.2.3, the interval between each two tubes is W and the length of each tube is L . Since the circulated water transfers heat to the tube wall while flowing inside the tubes, the water temperature declines along the flow direction. Moreover, the tubes do not cover the whole area of the floor. As a result, heat transfer happens in both horizontally and vertically between the water tube and the contacting medium, which results in non uniform temperature in floor slab. Based on this point, the temperature distribution inside the whole floor slab should be monitored in order to fully understand the characteristics of RFH systems. However, this is the main problem that the models stated in the literature review do not address adequately. Therefore, a model, which focuses on analysing the temperature distribution inside the floor slab, will be developed as described below.

Firstly, to simplify the analysis, the water temperature inside a short length of tube is considered uniform. Thus, the water temperature could be tracked by monitoring a number of water nodes.

Secondly, since mortar and concrete have huge thermal capacity which would affect the performance of RFH systems, the temperature of both mortar and concrete will be

analysed. That is to say, the temperature distribution in the tube layer (bottom layer of mortar), mortar layer (up layer of mortar) and concrete layer will be analysed.

Thirdly, by assuming well mixed air inside the air layer, the temperature of the air in the air layer is treated as uniform. Also, the temperature of gypsum layer is regarded as uniform as well. Therefore, the heat transfer model of one vertical layer (one short length of tube and contacting medium) inside floor slab has been established, which is described in Figure 3.2.5.

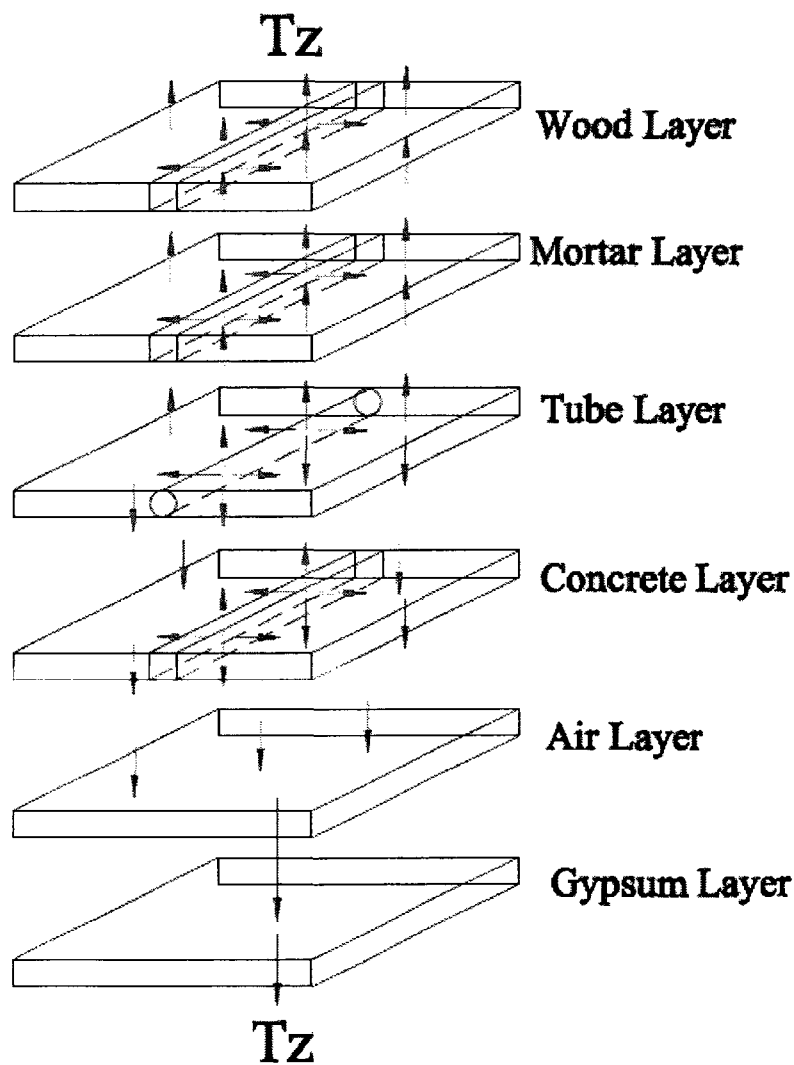


Figure 3.2.5 Heat transfer model in slab (arrow represent the heat transfer direction, circle represent the water pipe)

Finally, the slab surface (wood surface) temperature could be determined according to the temperature distribution of mortar, convective heat transfer coefficient between the slab surface and the heated zone, and radiative heat transfer coefficient between the slab surface and other interior surfaces. Figure 3.2.6 shows the details of the mesh of the nodes inside the floor slab.

Floor/Ceiling

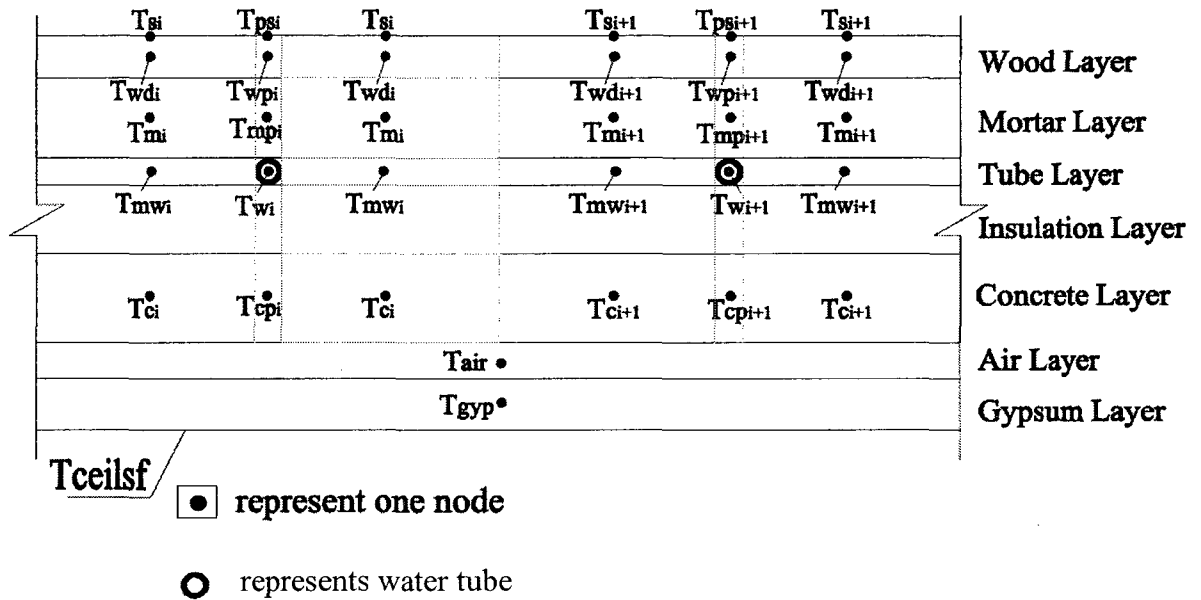


Figure 3.2.6 Nodes mesh in floor slab

Where, T_{wi} represents water temperature at i^{th} tube, °C

T_{mwi} represents mortar temperature around i^{th} tube in tube layer, °C

T_{mpi} represents mortar temperature above i^{th} tube in mortar layer, °C

T_{mi} represents mortar temperature at i^{th} node in mortar layer, °C

T_{wpi} represents wood temperature above i^{th} tube in wood layer, °C

T_{wdi} represents wood temperature at i^{th} node in wood layer, °C

T_{psi} represents wood surface temperature above i^{th} tube, °C

T_{si} represents wood surface temperature at i^{th} node, °C

T_{cpi} represents concrete temperature underneath i^{th} tube, °C

T_{ci} represents concrete temperature at i^{th} node in concrete layer, °C

T_{ceilsf} represents ceiling surface temperature, °C

T_{gyp} represents gypsum layer temperature, °C

T_{air} represents the air temperature in the air layer, °C

Even though there are a lot of nodes which may result in a complex model, these equations are necessary to accurately predict the complete temperature distribution inside the floor slab. And the dynamic equation of each node inside the slab is given below:

$$\begin{aligned} \frac{dT_{w,i}}{dt} = & C_{w,i}^{-1} [U_w m_{wd} c_w (T_{w,i-1} - T_{w,i}) - 2U_{w,wmor} L(T_{w,i} - T_{mw,i}) \\ & - U_{w,mor} L(T_{w,i} - T_{mp,i}) - U_{w,crt} L(T_{w,i} - T_{cp,i})] \end{aligned} \quad (3.2.9)$$

$$\begin{aligned} \frac{dT_{mw,i}}{dt} = & C_{wmor,i}^{-1} [2U_{w,wmor} L(T_{w,i} - T_{mw,i}) - \\ & U_{wmor,mor} WL(T_{mw,i} - T_{m,i}) - U_{wmor,crt} WL(T_{mw,i} - T_{c,i})] \end{aligned} \quad (3.2.10)$$

$$\begin{aligned} \frac{dT_{mp,i}}{dt} = & C_{mor,p,i}^{-1} [U_{w,mor} L(T_{w,i} - T_{mp,i}) - U_{mor,wd} D_o L(T_{mp,i} - T_{wp,i}) \\ & - 2U_{mor,mor} H_{mor} L(T_{mp,i} - T_{m,i})] \end{aligned} \quad (3.2.11)$$

$$\begin{aligned} \frac{dT_{m,i}}{dt} = & C_{mor,i}^{-1} [2U_{mor,mor} H_{mor} L(T_{mp,i} - T_{m,i}) - \\ & U_{mor,wd} WL(T_{m,i} - T_{w,i}) + U_{wmor,mor} WL(T_{mw,i} - T_{m,i})] \end{aligned} \quad (3.2.12)$$

$$\begin{aligned} \frac{dT_{wp,i}}{dt} = & C_{wdp,i}^{-1} [U_{mor,wd} D_o L(T_{mp,i} - T_{wp,i}) - U_{wd,wdsf} D_o L(T_{wp,i} - T_{ps,i}) \\ & - 2U_{wd,wd} H_{wd} L(T_{wp,i} - T_{wd,i})] \end{aligned} \quad (3.2.13)$$

$$\begin{aligned} \frac{dT_{wd,i}}{dt} = & C_{wd,i}^{-1} [U_{mor,wd} WL(T_{m,i} - T_{wd,i}) - U_{wd,wdsf} WL(T_{wd,i} - T_{s,i}) \\ & + 2U_{wd,wd} H_{wd} L(T_{wp,i} - T_{wd,i})] \end{aligned} \quad (3.2.14)$$

$$\frac{dT_{ps,i}}{dt} = T_{ps,i} - [T_{wp,i} - (q_{pconv} - q_{prad}) / U_{wd,wdsf}] \quad (3.2.15)$$

$$\frac{dT_{s,i}}{dt} = T_{s,i} - [T_{wd,i} - (q_{conv} - q_{rad}) / U_{wd,wdsf}] \quad (3.2.16)$$

$$\begin{aligned} \frac{dT_{cp,i}}{dt} = & C_{crt,i}^{-1} [U_{w,crt} L(T_{w,i} - T_{cp,i}) - U_{crt,air} D_o L(T_{cp,i} - T_{air}) \\ & + 2U_{crt,crt} H_{crt} L(T_{cp,i} - T_{c,i})] \end{aligned} \quad (3.2.17)$$

$$\begin{aligned} \frac{dT_{c,i}}{dt} = & C_{crt,i}^{-1} [U_{mor,crt} WL(T_{mw,i} - T_{c,i}) - U_{crt,air} WL(T_{c,i} - T_{air}) \\ & + 2U_{crt,crt} H_{crt} L(T_{cp,i} - T_{c,i})] \end{aligned} \quad (3.2.18)$$

$$\begin{aligned} \frac{dT_{air}}{dt} = & C_{air}^{-1} \left[\sum_{i=1}^n U_{crt,air} D_o L(T_{cp,i} - T_{air}) + \sum_{i=1}^n U_{crt,air} WL(T_{c,i} - T_{air}) \right. \\ & \left. - U_{air,gyp} A_f (T_{air} - T_{gyp}) \right] \end{aligned} \quad (3.2.19)$$

$$\frac{dT_{gyp}}{dt} = C_{gyp}^{-1} [U_{air,gyp} A_f (T_{air} - T_{gyp}) - U_{gyp,ceilsf} A_f (T_{gyp} - T_{ceilsf})] \quad (3.2.20)$$

Note: if $i=1$, $T_{w,i-1} = T_{sp}$ and if $i = \max imum$, $T_{w,i} = T_r$. All other symbols are defined in

Table 3.2.2, based on reference [18].

Item	Symbol	Magnitude	Dimension
Area of window	A_{win}	6	m^2
U-value of window	U_{win}	2.7	$w/(m^2 \cdot K)$
Area of south direction wall	A_{sw}		m^2
Area of north direction wall	A_{nw}		m^2
Outer diameter of tube	D_o	0.020	m
Inner diameter of tube	D_i	0.016	m
Length of each tube	L		m
Density of water	d_w	990	Kg/m^3
Specific heat of water	c_w	4187	$J/(kg \cdot K)$
Thermal capacity of the water in each tube	C_w	$C_w = 0.25L\pi D_o^2 d_w c_w$	$J/^\circ C$
Heating load of the each heating zone	Q_{hd}		w
Design supply water temperature	T_{spd}	60	$^\circ C$
Design return water temperature	T_{rd}	45	$^\circ C$
Water mass flow rate under design condition	m_w	$m_w = Q_{hd} / [c_w (T_{spd} - T_{rd})]$	Kg/s
Water velocity in the tube	V_m	$V_m = 4m_w / (\pi D_i^2)$	m/s

Kinematic viscosity	ν_m	$0.556 \cdot 10^{-6}$	m^2/s
Conductivity of water	K_w	0.648	$w/m \cdot K$
Reynolds Number	R_e	$R_e = V_m D_i / \nu_m$	
Prandtl Number	P_r	3.54	
Nusselt Number	N_u	$N_u = 0.12(R_e^{0.87} - 280)P_r^{0.4}$	
Convective heat transfer coefficient between water and tube wall (unit length)	h_{it}	$h_{it} = N_u K_w \pi$	$w/m \cdot K$
Conductivity of tube wall	K_{tube}	0.38	$w/m \cdot K$
Resistance of tube wall (unit length)	R_{tube}	$R_{tube} = \frac{\log(D_o / D_i)}{2\pi K_{tube}}$	$m \cdot K/w$
The thickness of mortar layer	H_{mor}	0.060	m
Interval between tubes	W	0.220	m
Length of each mortar node	W_m	0.200	m
U-value between water node and mortar node horizontally(unit length)	$U_{w,mor}$	$U_{w,mor} = (4/h_{it} + 4R_{tube} + \frac{0.5W_m}{D_o K_{mor}})^{-1}$	$w/(m \cdot K)$
U-value between water node and mortar node vertically(unit length)	$U_{w,mor}$	$U_{w,mor} = (4/h_{it} + 4R_{tube} + \frac{0.5H_{mor}}{D_o K_{mor}})^{-1}$	$w/(m \cdot K)$

U-value between water node and concrete node in unit length	$U_{w,crt}$	$U_{w,crt} = (4/h_{it} + 4R_{tube} + \frac{H_{ins}}{D_o K_{ins}} + \frac{0.5H_{crt}}{D_o K_{crt}})^{-1}$	w/(m*K)
Thermal capacity of mortar node in tube layer	$C_{wmor,i}$	$C_{wmor,i} = W_m D_o L d_{mor} c_{mor}$	J/°C
U-value between mortar node in tube layer and mortar node in mortar layer vertically	$U_{wmor,mor}$	$U_{wmor,mor} = \frac{K_{mor}}{(D_o + H_{mor})}$	w/K*m ²
U-value between mortar node in tube layer and concrete node vertically	$U_{wmor,crt}$	$U_{wmor,crt} = (\frac{D_o}{K_{mor}} + \frac{H_{ins}}{K_{ins}} + \frac{0.5H_{crt}}{K_{crt}})^{-1}$	w/K*m ²
Thermal capacity of mortar node in mortar layer, above the tube node	$C_{morp,i}$	$C_{morp,i} = D_o H_{mor} L d_{mor} c_{mor}$	J/°C
U-value between mortar node in mortar layer and wood node	$U_{mor,wd}$	$U_{mor,wd} = (\frac{0.5H_{mor}}{K_{mor}} + \frac{0.5H_{wd}}{K_{wd}})^{-1}$	w/K*m ²
U-value between mortar node and mortar node, in mortar layer	$U_{mor,mor}$	$U_{mor,mor} = \frac{K_{mor}}{W}$	w/K*m ²
Thermal capacity of mortar node in mortar layer	$C_{mor,i}$	$C_{mor,i} = W_m H_{mor} L d_{mor} c_{mor}$	J/°C
Thermal capacity of wood node i	$C_{wdp,i}$	$C_{wdp,i} = D_o H_{wd} L c_{wd} d_{wd}$	J/°C
U-value between wood node and wood surface	$U_{wd,wdsf}$	$U_{wd,wdsf} = \frac{2K_{wd}}{H_{wd}}$	w/K*m ²

U-value between wood node and wood node horizontally	$U_{wd,wd}$	$U_{wd,wd} = \frac{K_{wd}}{W}$	w/K*m ²
Thermal capacity of wood node i	$C_{wd,i}$	$C_{wd,i} = W_m H_{wd} L c_{wd} d_{wd}$	J/°C
Thermal capacity of concrete node i	$C_{crt,i}$	$C_{crt,i} = D_o H_{crt} L c_{crt} d_{crt}$	J/°C
U-value between concrete node and air node	$U_{crt,air}$	$U_{crt,air} = \left(\frac{0.5 H_{crt}}{K_{crt}} + 0.5 R_{air} \right)^{-1}$	w/K*m ²
U-value between concrete nodes	$U_{crt,crt}$	$U_{crt,crt} = \frac{K_{crt}}{W}$	w/K*m ²
Thermal capacity of concrete node i	$C_{crt,i}$	$C_{crt,i} = W_m H_{crt} L c_{crt} d_{crt}$	J/°C
Height of air layer	H_{air}	0.02	m
Specific heat of air	c_{air}	1005	J/kg*°C
Density of air	d_{air}	1.2	kg/m ³
Thermal capacity of the air layer	C_{air}	$C_{air} = A_f H_{air} c_{air} d_{air}$	J/°C
U-value between air node and gypsum node	$U_{air,gyf}$	$U_{air,gyf} = \left(0.5 R_{air} + \frac{0.5 H_{gyf}}{K_{gyf}} \right)^{-1}$	w/K*m ²
Thermal capacity of gypsum layer	C_{gyf}	$C_{gyf} = A_f H_{gyf} c_{gyf} d_{gyf}$	J/°C
Height of gypsum layer	H_{gyf}	0.013	m
U-value between gypsum and ceiling surface	$U_{gyf,ceilsf}$	$U_{gyf,ceilsf} = \frac{2 K_{gyf}}{H_{gyf}}$	w/K*m ²

U-value between block layer and insulation layer	$U_{blo,ins}$	$U_{blo,ins} = \left(\frac{0.5L_{blo}}{K_{blo}} + \frac{0.5L_{ins}}{K_{ins}} \right)^{-1}$	w/K*m ²
U-value between block layer and outside	$U_{blo,o}$	$U_{blo,o} = \left(\frac{0.5L_{blo}}{K_{blo}} + \frac{1}{h_o} \right)^{-1}$	w/K*m ²
U-value between insulation layer and gypsum layer	$U_{ins,gy}$	$U_{ins,gy} = \left(\frac{0.5L_{ins}}{K_{ins}} + \frac{0.5L_{gy}}{K_{gy}} \right)^{-1}$	w/K*m ²
U-value between cement layer and gypsum layer	$U_{cem,gy}$	$U_{cem,gy} = \left(\frac{0.5L_{cem}}{K_{cem}} + \frac{0.5L_{gy}}{K_{gy}} \right)^{-1}$	w/K*m ²
U-value between cement layer and wall interior surface	$U_{cemsf,cem}$	$U_{cemsf,cem} = \left(\frac{0.5L_{cem}}{K_{cem}} + \frac{1}{h_i} \right)^{-1}$	w/K*m ²
Thermal capacity of block layer in south direction wall	C_{blos}	$C_{blos} = A_{sw} L_{blo} d_{blo} c_{blo}$	J/°C
Thermal capacity of block layer in north direction wall	C_{blon}	$C_{blon} = A_{nw} L_{blo} d_{blo} c_{blo}$	J/°C
Thermal capacity of insulation layer in south direction wall	C_{inss}	$C_{inss} = A_{sw} L_{ins} d_{ins} c_{ins}$	J/°C

Thermal capacity of insulation layer in north direction wall	C_{insn}	$C_{insn} = A_{nw} L_{ins} d_{ins} c_{ins}$	J/°C
Thermal capacity of gypsum layer in south direction wall	C_{gypt}	$C_{gypt} = A_{sw} L_{gyp} d_{gyp} c_{gyp}$	J/°C
Thermal capacity of gypsum layer in north direction wall	C_{gypn}	$C_{gypn} = A_{nw} L_{gyp} d_{gyp} c_{gyp}$	J/°C
Thermal capacity of cemmol layer in south direction wall	C_{cems}	$C_{cems} = A_{sw} L_{cem} d_{cem} c_{cem}$	J/°C
Thermal capacity of cemmol layer in north direction wall	C_{cemn}	$C_{cemn} = A_{nw} L_{cem} d_{cem} c_{cem}$	J/°C

Table 3.2.2 Symbols used in the equations 3.2.1-3.2.20

3.2.3 Zone Model

The warm floor slab surface and ceiling surface exchange heat with the cold enclosure surfaces, occupants and other objects inside the space by radiation, and exchange heat with the zone air by convection. At the same time, the zone air exchanges heat with the interior cold surfaces of the enclosure by convection. Simultaneously, the zone air losses some heat because of infiltration. Therefore, the zone air temperature is impacted by a number of factors listed below:

1. Slab surface temperature, T_{flrsf}
2. Internal heat generation, Q_{int}

3. Heat loss rate due to infiltration, Q_{inf}
4. Outside air temperature, T_o
5. Solar radiation, q_{sol} , including the solar gain from south direction windows and solar radiation on the exterior surface of external walls.
6. Average enclosure interior surfaces temperature, T_{en} , including wall, window, ceiling and door.

All of the above factors are time dependent variables and are considered as discrete inputs in the model equations.

In the zone model, the air temperature T_z , ceiling surface temperature T_{ceilsf} , interior surface temperature of south direction wall T_{swsf} , interior surface temperature of north wall T_{nwsf} , interior surface temperature of door T_{doorsf} and interior surface temperature of window T_{winsf} are taken as uniform in the process of simulation. That is to say that those temperatures depend on time rather than location.

The radiation heat flux q_{rad} from each slab surface element to the enclosure interior surfaces is modeled as in reference [48] (2001)

$$q_{radi} = 5 * 10^{-8} F_{i-en} A_i [(T_{flrsfi} + 273)^4 - (T_{en} + 273)^4] \quad (3.2.21)$$

Where,

F_{i-en} is radiation angle factor between i^{th} wood surface node and enclosure

T_{en} is area-average temperature of interior surfaces, except for slab surface, °C

A_i is the slab surface area covered by i^{th} node, m^2

T_{flrsfi} is the i^{th} slab surface temperature, $^{\circ}\text{C}$

Furthermore, as in reference [23] (2008),

$$T_{en} = (A_{iw}T_{iwsf} + A_{ew}T_{ewsf} + A_{win}T_{winsf} + A_{door}T_{doorsf} + A_{ceil}T_{ceilsf}) / (A_{iw} + A_{ew} + A_{win} + A_{door} + A_{ceil}) \quad (3.2.22)$$

Where,

$A_{iw}, A_{ew}, A_{win}, A_{door}, A_{ceil}$ is the area of internal wall, external wall, window, door and ceiling respectively, m^2

$T_{iwsf}, T_{ewsf}, T_{winsf}, T_{doorsf}, T_{ceilsf}$ is the surface temperature of internal wall, external wall, window, door and ceiling respectively, $^{\circ}\text{C}$

According to reference [48] (2001), the convective heat flux q_{conv} from each slab surface element to the zone air directly is expressed as

$$q_{conv} = 2.17 A_i (T_{flrsfi} - T_z)^{1.31} \quad (3.2.23)$$

Therefore, the total heat flux from the whole floor slab to the zone air is:

$$Q_{rad,conv} = \sum_{i=1}^n (q_{radi} + q_{conv}) \quad (3.2.24)$$

Besides the heat gain from slab surfaces, the zone air also receives some heat from the internal heat production and solar radiation, which should be considered as well.

Solar radiation model has two components. One represents solar gains through windows. Solar energy directly transmits through south direction window and is received by enclosure interior surfaces and indoor objects. The other component is the solar radiation which impinges on the external wall surface. If I_c is the solar radiation intensity, τ is the transmittance of the glass, SF is the shading factor, and CF is cloud factor, then Q_{sols} , directly transmits through the south direction window in A_{wins} of area can be expressed as:

$$Q_{sols} = A_{wins} SF CF I_c \tau \quad (3.2.25)$$

Besides, because the solar radiation does have some impact on enclosure exterior surface's heat balance, when considering the heat balance of the exterior surfaces of the enclosure, two heat fluxes, Q_{sol} , Q_o should be considered. Since the solar radiation mainly impinges on the south direction wall, the effect of solar radiation on the other 3 direction walls is ignored. If A_{sw} is the area of south direction wall, then Q_{solsw} is computed by:

$$Q_{solsw} = A_{sw} SF CF I_c \quad (3.2.26)$$

In addition, the internal heat gains Q_{int} are the heat produced by cooking, occupants, lighting and equipments, etc.

The heat transfer by convection between the zone air and windows, doors and walls, can be simply expressed by the following equations.

$$Q_{loss} = \sum_{j=1}^n h_j A_j (T_z - T_{jsf}) \quad (3.2.27)$$

Assuming ACH is the rate of air change per hour, and then the infiltration heat loss rate Q_{inf} can be computed from:

$$Q_{inf} = A_f H d_{air} c_{air} (T_z - T_o) ACH / 3600 \quad (3.2.28)$$

Where H is the height of zone, A_f is total floor area in m^2 , d_{air} , c_{air} are density and specific heat of air, with units Kg/m^3 and $J/(Kg*^{\circ}C)$ respectively.

Therefore, by combining the heat gains and heat losses of the zone, the heat balance of the zone can be expressed as:

$$\begin{aligned} \frac{dT_z}{dt} = C_z^{-1} [& Q_{rad,conv} + Q_{int} + Q_{sols} - Q_{inf} + h_i A_{ceil} (T_{ceilsf} - T_z) \\ & + h_i A_{sw} (T_{swsf} - T_z) + h_i A_{nw} (T_{nwsf} - T_z) - h_i A_{win} (T_z - T_{winsf})] \end{aligned} \quad (3.2.29)$$

Where h_i represents the heat transfer coefficient of interior surface film, $w/(m^2*^{\circ}C)$, and T_{jsf} is the interior surface temperature of j surface, $^{\circ}C$, including walls, windows and doors.

3.2.4 Boiler Model

Usually, a gas-fired boiler is used in a small RFH system. The temperature of supply water of boiler is function of the capacity of the boiler, the efficiency of boiler, mass flow rate of supply-return water and the rate of fuel consumption. According to reference [23] (2008), the efficiency of a boiler is function of return water temperature and the accurate value can be obtained from experiments. The energy balance equation of the boiler can be described as

$$\frac{dT_b}{dt} = C_b^{-1} [U_f m_{f_{\max}} HVeb - m_{wd} c_w U_w (T_b - T_{rb})] \quad (3.2.30)$$

Where, C_b is the thermal capacity of the boiler, J/(Kg*°C)

$m_{f_{\max}}$ is maximum fuel consumption, based on design condition, Kg/s

HV is the specific heat of natural gas, J/Kg

eb represents the efficiency of the boiler.

T_b is the supply water temperature from boiler, °C

T_{rb} is the return water temperature to boiler, °C

U_f represents the control signal for mass flow rate of gas

U_w represents the control signal for mass flow rate of water

Note that both U_f, U_w vary between 0 and 1. The control signal U_f can be obtained from the error between the set-point of boiler water temperature T_{bset} and real boiler supply water temperature T_b , and U_w can be obtained from the thermostat for measuring room air temperature or floor slab temperature.

Besides, the heat loss from pipe network should be considered as well, which is related to the boiler supply water temperature T_b , ground temperature T_g , type of pipe, thickness of insulation layer and the total length of pipe. All of them affect the supply water temperature T_{sp} to the radiant floor. Since the supply water from the boiler would lose some heat, the temperature of the water sent to the radiant floor is lower than the water temperature at the outlet of boiler. The same theory applies on the return water pipe

network which would result in the return water temperature to boiler being lower than that of water returning from the zone. Therefore, the temperature of supply water T_{sp} to the RFH zone and the temperature of return water T_{rb} to boiler are expressed as:

$$T_{sp} = (U_w m_w c_w T_b - 0.5U_p T_b + U_p T_g) / (U_w m_w c_w + 0.5U_p) \quad (3.2.31)$$

$$T_{rb} = (U_w m_w c_w T_r - 0.5U_p T_r + U_p T_g) / (U_w m_w c_w + 0.5U_p) \quad (3.2.32)$$

Where,

$$U_p = (1/h_{it} + R_p + \{\log[(D_o + 2H_{insp})/D_o]\} / (2\pi k_{ins} L_p))^{-1} \quad (3.2.33)$$

L_p is the total length of the pipe from boiler to RFH zone, m; H_{insp} , D_o are thickness of insulation layer and outer diameter of pipe respectively, m. h_{it} is the convective heat transfer coefficient between water and tube surface, $w/(m^2 \cdot ^\circ C)$, and R_p is the thermal resistance of tube wall, $(m^2 \cdot ^\circ C)/w$.

3.3 Overall RFH System Model

The equations described above were linked together to formulate a complete model of RFH system. These equations were programmed in MATLAB and solved using subroutines.

3.4 Open loop simulations of a single zone RFH system

A single zone RFH system was simulated. The size of the room is 5m(L)*5.2m(W)*2.8m(H) and located in Teajon, South Korea, Latitude 37.5° north where the outside air design temperature T_{od} is -15°C. The size of the south facing window is 3m (L)*2m (H). The elevation view and floor plan view is depicted in Figure 3.4.1.

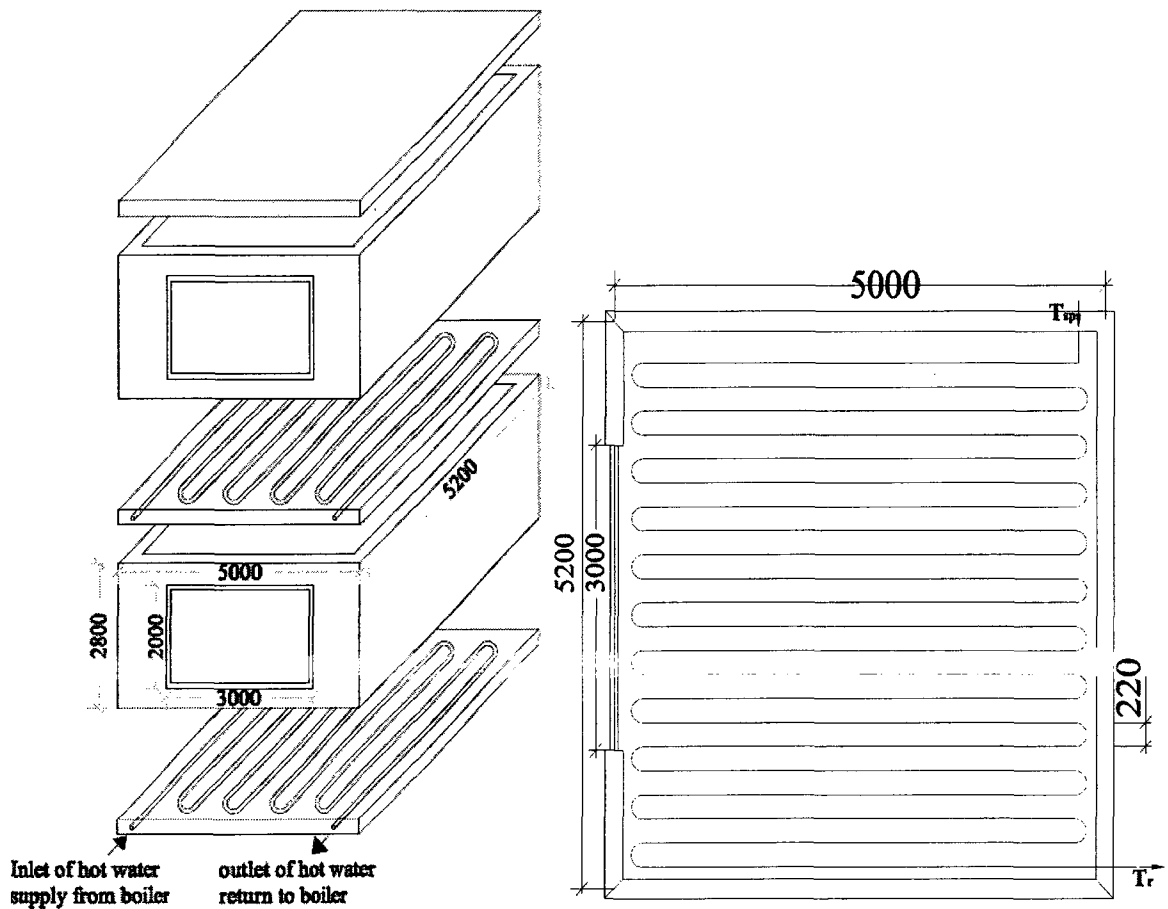


Figure 3.4.1 Elevation view and floor plan view of the single zone RFH system

As shown in Figure 3.4.1, the interval between the tubes is 220mm. The east wall and west wall are assumed as internal walls, from which no heat losses and gains occur. The

air infiltration rate is 0.5 ACH. From the properties of the construction materials stated in chapter 3, the design heating load Q_{hd} for this single zone is 1379.6w when the indoor air design temperature T_{id} is 20°C.

The hot water system consists of a 2500W capacity gas-fired boiler and the inner/outer diameter of the pipe is 16/20mm. The supply water pipe from boiler to the heated zone is 25m long, and thickness of the insulation layer is 20mm. Under design condition, the temperature difference between supply water to the zone and return water from the zone is 15°C. Therefore, under design condition, the mass flow rate of the hot water m_{wd} is 0.0310 Kg/s. Using these design parameters, open loop simulation runs were made. The results are discussed in the following.

3.4.1 Simulation results of the single zone model under design condition

Figure 3.4.2 and 3.4.3 show the zone air temperature, ceiling surface temperature, external walls temperature, and boiler water, supply water and return water temperatures, as a function of time.

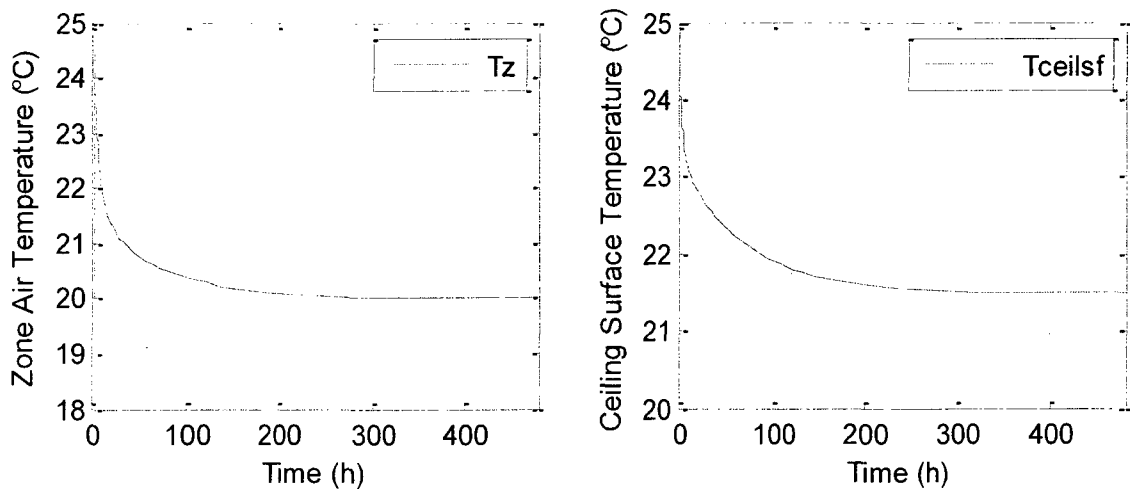


Figure 3.4.2 Predicted zone air temperature and ceiling surface temperature

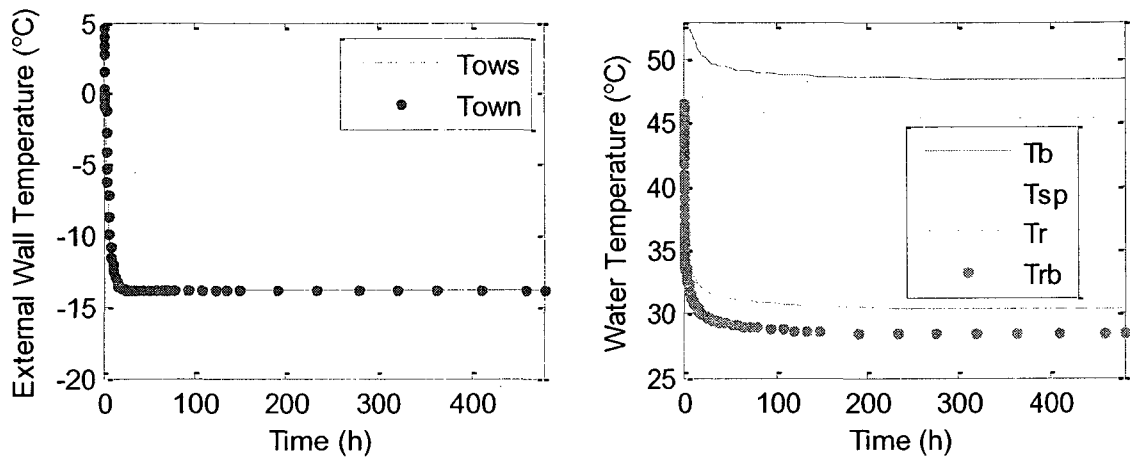
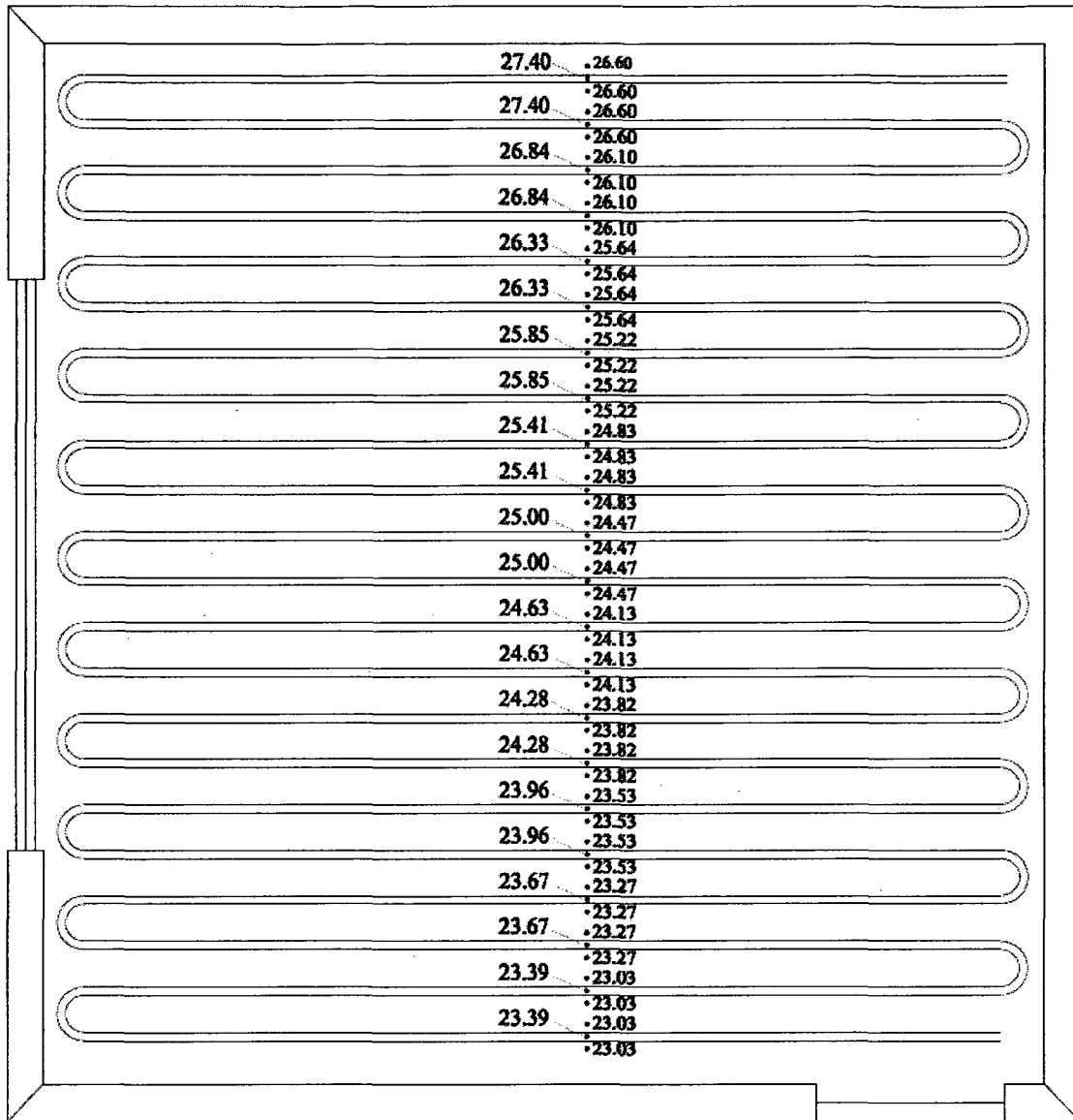


Figure 3.4.3 Predicted external wall temperature and water temperature

From Figures 3.4.2 and 3.4.3, it can be seen clearly that the temperatures reach steady state after about 100 hours. This reflects the large thermal capacity of the system giving rise to slow response. At the steady state, the zone air temperature is 20.00°C , the supply water temperature from boiler is 48.51°C , the supply water to the radiant floor is 45.36°C , the return water temperature from the zone is 30.36°C , the water temperature return to the boiler is 28.44°C , and the ceiling surface temperature is 21.49°C . Also, Figure 3.4.4 shows the surface temperature of each surface element under steady state:



● represent one node
 the number represent the temperature of the node, °C

scale: 1:2

Figure 3.4.4 Surface temperature distribution

From Figure 3.4.4, we can see that the maximum surface temperature is 27.40°C and the minimum surface temperature is 23.03°C, a difference of 4.37°C. In comparison, the difference between the water temperature nodes is 15°C, which is much higher than the surface temperature gradient. That is because the higher surface temperature, more

radiative and convective heat is transferred to the zone which lowers the surface temperature. In contrast, the lower the slab surface temperature, the less heat is transferred to the zone. Thus, the temperature distribution of slab surface is relatively even.

Based on the design conditions (control signal $U_w = 1$ and boiler capacity $Q_{boiler} = 2500 \text{ w}$), by changing outside air temperature and the rate of gas combustion in the boiler, the zone air temperature, the ceiling temperature, the supply water temperature to the radiant zone and the return water temperature from the radiant floor were simulated. The results are summarized in Table 3.4.1.

T_o °C	u_f %	T_z °C	T_b °C	T_{sp} °C	T_r °C	T_{rb} °C	T_{ceilsf} °C
-15	70.8	20.00	48.51	45.36	30.36	28.44	21.49
-10	61.77	20.00	44.69	41.79	28.94	27.11	21.29
-5	52.79	20.00	40.85	38.21	27.50	25.77	21.08
0	43.86	20.00	36.99	34.62	26.05	24.42	20.87
5	34.99	20.00	33.12	31.01	24.58	23.05	20.66
10	26.17	20.00	29.22	27.38	23.10	21.67	20.45

Table 3.4.1 Open loop test of the single zone RFH system model

From the above simulation results, a relationship between the boiler control signal and outside air temperature, water temperatures and outside air temperature, of the single zone were plotted as shown in Figure 3.4.5.

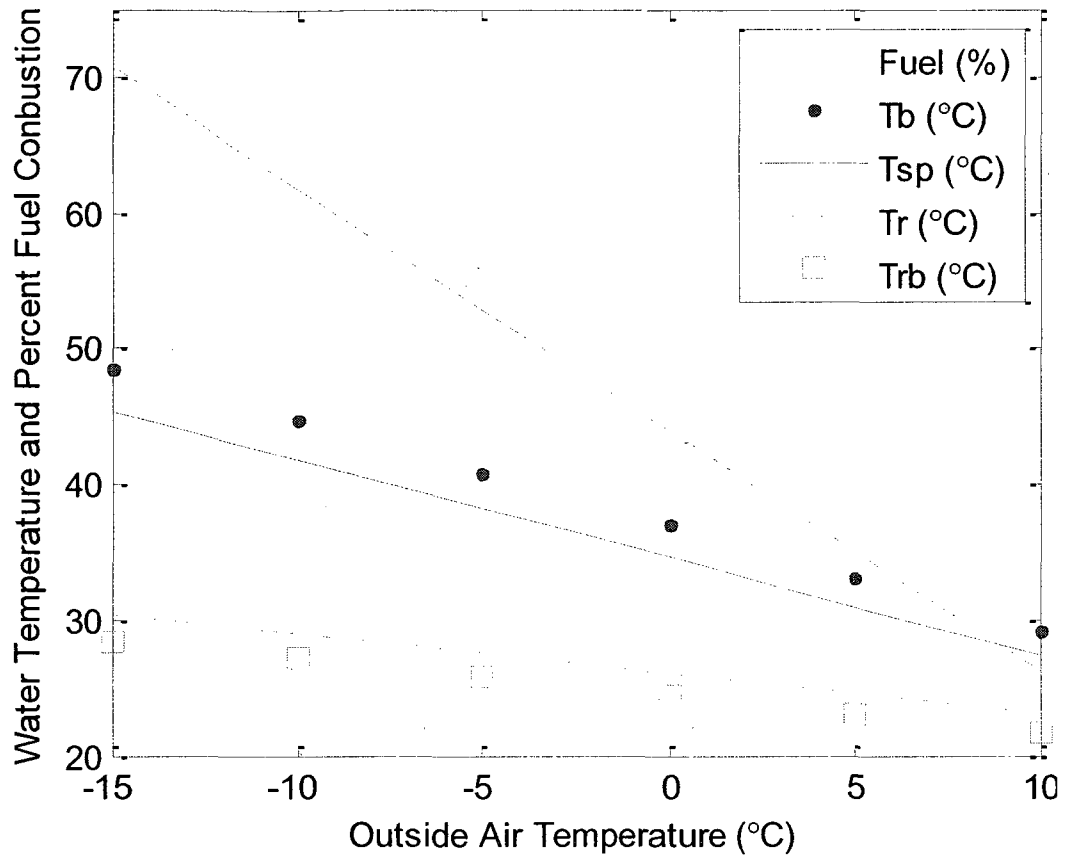


Figure 3.4.5 Open loop test of the single zone RFH system

From above figure, it can be clearly seen that the fuel combustion rate is a linear function of the outside air temperature. Besides, the difference between the supply water temperature T_{sp} and return water temperature T_r is smaller when the outside air temperature increases, which is correct, because the water flow rate is held constant and less heat is required to maintain the zone air temperature.

3.5 Zonal model of single zone RFH system

From Figure 3.4.4, it was noted that the floor slab surface temperature shows maximum variation of 4°C between the first and last node. This is also likely to impact

on the zone air temperature distribution in the room. To study this effect, a zonal model of single zone RFH system was developed. The model and simulation results are described in the following section.

3.5.1 The formulation of the zonal model

The single zone described in previous section will be divided into several small cells. All these cells are inter-connected by mass air flows, and the mass and thermal balances are given for each of them to calculate the indoor temperature field.

By assuming uniform temperature and density in each small cell, the pressure at the middle of a zone obeys the perfect gas law [44] (1999) is expressed by:

$$P_{middle} = \rho R(T + 273) \quad (3.5.1)$$

Where ρ is the density of the air in the cell, Kg/m³,

R is the perfect gas constant, Pa*m³/(Kg*K)

T is the temperature of the zone, °C

Therefore, the pressure at height z above the bottom of a cell is given by:

$$P = p_0 - \rho g z \quad (3.5.2)$$

Where p_0 is the pressure at the bottom of the cell, Pa

According to reference [19] (1996), the mass transfer rate from one cell to the other is mainly governed by variation in the driving pressure, which is expressed by the following equation:

$$0.5\rho v^2 = Cd_v^2 \Delta P \quad (3.5.3)$$

Where ρ donates density of the air in the cell from which air leaves, Kg/m^3

v is the velocity of mass transfer, m/s

Cd_v is the discharge coefficient, dimensionless,

ΔP is the pressure difference between the two neighbour cells, Pa

Thus, the mass transfer rate at the interface level between two neighbour cells is:

$$m = \rho A v \quad (3.5.4)$$

Where m is the mass transfer rate, Kg/s

A is the area of the interface, m^2 .

Since the density ρ in equations 3.5.3 and 3.5.4 is determined by the direction of the mass transfer, the pressure difference ΔP would determine density ρ . Meanwhile, because hydrostatic effects are taken into account, the mass flow for horizontal interfaces and vertical interfaces is calculated differently [29] (2002). The next part is to calculate the mass transfer under the two cases.

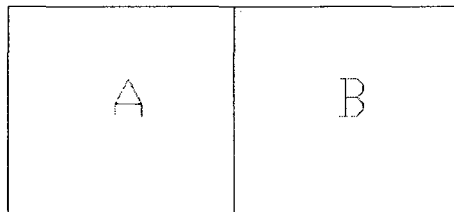


Figure 3.5.1 Vertical interface of mass transfer between cells

Figure 3.5.1 has described a vertical interface. The mass flow rate can be calculated as follow:

$$\text{If } \Delta P = P_A - P_B \geq 0, \quad m_{AB} = CdA(2\rho_A)^{0.5}(P_A - P_B)^{0.5} \quad (3.5.5)$$

$$\text{and if } \Delta P = P_A - P_B < 0, \quad m_{AB} = -CdA(2\rho_B)^{0.5}(P_B - P_A)^{0.5} \quad (3.5.6)$$

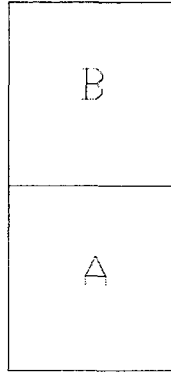


Figure 3.5.2 Horizontal interface of mass transfer between cells

Figure 3.5.2 describes a horizontal interface. The mass flow rate can be expressed by:

$$\text{If } \Delta P = (P_A - 0.5\rho_A gh_A) - (P_B + 0.5\rho_B gh_B) \geq 0,$$

$$m_{AB} = CdA(2\rho_A)^{0.5}[(P_A - 0.5\rho_A gh_A) - (P_B + 0.5\rho_B gh_B)]^{0.5} \quad (3.5.7)$$

$$\text{And if } \Delta P = (P_A - 0.5\rho_A gh_A) - (P_B + 0.5\rho_B gh_B) < 0,$$

$$m_{AB} = -CdA(2\rho_B)^{0.5}[-(P_A - 0.5\rho_A gh_A) + (P_B + 0.5\rho_B gh_B)]^{0.5} \quad (3.5.8)$$

Where P_A, P_B is the pressure in the middle of cell A and cell B respectively, Pa

ρ_A, ρ_B is the density of cell A and cell B respectively, Kg/m^3

g is the gravitational acceleration, m/s^2

h_A, h_B is the height of cell A and cell B respectively, m

m_{AB} is the rate of mass transfer from cell A to cell B, Kg/s

A is the area of the interface between cell A and cell B, m^2

As stated in reference [19] (1996), the computed values of mass transfer rate are not very sensitive to the cell number in the lengthwise direction and the widthwise direction of the cell owing to low air temperature gradients along these coordinates. However, it was noticed that the simulation results depend on the cell number over the height. As result, the small room is divided into 9 cells with three meshes in the lengthwise direction and 3 meshes over the height of the room. Each cell and the size of each cell are shown in the following figure.

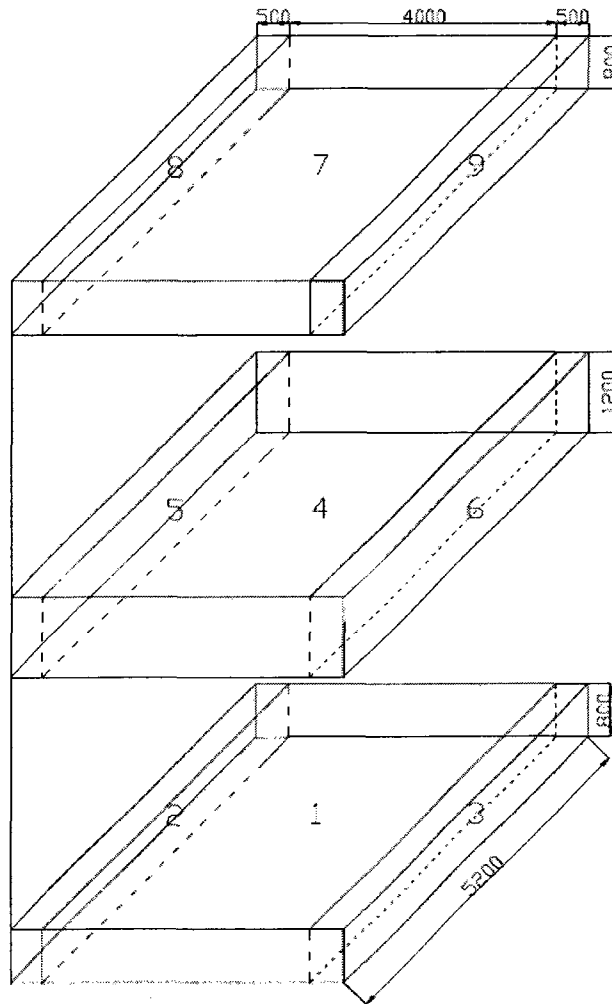


Figure 3.5.3 9 cells in the single room

According to equations 3.5.7 and 3.5.8, we have:

$$\text{If } P_1 \leq P_2, \quad m_{21} = CdA_{12}(2\rho_2)^{0.5}(P_2 - P_1)^{0.5} \quad (3.5.9)$$

$$Q_{21} = m_{21}c_{air}T_2 \quad (3.5.10)$$

$$\text{and if } P_1 > P_2, \quad m_{21} = -CdA_{12}(2\rho_1)^{0.5}(P_1 - P_2)^{0.5} \quad (3.5.11)$$

$$Q_{21} = m_{21}c_{air}T_1 \quad (3.5.12)$$

$$\text{If } P_1 \leq P_3, \quad m_{31} = CdA_{13}(2\rho_3)^{0.5}(P_3 - P_1)^{0.5} \quad (3.5.13)$$

$$Q_{31} = m_{31}c_{air}T_3 \quad (3.5.14)$$

$$\text{and if } P_1 > P_3, \quad m_{31} = -CdA_{13}(2\rho_1)^{0.5}(P_1 - P_3)^{0.5} \quad (3.5.15)$$

$$Q_{31} = m_{31}c_{air}T_1 \quad (3.5.16)$$

$$\text{If } P_1 - 0.5\rho_1gh_1 \geq P_4 + 0.5\rho_4gh_4,$$

$$m_{14} = CdA_{14}(2\rho_1)^{0.5}[(P_1 - 0.5\rho_1gh_1) - (P_4 + 0.5\rho_4gh_4)]^{0.5} \quad (3.5.17)$$

$$Q_{14} = m_{14}c_{air}T_1 \quad (3.5.18)$$

$$\text{and if } P_1 - 0.5\rho_1gh_1 < P_4 + 0.5\rho_4gh_4,$$

$$m_{14} = -CdA_{14}(2\rho_1)^{0.5}[-(P_1 - 0.5\rho_1gh_1) + (P_4 + 0.5\rho_4gh_4)]^{0.5} \quad (3.5.19)$$

$$Q_{14} = m_{14}c_{air}T_4 \quad (3.5.20)$$

If $P_4 \geq P_5$,

$$m_{45} = CdA_{45}(2\rho_4)^{0.5}(P_4 - P_5)^{0.5} \quad (3.5.21)$$

$$Q_{45} = m_{45}c_{air}T_4 \quad (3.5.22)$$

and if $P_4 < P_5$,

$$m_{45} = -CdA_{45}(2\rho_5)^{0.5}(P_5 - P_4)^{0.5} \quad (3.5.23)$$

$$Q_{45} = m_{45}c_{air}T_5 \quad (3.5.24)$$

If $P_4 \geq P_6$,

$$m_{46} = CdA_{46}(2\rho_4)^{0.5}(P_4 - P_6)^{0.5} \quad (3.5.25)$$

$$Q_{46} = m_{46}c_{air}T_4 \quad (3.5.26)$$

and if $P_4 < P_6$,

$$m_{46} = -CdA_{46}(2\rho_6)^{0.5}(P_6 - P_4)^{0.5} \quad (3.5.27)$$

$$Q_{46} = m_{46}c_{air}T_6 \quad (3.5.28)$$

If $P_4 - 0.5\rho_4gh_4 \geq P_7 + 0.5\rho_7gh_7$,

$$m_{47} = CdA_{47}(2\rho_4)^{0.5}[(P_4 - 0.5\rho_4gh_4) - (P_7 + 0.5\rho_7gh_7)]^{0.5} \quad (3.5.29)$$

$$Q_{47} = m_{47}c_{air}T_4 \quad (3.5.30)$$

and if $P_4 - 0.5\rho_4gh_4 < P_7 + 0.5\rho_7gh_7$

$$m_{47} = -CdA_{47}(2\rho_7)^{0.5} [-(P_4 - 0.5\rho_4gh_4) + (P_7 + 0.5\rho_7gh_7)]^{0.5} \quad (3.5.31)$$

$$Q_{47} = m_{47}c_{air}T_7 \quad (3.5.32)$$

$$\text{If } P_8 \leq P_7, m_{78} = CdA_{78}(2\rho_7)^{0.5}(P_7 - P_8)^{0.5} \quad (3.5.33)$$

$$Q_{78} = m_{78}c_{air}T_7 \quad (3.5.34)$$

$$\text{and if } P_8 > P_7, m_{78} = -CdA_{78}(2\rho_8)^{0.5}(P_8 - P_7)^{0.5} \quad (3.5.35)$$

$$Q_{78} = m_{78}c_{air}T_8 \quad (3.5.36)$$

$$\text{If } P_9 \leq P_7, m_{79} = CdA_{79}(2\rho_7)^{0.5}(P_7 - P_9)^{0.5} \quad (3.5.37)$$

$$Q_{79} = m_{79}c_{air}T_7 \quad (3.5.38)$$

$$\text{and if } P_9 > P_7, m_{79} = -CdA_{79}(2\rho_9)^{0.5}(P_9 - P_7)^{0.5} \quad (3.5.39)$$

$$Q_{79} = m_{79}c_{air}T_9 \quad (3.5.40)$$

Where m_{ij} presents the mass transfer rate (Kg/s) between cell i and cell j . If it is positive, it means the mass transfer direction is from cell i to cell j ; if it is negative, it means the mass transfer direction is from cell j and cell i . Besides, A_{ij} is the area of the interface between cell i and cell j , m^2 , and ρ_i , P_i and T_i represent the density, pressure and temperature of zone i respectively, with units kg/m^3 , Pa, °C and c_{air} represents the specific heat of air, J/(Kg*°C).

By applying air mass balance for each cell, the general equation can be written as :

$$\frac{dm_i}{dt} = \sum m_{ij} + m_{i\text{source}} - m_{i\text{sink}} \quad (3.5.41)$$

Where, m_i is the total air mass in cell i , Kg

$m_{i\text{source}}$ is the mass flow rate from sources in the cell i , Kg/s

$m_{i\text{sink}}$ is the mass flow rate to sinks in the cell i , Kg/s

In addition, under the steady condition, the derivative of the air mass $\frac{dm_i}{dt} = 0$, because of the natural convection in the room with RFH system, the air mass flow rates $m_{i\text{source}}$ and $m_{i\text{sink}}$ are also set to zero.

By assuming the air distribution in each small cell is uniform, the density depends on the total mass of the air in each cell. In other words, the air density in each cell is time dependent, resulting from the mass transfer rate between the connecting cells. Therefore, the dynamic equations for the density in each cell can be expressed by the following equations:

$$\frac{d\rho_1}{dt} = (m_{21} + m_{31} - m_{14})/V_1 \quad (3.5.42)$$

$$\frac{d\rho_2}{dt} = (m_{52} - m_{21})/V_2 \quad (3.5.43)$$

$$\frac{d\rho_3}{dt} = (m_{63} - m_{31})/V_3 \quad (3.5.44)$$

$$\frac{d\rho_4}{dt} = (m_{14} - m_{45} - m_{46} - m_{47})/V_4 \quad (3.5.45)$$

$$\frac{d\rho_5}{dt} = (m_{45} + m_{85} - m_{52})/V_5 \quad (3.5.46)$$

$$\frac{d\rho_6}{dt} = (m_{46} + m_{96} - m_{63})/V_6 \quad (3.5.47)$$

$$\frac{d\rho_7}{dt} = (m_{47} - m_{78} - m_{79})/V_7 \quad (3.5.48)$$

$$\frac{d\rho_8}{dt} = (m_{78} - m_{85})/V_8 \quad (3.5.49)$$

$$\frac{d\rho_9}{dt} = (m_{79} - m_{96})/V_9 \quad (3.5.50)$$

Where V_i represents the volume of cell i .

Since the zonal model is based on the single zone RFH system stated in previous section, it should be combined together with the RFH system. That is to say, besides the radiative heat transfer, cell 1, cell 2 and cell 3 would absorb some heat from the floor surface by convection, and cell 7, cell 8 and cell 9 would obtain some heat from the ceiling surface by convection. In addition, convective heat exchange exists between the air and the inside surfaces of walls and windows in each cell.

The infiltration from external walls and windows will be considered in the zonal model. Assume the direction of the wind is in south direction, which means some outside air will infiltrate into the room from south wall and infiltrate out of the room through north wall.

Assume both the window and the external wall is tight fitting. According to reference [2], the infiltration rate through the window is $v_{win}=0.5L/(s*m)$ and the infiltration rate through the wall is $v_w=0.48L/(s*m^2)$. Then, the total infiltration rate to each cell can be written as follow.

$$V_{z2inf} = A_{z2w}v_w + A_{z2win}v_{win} \quad (3.5.51)$$

$$V_{z5inf} = A_{z5w}v_w + A_{z5win}v_{win} \quad (3.5.52)$$

$$V_{z8inf} = A_{z8w}v_w \quad (3.5.53)$$

$$V_{z3inf} = -(V_{z2inf} + V_{z5inf} + V_{z8inf}) \frac{A_{z3w}}{A_{z3w} + A_{z6w} + A_{z9w}} \quad (3.5.54)$$

$$V_{z6inf} = -(V_{z2inf} + V_{z5inf} + V_{z8inf}) \frac{A_{z6w}}{A_{z3w} + A_{z6w} + A_{z9w}} \quad (3.5.55)$$

$$V_{z9inf} = -(V_{z2inf} + V_{z5inf} + V_{z8inf}) \frac{A_{z9w}}{A_{z3w} + A_{z6w} + A_{z9w}} \quad (3.5.56)$$

Where, V_{zinf} refers to the infiltration rate in m^3/s to zone i ,

A_{ziw} and A_{ziwin} present the area of the wall and window respectively

in zone i , m^2 ,

By applying energy conservation law to each cell, a series of temperature dynamic equations are expressed as follow:

$$C_{z1} \frac{dT_1}{dt} = Q_{z1rad} + Q_{z1sur1} + h_i A_{z1w} (T_{z1wsur} - T_1) + Q_{21} + Q_{31} - Q_{14} \quad (3.5.57)$$

$$C_{z2} \frac{dT_2}{dt} = Q_{z2rad} + Q_{flrsur2} + h_i A_{z2w} (T_{z2wsur} - T_2) + U_{win} A_{z2win} (T_o - T_2) - Q_{21} + Q_{52} + V_{z2inf} \rho_{o,air} c_{air} T_o \quad (3.5.58)$$

$$C_{z3} \frac{dT_3}{dt} = Q_{z3rad} + Q_{flrsur3} + h_i A_{z3w} (T_{z3wsur} - T_3) + Q_{63} - Q_{31} + V_{z3inf} \rho_3 c_{air} T_3 \quad (3.5.59)$$

$$C_{z4} \frac{dT_4}{dt} = Q_{z4rad} + h_i A_{z4w} (T_{z4wsur} - T_4) + Q_{14} - Q_{45} - Q_{46} - Q_{47} \quad (3.5.60)$$

$$C_{z5} \frac{dT_5}{dt} = Q_{z5rad} + h_i A_{z5w} (T_{z5wsur} - T_5) + U_{win} A_{z5win} (T_o - T_5) + Q_{45} + Q_{85} - Q_{52} + V_{z5inf} \rho_{o,air} c_{air} T_o \quad (3.5.61)$$

$$C_{z6} \frac{dT_6}{dt} = Q_{z6rad} + h_i A_{z6w} (T_{z6wsur} - T_6) + Q_{46} + Q_{96} - Q_{63} + V_{z6inf} \rho_6 c_{air} T_6 \quad (3.5.62)$$

$$C_{z7} \frac{dT_7}{dt} = Q_{z7rad} + h_i A_{z7w} (T_{z7wsur} - T_7) + h_i A_{z7ceil} (T_{z7ceilsur} - T_7) + Q_{47} - Q_{78} - Q_{79} \quad (3.5.63)$$

$$C_{z8} \frac{dT_8}{dt} = Q_{z8rad} + h_i A_{z8w} (T_{z8wsur} - T_8) + h_i A_{z8ceil} (T_{z8ceilsur} - T_8) + Q_{78} - Q_{85} + V_{z8inf} \rho_{o,air} c_{air} T_o \quad (3.5.64)$$

$$C_{z9} \frac{dT_9}{dt} = Q_{z9rad} + h_i A_{z9w} (T_{z9wsur} - T_9) + h_i A_{z9ceil} (T_{z9ceilsur} - T_9) + Q_{79} - Q_{96} - V_{z9inf} \rho_9 c_{air} T_9 \quad (3.5.65)$$

Where, C_{z_i} is the thermal capacity of the air in cell i , J/°C

T_{ziwsur} and $T_{ziceilsur}$ represent the interior surface of the wall and ceiling

in cell i , °C

$\rho_{o,air}$ is the density of outside air, Kg/m³,

T_o is the outside air temperature, °C.

In equations 3.5.57~3.5.59, $Q_{flrsur1}$, $Q_{flrsur2}$ and $Q_{flrsur3}$ refer to the convective heat transfer rate in unit w to cell 1, 2 and 3 from the radiant floor surface respectively, which can be expressed as:

$$Q_{flrsur1} = 2.17 A_{z1,flr} (T_{flrsur} - T_1)^{1.31} \quad (3.5.66)$$

$$Q_{flrsur2} = 2.17 A_{z2,flr} (T_{flrsur} - T_2)^{1.31} \quad (3.5.67)$$

$$Q_{flrsur3} = 2.17 A_{z3,flr} (T_{flrsur} - T_3)^{1.31} \quad (3.5.68)$$

Where $A_{z1,flr}$, $A_{z2,flr}$ and $A_{z3,flr}$ present the floor area in cell 1, 2 and 3 respectively, m²

T_{flrsur} is the floor surface temperature, °C.

Besides, in above equations, Q_{zirad} represents the radiative heat to cell i , which will be calculated later.

Because the conduction of air is very small, the heat conduction of air between the cells is assumed to be negligible. Hence, in equation 3.5.(57~65), the net heat stored in each zone is equal to the heat transfer from the radiant floor surface and/or the air mass flow entering into the cell minus the heat from air mass flow leaving the cell, and the heat transfer between the cells and interior surfaces of the enclosure.

From the simulation results of RFH single zone model, it can be seen that radiative heat transfer accounts for a large proportion in the total heat transfer in RFH system. In the zonal model, floor, ceiling and internal wall will be considered as heat sources which

radiate heat to cold surfaces, such as window, external walls. Ceiling and internal wall would also receive some radiative heat from floor surface, resulting from that the temperature of floor surface is the highest in the room. According to reference [18], the radiative heat can be expressed by:

$$Q_{rad} = \sigma A_1 F_{1-2} \frac{1}{1/\varepsilon_1 + 1/\varepsilon_2 - 1} (T_{sur1}^4 - T_{sur2}^4) \quad (3.5.69)$$

Where Q_{rad} is the total radiative heat from surface 1 to surface 2, w

σ is constant, $5.67 \cdot 10^{-8} \text{ w}/(\text{m}^2 \cdot \text{K}^4)$

A_1 is the area of surface 1, m^2

F_{1-2} is the angle factor between the two surface

$\varepsilon_1, \varepsilon_2$ is the emissivity of surface 1 and 2 respectively

T_{sur1}, T_{sur2} is the temperature of surface 1 and 2 respectively, K

The dynamic equations of the other nodes, such as nodes in enclosure and floor, supply/return water, and boiler system have been explained in previous section, and they remain the same as given in equations (3.2.1) ~ (3.2.33).

3.5.2. Simulation results of the zonal model

By programming the dynamic equations in MATLAB and solving the equations, the mass transfer rates in each cell were obtained. The results are depicted in Figure 3.5.4.

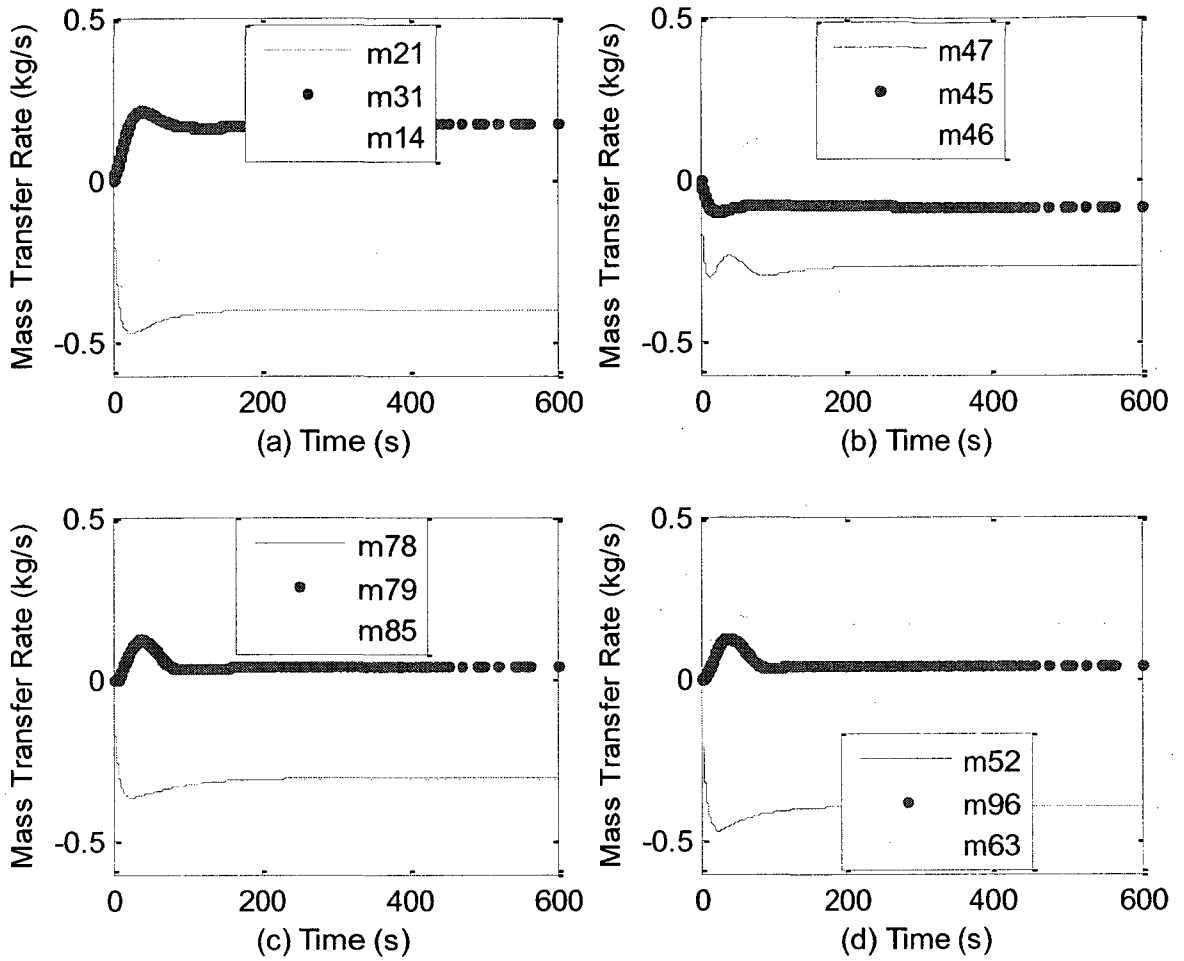


Figure 3.5.4 Simulation results of air mass transfer rate in each cell

In Figure 3.5.4, when m_{ij} is negative, it means the mass transfer direction is from cell i to cell j . In reverse, when m_{ij} is positive, it means the mass transfer direction is from cell j to cell i . Under the steady state design condition, both mass transfer rate and direction are represented in the following grid.

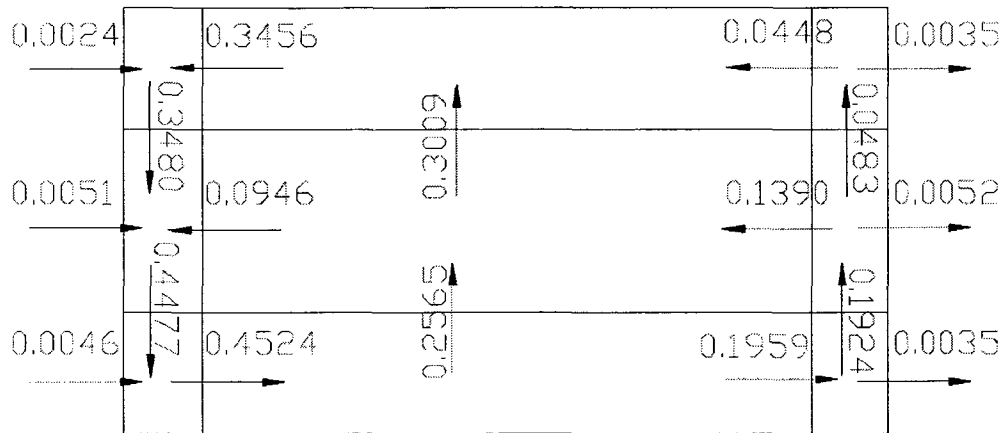


Figure 3.5.5 Mass transfer rate (Kg/s) and direction in the boundary layers

In addition, the simulation results of air temperature in each cell are plotted in Figure 3.5.6.

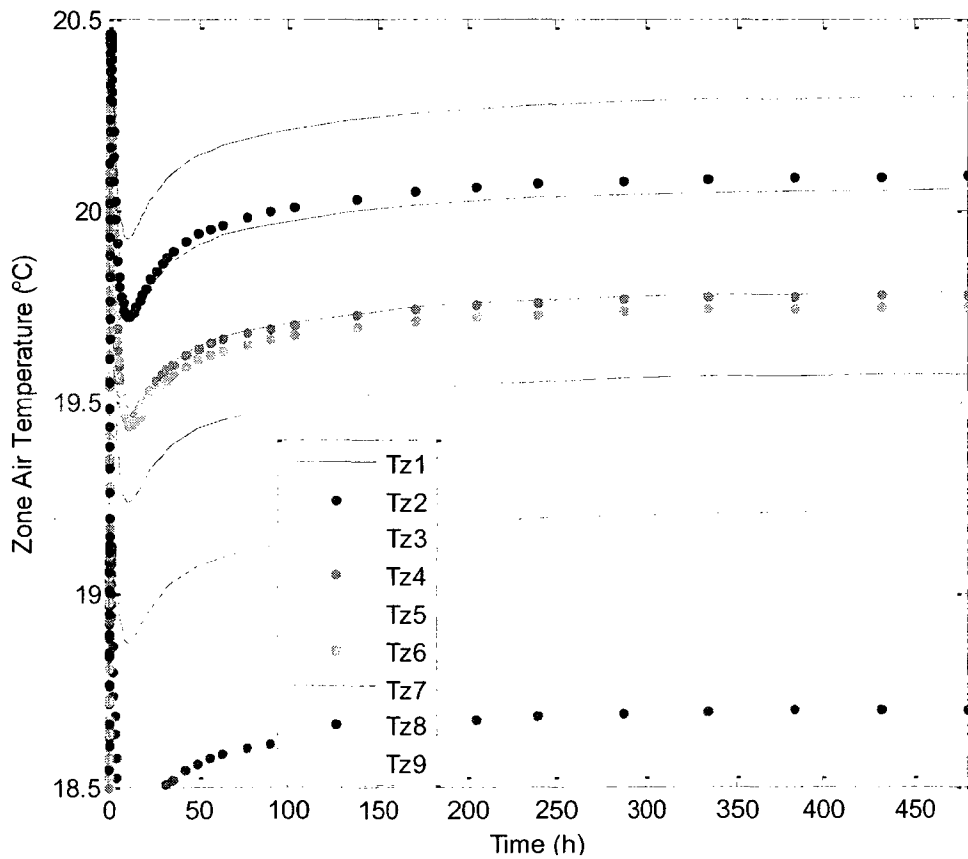


Figure 3.5.6 Simulation results of air temperature in each cell

Figure 3.5.6 shows that, after about 100 hours, the dynamic model reaches steady state.

The air temperature in each cell in the zone is shown in Figure 3.5.7.

20.09	20.30	20.05
19.22	19.78	19.75
18.70	19.57	19.79

Figure 3.5.7 Cell temperature under steady state

Figure 3.5.7 shows that cell 7 has the highest temperature 20.30°C and cell 2 has the lowest temperature of 18.70°C. The simulation results are reasonable because cell 7 could obtain some convective heat from the ceiling which has higher temperature and some radiative heat from the floor surface, results from relative large angle factor between the two surfaces, and it does not lose heat to outside. By comparison, although cell 1 receives a large amount of convective heat from floor surface, a lot of cold air comes from cell 2 and cell 3 into cell 1 to counteract the heat. The cell 2 loses too much heat through the wall, window and by infiltration. Although cell 5 loses more heat than cell 2, it gets some warm air from cell 8 and cell 4.

In addition, from the simulation results, we can find that the maximum temperature difference among the cells is 1.6°C. Moreover, the temperature difference is less than that in other heating systems, such as board heater and traditional air-conditioning system.

3.5.3 Open-loop test of the zonal model

The open-loop simulation results are described in Table 3.5.1.

Outside air temperature	Temperature in each zone °C								
	cell	cell	cell	cell	cell	cell	cell	cell	cell
	1	2	3	4	5	6	7	8	9
-15°C	19.57	18.70	19.79	19.78	19.22	19.75	20.30	20.09	20.05
-10°C	19.68	18.94	19.88	19.84	19.38	19.89	20.29	20.12	20.22
-5°C	19.72	19.08	19.89	19.88	19.47	19.91	20.28	20.13	20.19
0°C	19.73	19.18	19.87	19.86	19.52	19.90	20.23	20.10	20.19
5°C	19.76	19.33	19.89	19.88	19.60	19.90	20.20	20.09	20.16

Table 3.5.1 Open loop runs of air temperature in each cell

From Table 3.5.1, it can be seen that the air temperature in cell 2 is the lowest and in cell 7 is the highest. In addition, it shows that the temperature difference between the cells decreases when the outside air temperature increases, due to less heat loss to outside through structure when outside air temperature is higher. Thus, heat is distributed more evenly among the cells.

3.5.4 Summary

As can be noted, the air temperature distribution in the zone is not uniform resulting in a maximum variation of 1.6°C. Therefore, in order to study the zone temperature

distribution, it is necessary to use zonal models for evaluating thermal comfort in the zone.

This increases the complexity of the model. Since such complex models are not suitable for control analysis, the single and multi-zone models with uniform air temperature were used for designing control strategies presented in chapter 4.

3.6 Open loop simulation of multi-Zone RFH system

An apartment with 4 zones shown in Figure 3.6.1 was considered as a multi-zone RFH system. The area being heated is 66.77m^2 and the unheated area is 86.23m^2 . The apartment is assumed to be located in the middle of a high-rise building. The water circuit consists of 4 tube loops. The tube pitch in room 1 is 150mm and it is 220mm in other 3 rooms. The construction details of external walls, internal walls and floor slab is the same as mentioned before. Under the design condition with the outside air temperature of -15°C and the air infiltration rate of 0.5ACH, the design heating load of the apartment is 4270w.

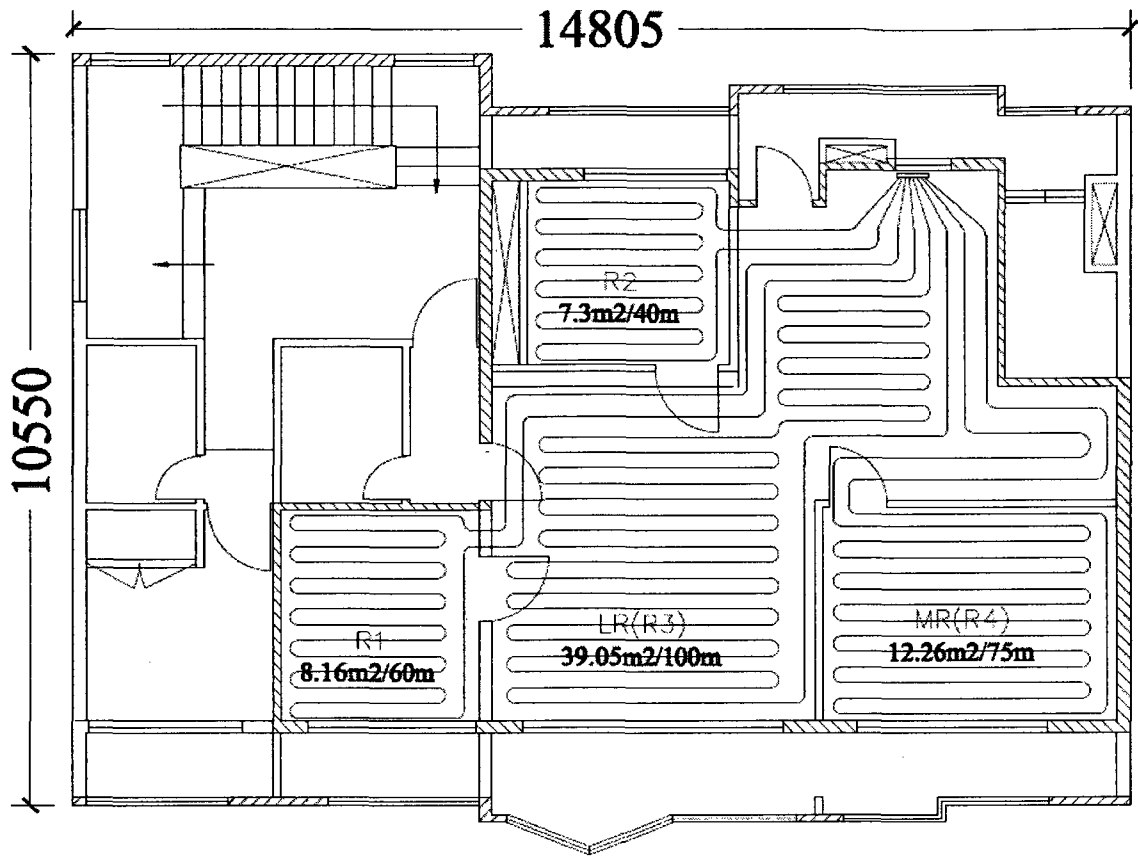


Figure 3.6.1 Plan view of the 4-zone apartment with RFH system

3.6.1 Nodes in the multi-zone RFH system

By assuming the air mass in each zone, including the unheated zone, as well mixed, 5 air temperature nodal equations were used to describe the four zone RFH system model. In addition, the model equations for walls and slab remain the same as in the single zone RFH system model. However, the difference between the single zone RFH model and multi-zone RFH model is that, in multi-zone model, the supply water temperature to all the zones is the same, the heat transfer by conduction between the zones through walls will be considered and the return water from 4 loops is first mixed and then sent back to the boiler. The design condition is such that the water temperature difference between the

supply water to the apartment and return water from the apartment is 10°C instead of 15°C in the single zone RFH system model. The boiler capacity for the apartment is 8000w. In summary, there are 463 nodes in this multi-zone RFH system model. The dynamic equation for the air node of unheated zone and for the return water temperature can be written as follows:

$$\frac{dT_{znh}}{dt} = Q_{z1} + Q_{z2} + Q_{z3} + Q_{z4} - Q_{nh_o} - Q_{inf_nh} + Q_{sols} + Q_{int_nh} \quad (3.6.1)$$

$$\frac{dT_r}{dt} = T_r - \frac{u_{w1}m_{w1}T_{r1} + u_{w2}m_{w2}T_{r2} + u_{w3}m_{w3}T_{r3} + u_{w4}m_{w4}T_{r4}}{u_{w1}m_{w1} + u_{w2}m_{w2} + u_{w3}m_{w3} + u_{w4}m_{w4}} \quad (3.6.2)$$

Where $Q_{z1}, Q_{z2}, Q_{z3}, Q_{z4}$ are the total heat transfer from zone 1, zone 2, zone 3 and

zone 4 to the unheated zone by conduction respectively, including heat transfer from walls, windows and doors, w.

Q_{nh_o} is the heat transfer from unheated area to outside by conduction, w.

Q_{inf_nh} is the heat loss by infiltration, w.

Q_{int_nh} is the internal heat gains of unheated zone, w.

T_r is the return water temperature from the apartment, °C.

$T_{r1}, T_{r2}, T_{r3}, T_{r4}$ is the return water temperature from each loop respectively, °C.

$u_{w1}, u_{w2}, u_{w3}, u_{w4}$ is the control signal of water flow rate in each

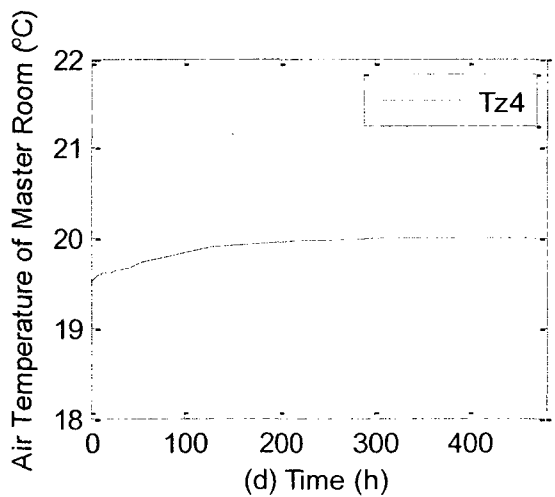
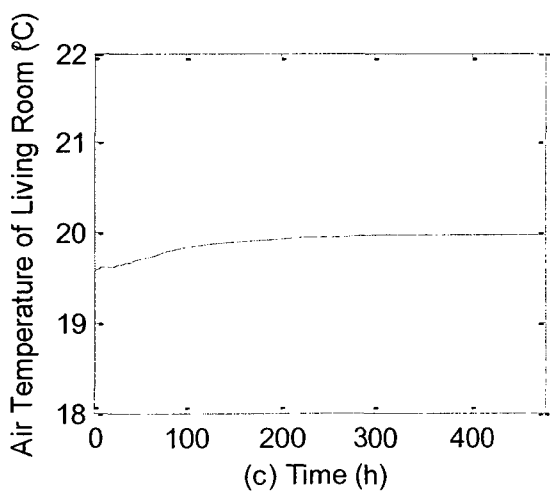
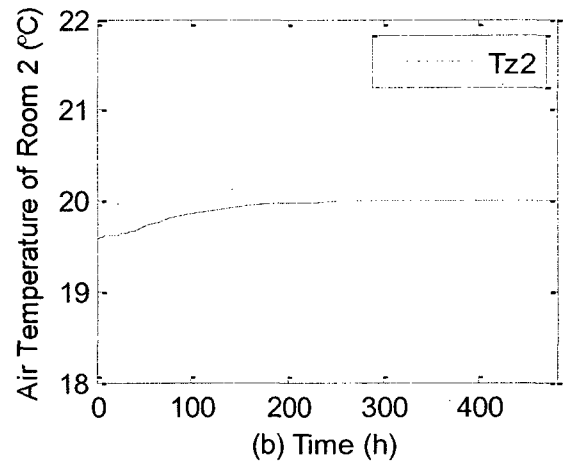
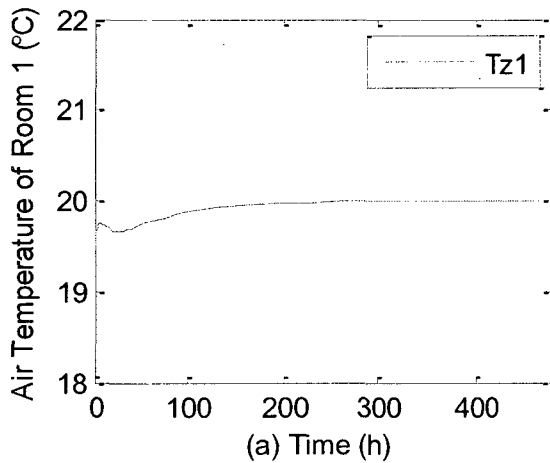
loop respectively.

$m_{w1}, m_{w2}, m_{w3}, m_{w4}$ is the design water mass flow rate in each loop respectively,

Kg/s.

3.6.2 Simulation results of multi-zone model under design condition

From Figure 3.6.1, we can see that the water-tube loops for room 1, room 2 and master room have to go through living room first, which would obtain some heat from the loops, and then get into room 1, room 2 and master room respectively. Therefore, we have to balance the water mass flow rate for all the tube loops. By adjusting the mass flow rate in each loop and running the MATLAB programming, the zone air temperature, water temperature, and unheated zone air temperature response as a function time is plotted in the following figures.



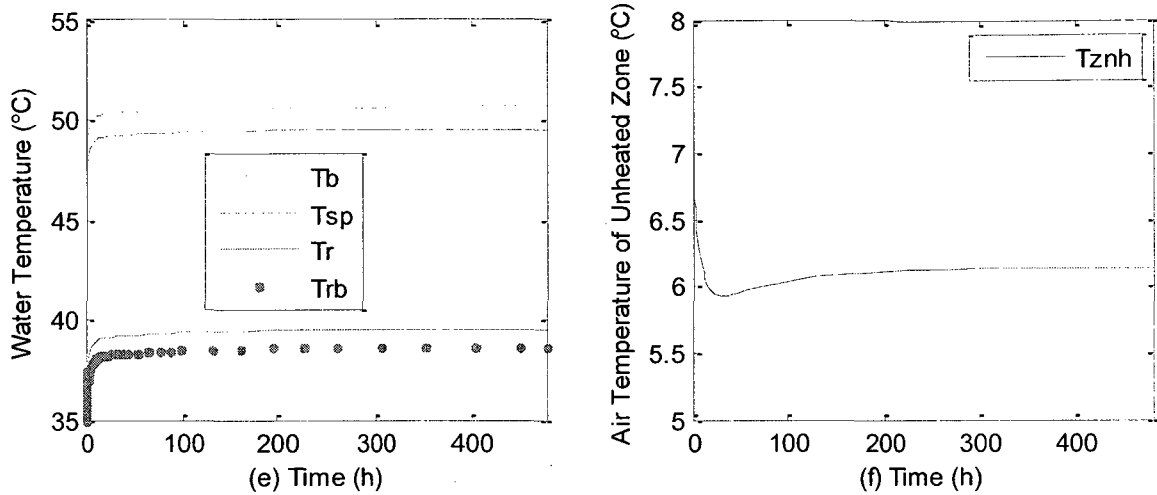


Figure 3.6.2 Simulation results of multi-zone model under design condition

From Figure 3.6.2, we can see that the system could reach near steady state after about 100-150 hours. Under the steady state, the air temperature of the heated zones is about 20°C, the unheated zone air temperature is about 6.1°C, and the water temperature difference between supply water to the apartment and return water from the apartment is about 10°C.

Several simulation runs were made, by changing outside air temperature and the rate of gas combustion in the boiler to determine the air temperature T_z in each zone, supply water temperature T_{sp} to the apartment, and return water temperature T_r from the zone.

The results are summarised in Table 3.6.1.

Outside air temperature T_o (°C)	Control signal u_f of boiler %	Zone air temperature (°C)					Water temperature °C	
		Room 1	Room 2	Living room	Master room	Unheated zone	supply	return
-15	67.113	20.01	20.01	19.99	20.00	6.14	49.50	39.50
-10	57.97	20.00	20.02	20.01	20.02	8.13	45.39	36.83
-5	48.89	19.98	20.01	20.01	20.01	10.10	41.24	34.10
0	39.92	19.96	20.00	20.00	20.01	12.08	37.06	31.35
5	31.09	19.95	20.01	20.01	20.01	14.06	32.87	28.59
10	22.36	19.95	20.00	20.01	20.01	16.04	28.65	25.79

Table 3.6.1 Simulation results of open loop test of multi-zone RFH system

Besides, from the simulation results, the relationship between the boiler control signal and outside air temperature, water temperature and outside air temperature in the multi-zone is plotted in Figure 3.6.3.

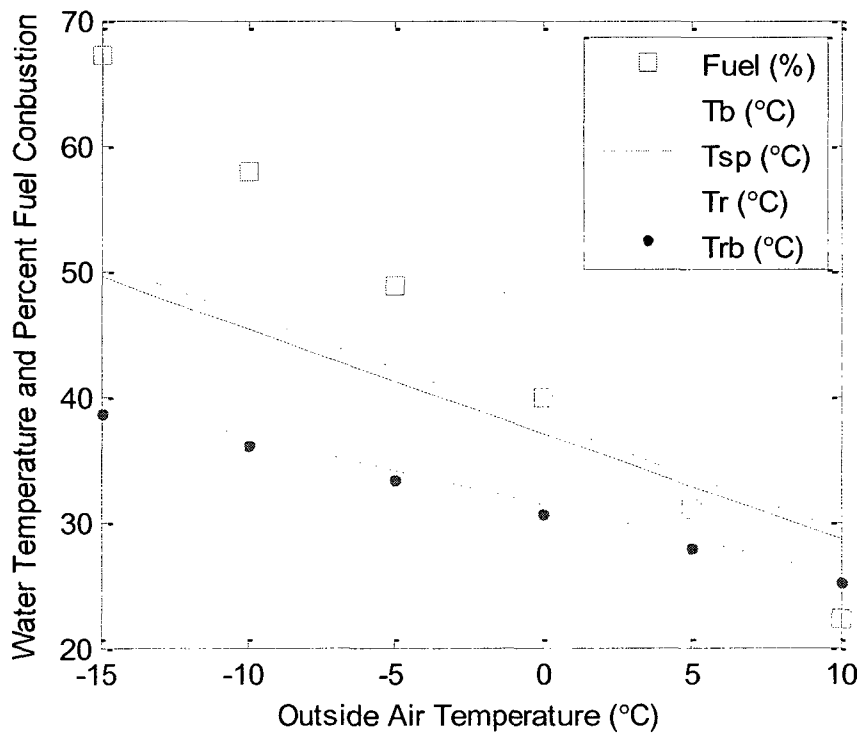


Figure 3.6.3 Open-loop test of the multi-zone model

From above figure, it can be seen clearly that the fuel combustion rate is linear function of outside air temperature. The temperature trends are similar to those discussed in the single zone RFH system.

3.7 Summary

The dynamic model for RFH system, which focuses on calculating the floor slab surface temperature distribution, temperature distribution in floor slab and zone air temperature, etc., has been built. The model was applied to a single zone and multi-zone RFH systems respectively. From the simulation results, it was noted that maximum surface temperature does not exceed 29°C under design condition. Meanwhile, the maximum floor slab surface temperature difference is less than 4°C.

In addition, to study the zone air temperature distribution in the room with RFH system, a zonal model was developed. The simulation results show maximum temperature variation of 1.6°C in the zone.

By carrying out open loop simulation runs of single zone and multi-zone RFH system, it was possible to show functional relationship between boiler temperature, return water temperature and outdoor air temperature. The simulation results for both single zone and multi-zone RFH systems are useful in determining potential operating set-point of RFH system as a function of outdoor air temperature.

CHAPTER 4

Control Strategies for RFH System

4.1 Introduction

In this chapter, before applying any control strategies on RFH system, the impact of the fluctuating outside air temperature, solar radiation and internal heat gains on the RFH system would be examined. Then, the conventional suitably-tuned PI (proportional plus integral) control, which is expected to improve the temperature regulation performance of the RFH systems, will be applied to the single zone and multi-zone RFH system developed in Chapter 3. Although PI controllers are much more expensive than on/off controllers, from references [11] (1999) and [8] (1997), PI controllers have a much better temperature regulation performance than on/off control. The objective of this chapter is to study the closed loop performance of conventional PI control, in which the set-point of boiler water temperature is constant, which is an effective base case control strategy. In the later chapters, improved control strategies will be proposed and their performance will be compared with the base case PI control strategy.

4.2 The impact of load disturbances on the single zone RFH system

The disturbances on RFH system mainly include outside air temperature, solar radiation gain and internal heat gain. Actually, heating design is based on the worst situation when the outside air temperature reaches the lowest point in winter, and there is no solar gain and no internal heat production. However, the outdoor air temperature is always higher

than the outside air design temperature, and the heating space could get some solar radiation gain and internal heat gain. As a result, the zone air temperature is always higher than the design air temperature if there is no zone air temperature control, which not only wastes energy, but also it may make occupants feel uncomfortable.

To carry out simulation runs, predicted outdoor air temperatures were used. The outdoor air temperatures over a 24-hour period were predicted using the equations given in reference [10]. The inputs to the model are the expected maximum (T_h) and minimum (T_m) temperatures and their time-of-day occurrence (t_{high}, t_{low}) respectively.

$$t \leq t_{low}, \quad T_o = T_v - T_d \cos\left[\left(\frac{\pi}{24 - (t_{high} - t_{low})}\right)(t - t_{low})\right] \quad (4.2.1)$$

$$t_{low} < t \leq t_{high}, \quad T_o = T_v - T_d \cos\left[\left(\frac{\pi}{t_{high} - t_{low}}\right)(t - t_{low})\right] \quad (4.2.2)$$

$$t > t_{high}, \quad T_o = T_v + T_d \cos\left[\left(\frac{\pi}{24 - (t_{high} - t_{low})}\right)(t - t_{high})\right] \quad (4.2.3)$$

$$\text{Where, } T_v = \frac{T_{high} + T_{low}}{2}, \quad \text{and} \quad T_d = \frac{T_{high} - T_{low}}{2}$$

Assuming a maximum temperature of 0°C at 13:00, and a minimum temperature is -10°C at 5:00, the predicted outdoor air temperature using equations 4.2.1-4.2.3 is plotted in Figure 4.2.1.

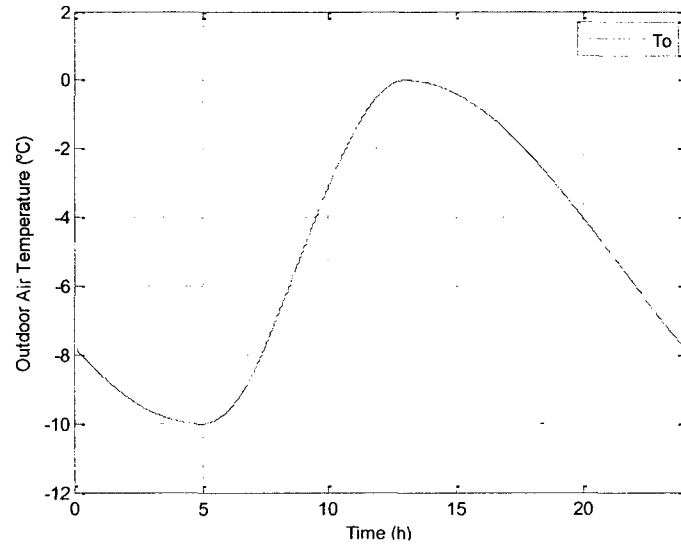


Figure 4.2.1 Predicted outdoor air temperature

By selecting $U_f = 0.53$ according to Figure 3.4.5 and Table 3.4.1, the responses of single zone RFH system without any control and subjected to the predicted daily outdoor air temperature profile shown in Figure 4.2.1 were studied. The results are plotted in Figure 4.2.2.

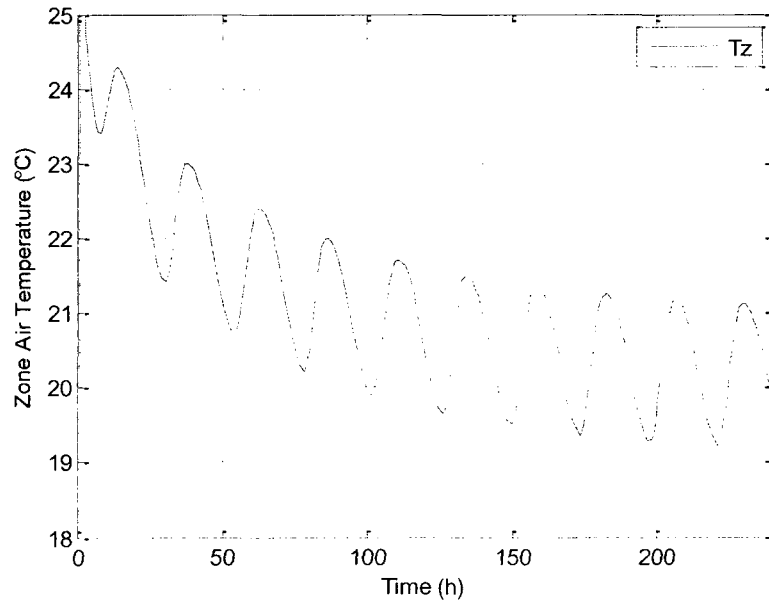


Figure 4.2.2 Predicted zone air temperature under predicted outside air temperature

Simulation runs conducted over 10 consecutive days until the periodic steady state was achieved. Under steady state condition, the zone air temperature fluctuates between 19.2°C and 21.2°C without any control. These fluctuations will increase if the solar radiation and internal heat generation are added to the single zone RFH system.

4.3 Closed loop PI control responses of the single zone RFH system

Usually, there are three methods to control a RFH system, which are: (i) by controlling only the supply water temperature, (ii) by controlling only the supply water mass flow rate, and (iii) by controlling the supply water temperature and supply water mass flow rate at the same time. In the conventional PI control method, both the temperature and the mass flow rate of supply water are controlled. Both set-points for supply water temperature and zone air temperature are constant and there are two thermostats, one measuring the temperature of boiler water and the other measuring the zone air temperature. The error between the real boiler water temperature and the boiler water temperature set-point is used to control the combustion rate U_w of natural gas and the signal from the error between the real zone air temperature and the zone air temperature set-point is used to control the water mass flow rate U_w , which is depicted in Figure 4.3.1.

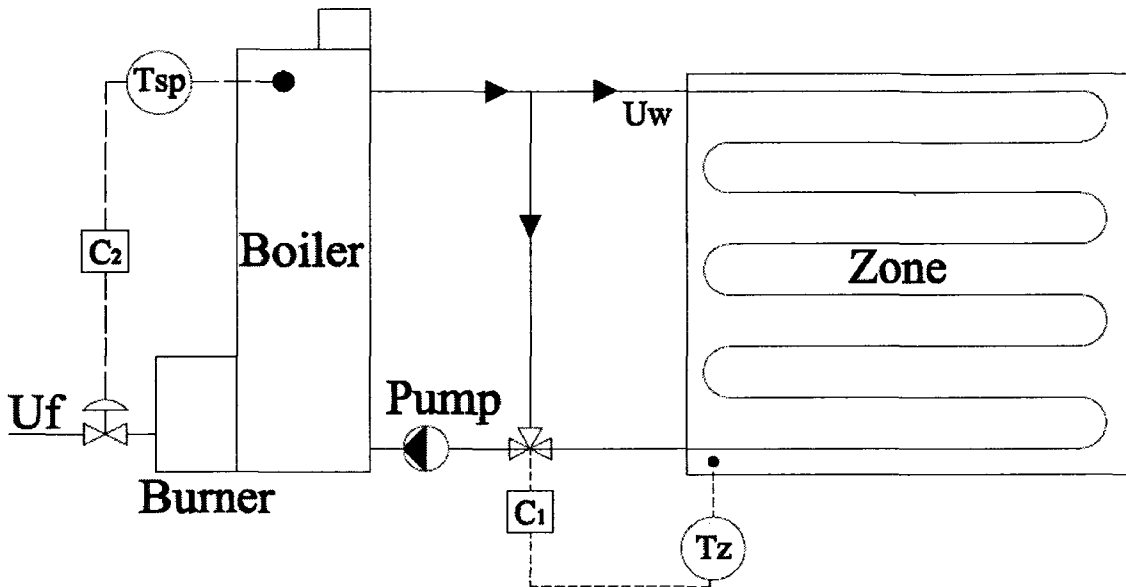


Figure 4.3.1 Control inputs for single zone RHF system

In Figure 4.3.1, zone air temperature T_z and boiler water temperature T_b are the outputs, and water flow rate U_w and natural gas combustion rate U_f are the inputs. If the zone air temperature is under the set-point, the mass flow rate of water is increased via the three-way valve controller C_1 . Simultaneously, the controller C_2 adjusts the gas burning rate in the burner such that the boiler water temperature would maintain at the chosen set-point. Figure 4.3.2 and Figure 4.3.3 describe the closed-loop control diagrams.

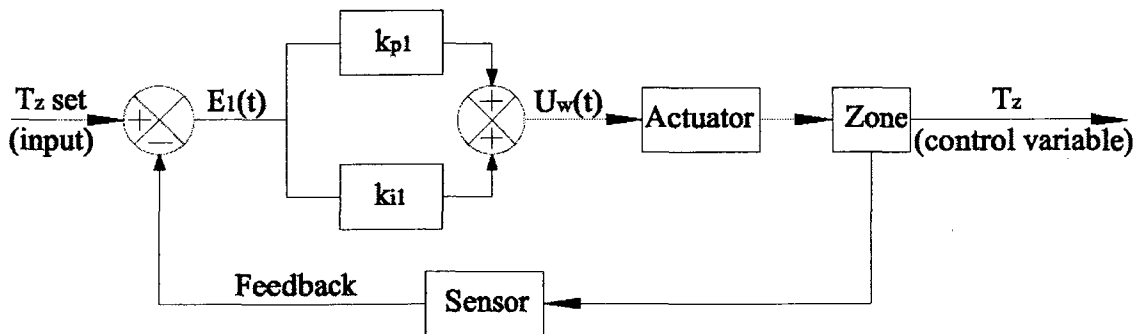


Figure 4.3.2 PI controller block diagram with zone air temperature feedback

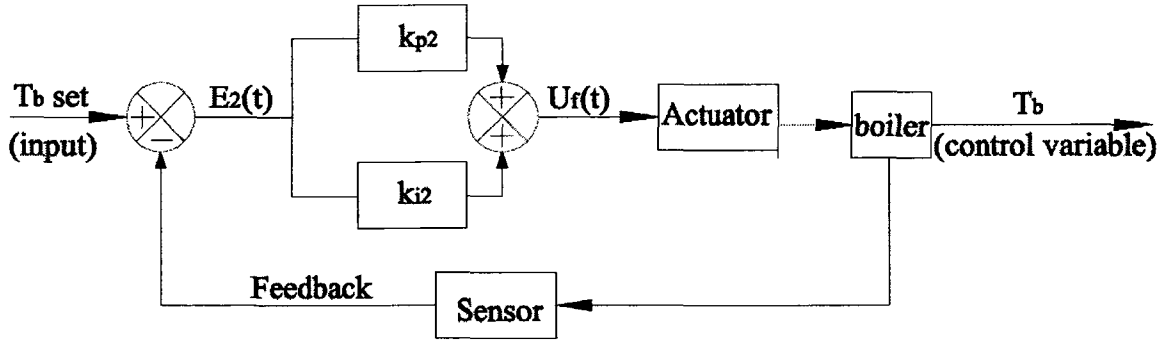


Figure 4.3.3 PI controller block diagram with boiler water temperature feedback

The PI control equations for Figure 4.3.2 and 4.3.3 are described below:

$$E_1(t) = T_{zset} - T_z \quad (4.3.1)$$

$$U_w(t) = k_{p1}E_1(t) + k_{i1} \int_0^t E_1(t)dt \quad (4.3.2)$$

$$E_2(t) = T_{bset} - T_b \quad (4.3.3)$$

$$U_f(t) = k_{p2}E_2(t) + k_{i2} \int_0^t E_2(t)dt \quad (4.3.4)$$

Where, k_p is the proportional gain and k_i is the integral gain, and T_{zset}, T_{bset} are the set-point of zone air temperature and boiler water temperature respectively. In the simulations, $T_{zset} = 20^\circ\text{C}$ and $T_{bset} = 60^\circ\text{C}$ were assumed.

The following set of controller gains $k_{p1} = 1, k_{i1} = 0.00333, k_{p2} = 0.03, k_{i2} = 0.00001$, which were obtained with a few trials, gave acceptable set-point tracking responses. Temperature responses subject to step change in outdoor air temperature from -10°C to -15°C are depicted in Figure 4.3.4.

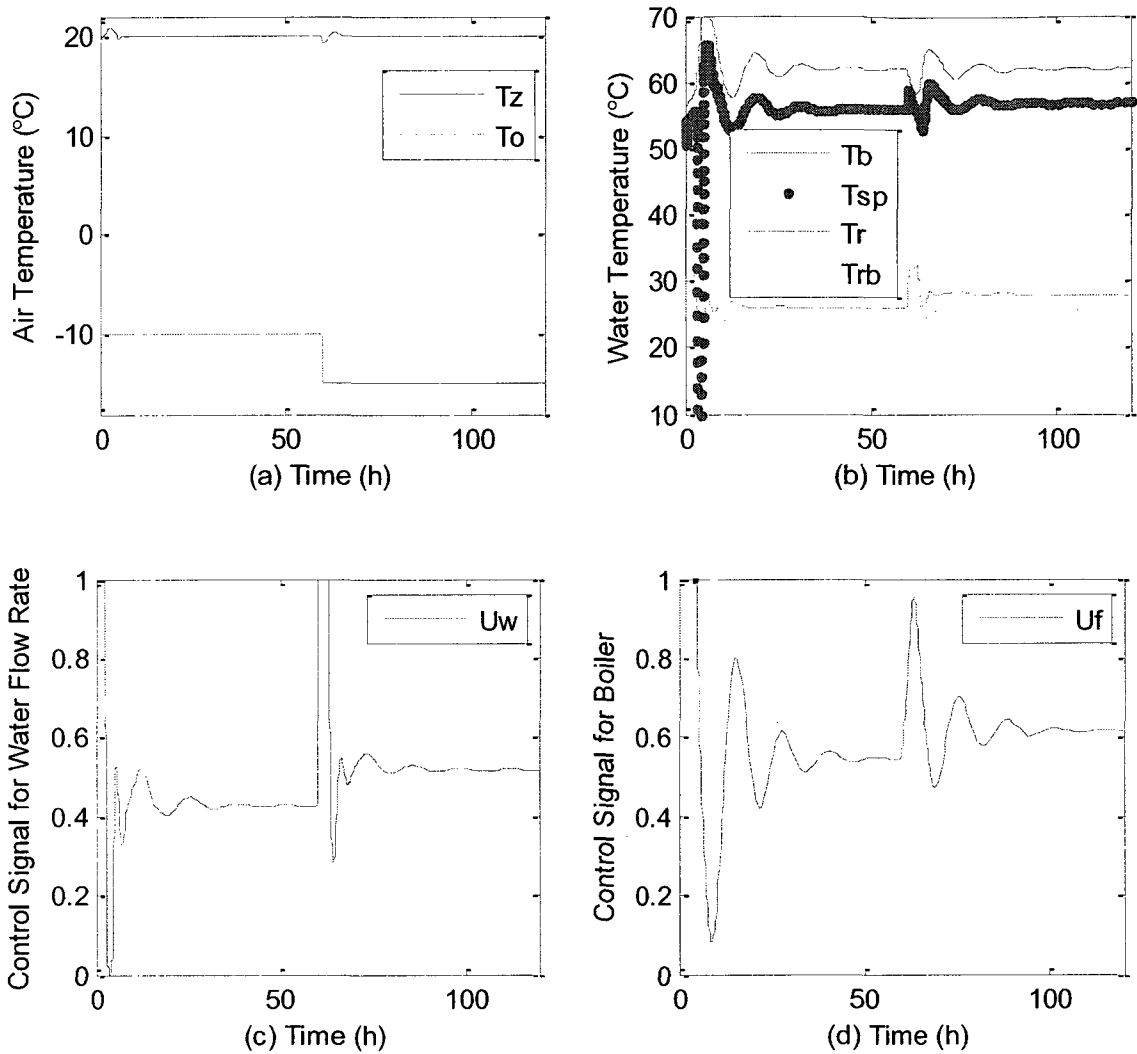


Figure 4.3.4 Validation of the constant gain values of PI controllers
for single zone RFH system

From Figure 4.3.4 (b), (c), (d), it can be clearly seen that the single zone RFH system responses converge and reach stable steady state. When the outside air temperature decreases from -10°C to -15°C , it takes the system about 10hrs to reach a new steady state. Since the outside air temperature decreases, the heating load increases correspondingly, this is shown in Figures (c), (d), in which the water mass flow rate and

gas burning rate increases. Most importantly, in both cases, the zone air temperature is held close to the set-point 20°C over the entire simulation period.

4.4 Closed-loop PI control of the multi-zone RFH system

Unlike the single zone, there are 5 PI controllers in multi-zone RFH system, one of which is used to control the gas burning rate, and the rest are used to control the water mass flow rate in water loop. Figure 4.4.1 shows the PI control loops of multi-zone RFH system.

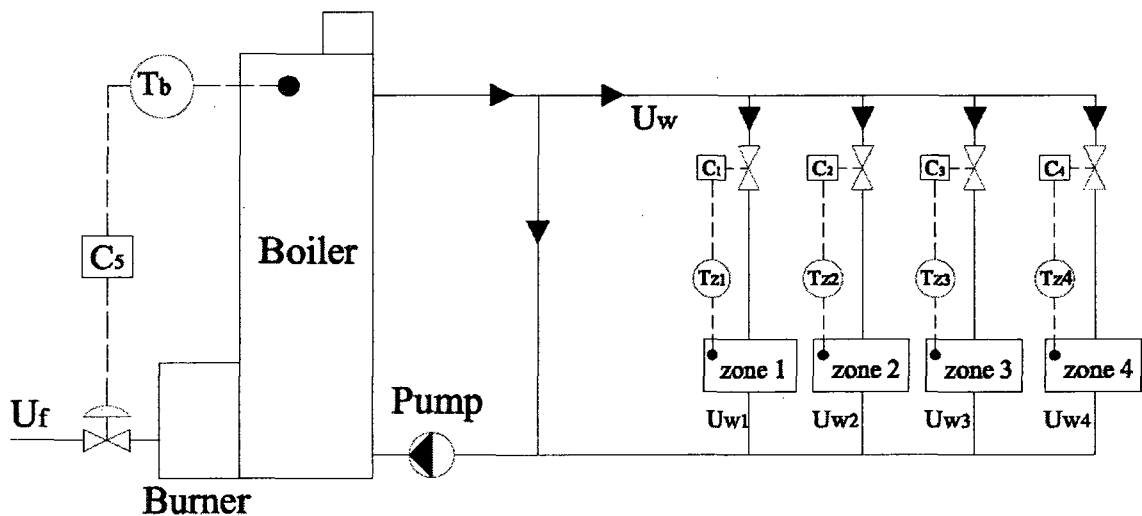
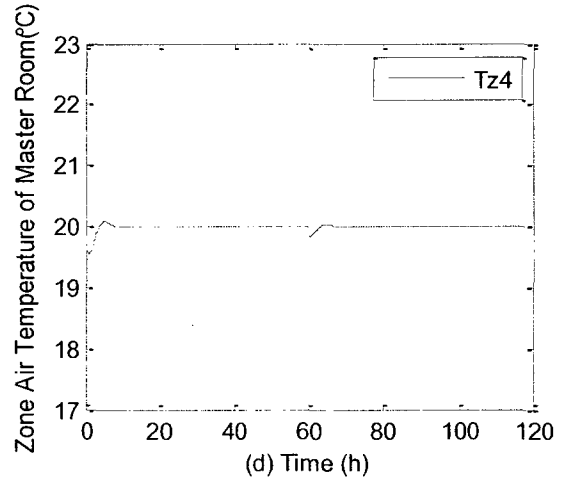
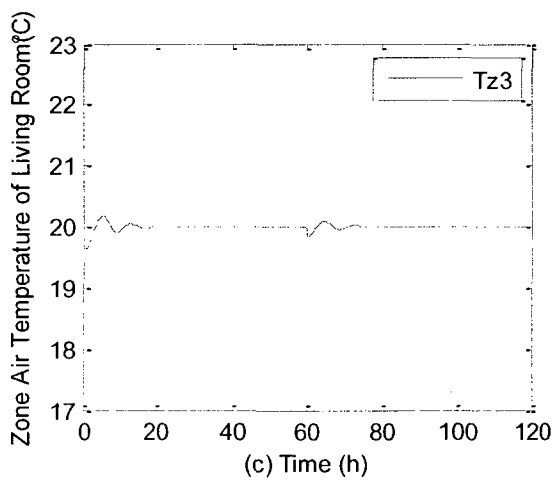
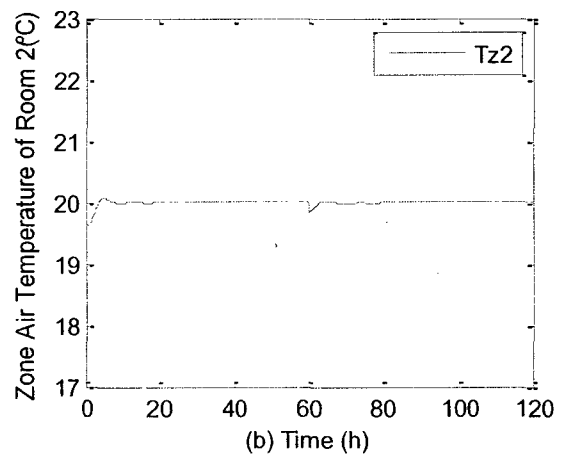
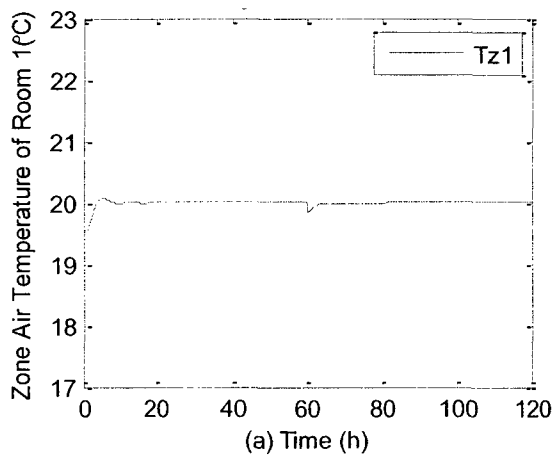


Figure 4.4.1 Control inputs for multi-zone RHF system

As stated previously, in the multi-zone RFH system depicted in Figure 3.5.1, the indoor air temperature of living room is affected by the flow rate in water loops 1, 2, 3 and 4. Therefore, the control is much more complex in this kind of multi-zone system than the multi-zone where each controller controls each zone separately.

By trial and error sets of controller gains which gave better performance were chosen. These are $k_{p1} = 0.5$, $k_{i1} = 0.0001$, $k_{p2} = 1$, $k_{i2} = 0.0002$, $k_{p3} = 1$, $k_{i3} = 0.0004$, $k_{p4} = 1$, $k_{i4} = 0.0002$, $k_{p5} = 0.2$, $k_{i5} = 0.00003$. Using these values, temperature responses of the system subjected to step change in outdoor air temperature from -10°C to -15°C were obtained. They are shown in Figure 4.4.2.



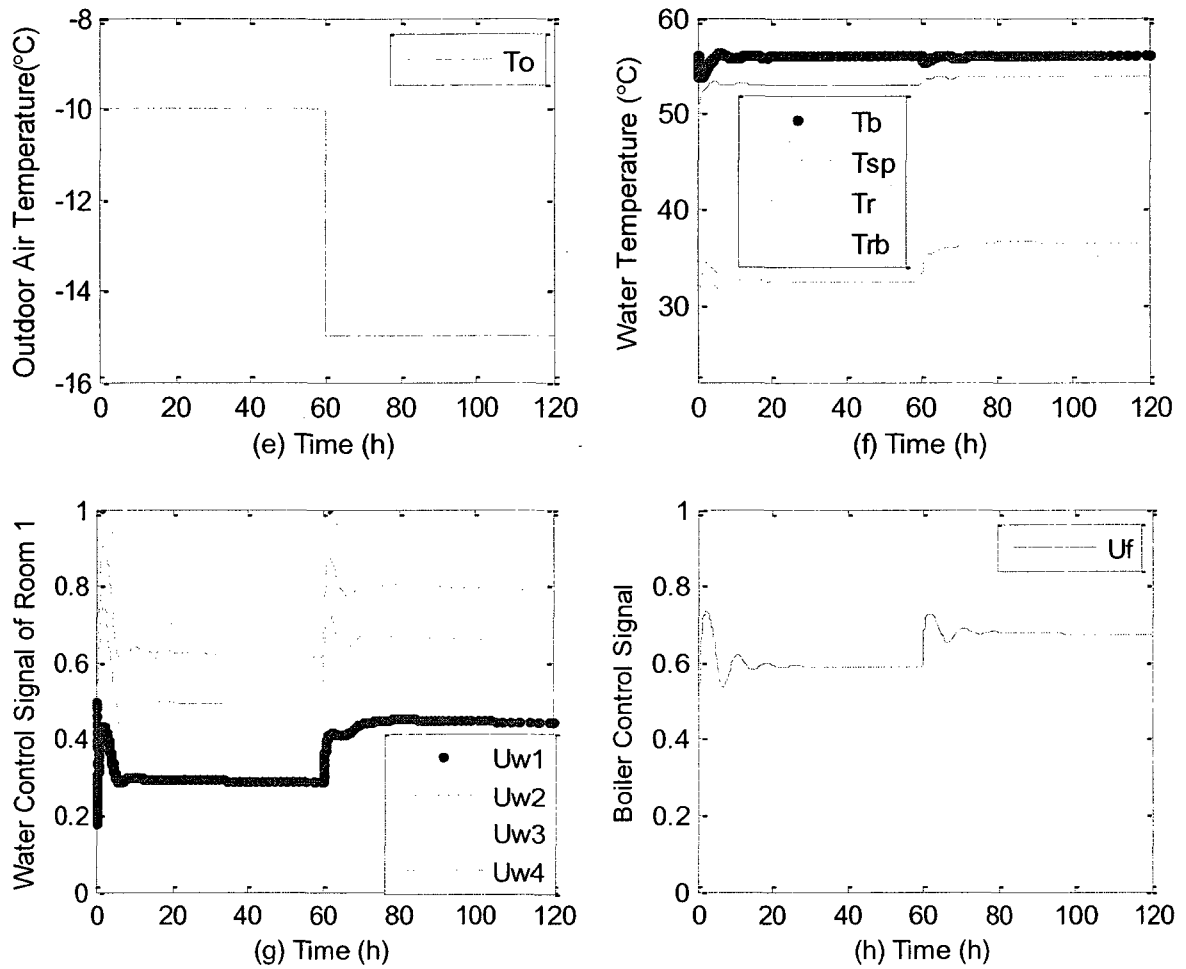
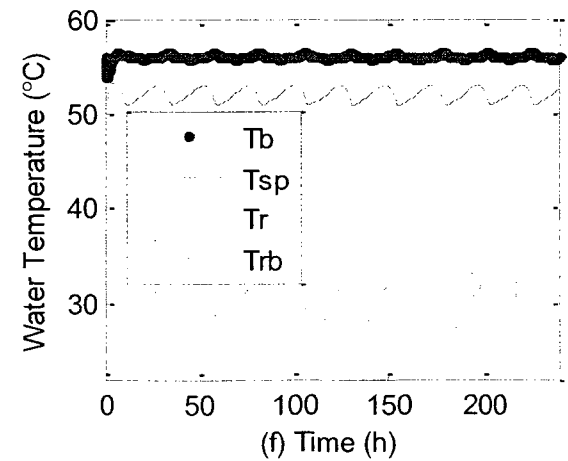
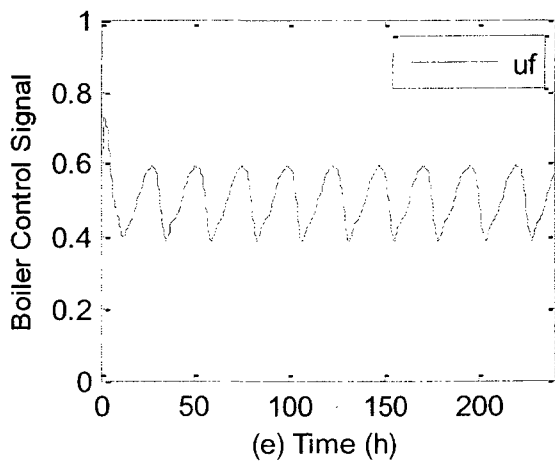
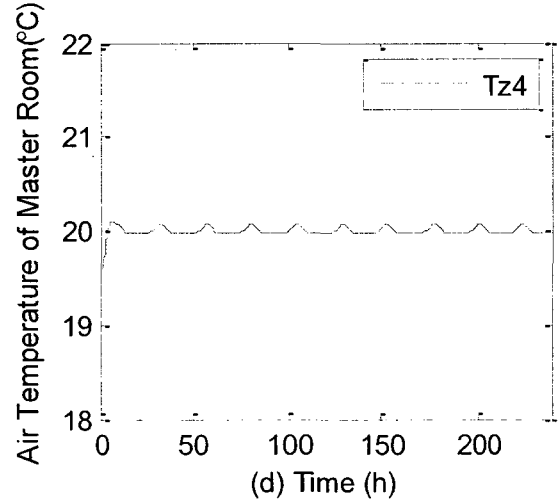
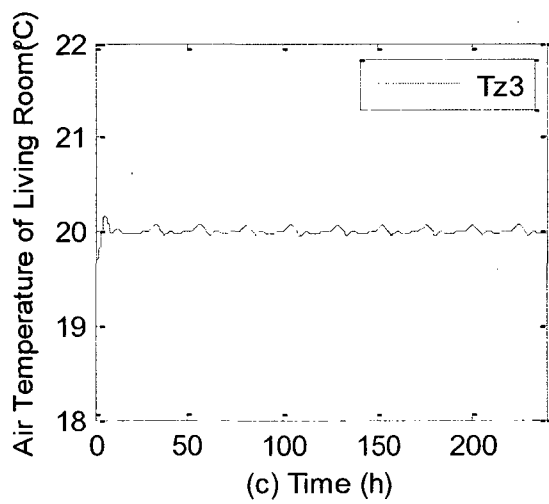
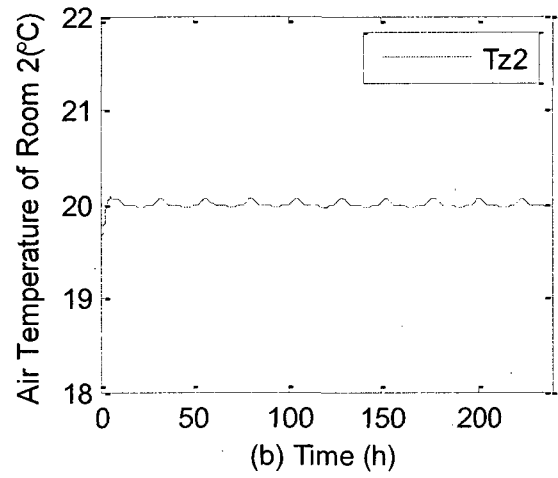
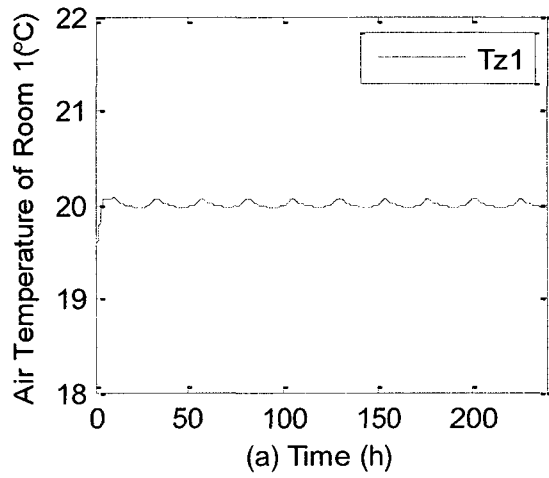


Figure 4.4.2 Validation of the constant gain values of PI controllers
for multi-zone RFH system

Figure 4.4.2 (f), (g) and (h) show that the multi-zone RFH system reaches stable state in less than 10hrs. Figure 4.4.2 (h) also shows that, to keep the zone air temperature around the set-point, more fuel is required when outside air temperature decreases. The constant gain values of the PI controllers for multi-zone RFH system are valid and yield better results. Simulation runs were conducted over a longer period by using outdoor air temperature profile shown in Figure 4.2.1. The results depicted in Figure 4.4.3 show that all zone temperatures are maintained close to the set-point and system responses remain

stable. This validates the stability of constant gain PI controllers as applied to the multi-zone RFH system and 4.4.3 (a)-(j) are the dynamic responses of zone air temperature, water temperature, water flow rate and gas burning rate of the multi-zone RFH system.



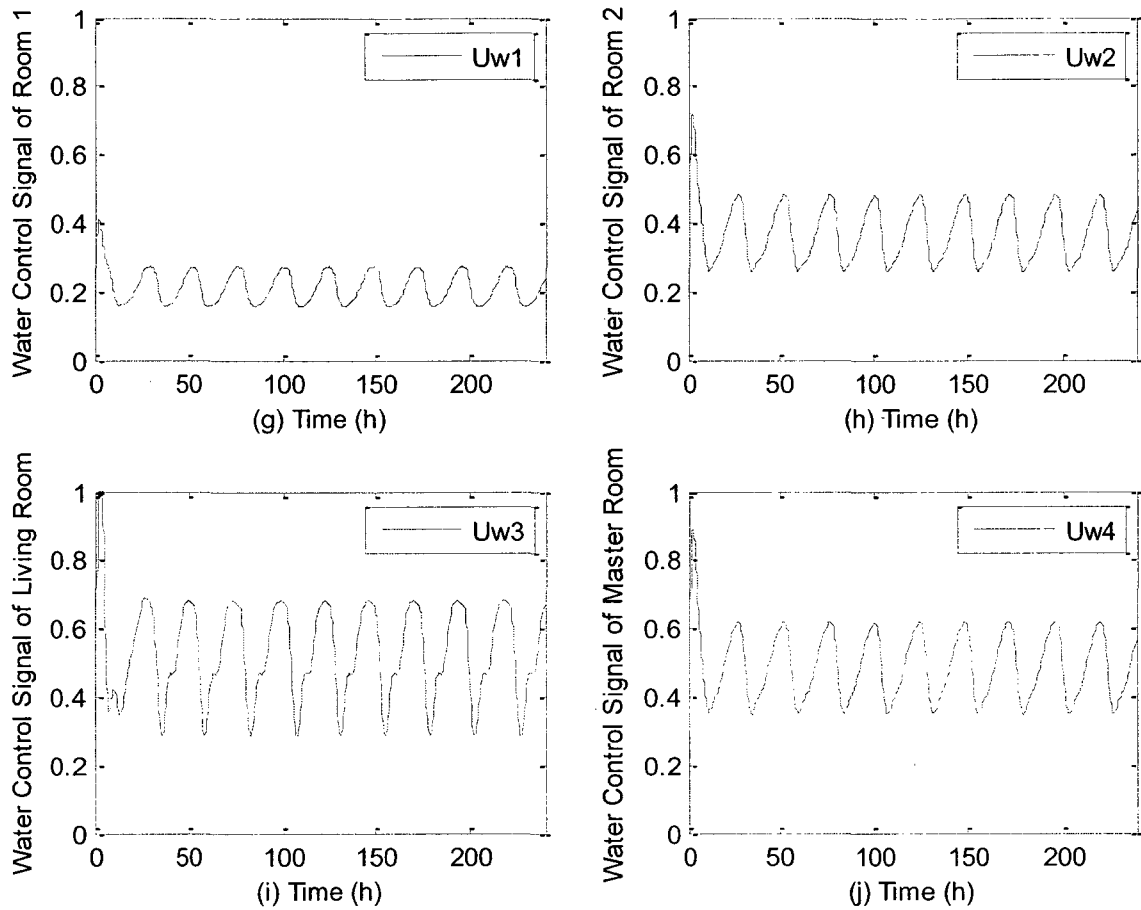


Figure 4.4.3 Simulation results of multi-zone RFH system under conventional PI control (only the disturbance of outside air temperature is considered)

It is apparent from Figure 4.4.3 (a), (b), (c) (d) that the zone air temperature in all the 4 rooms experiences a slight swing between 19.96°C and 20.08°C during the simulation period. It means that the PI controllers are able to regulate the zone air temperature well in this kind of complex multi-zone RFH system.

4.5 PI control of multi-zone RFH system under simulated operating condition

Multi-zone RFH system responses subject to variations in outdoor air temperature, variation in solar radiation gains and variation in internal heat gains were studied. The solar radiation intensity and assumed internal heat gain profiles are depicted in Figure 4.5.1 and Figure 4.5.2 respectively.

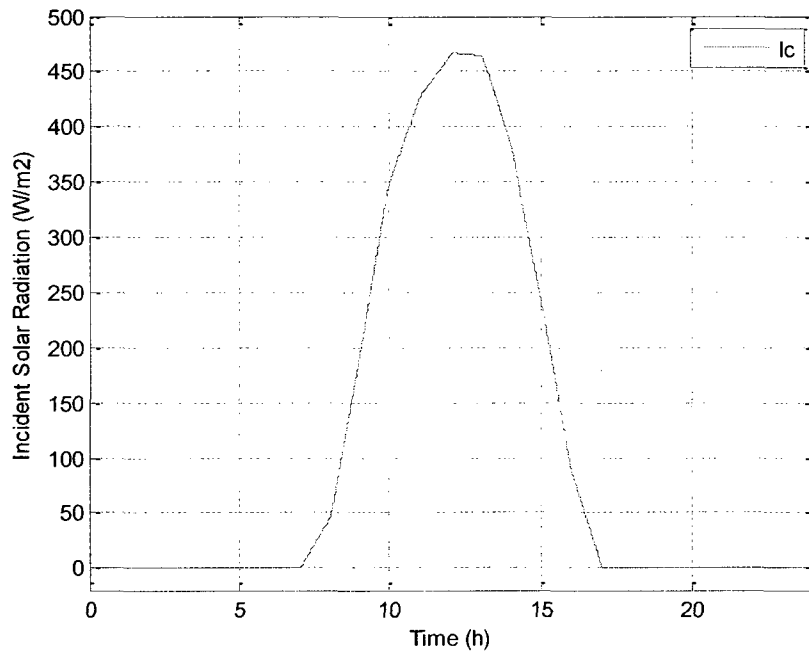


Figure 4.5.1 Incident Solar Radiation

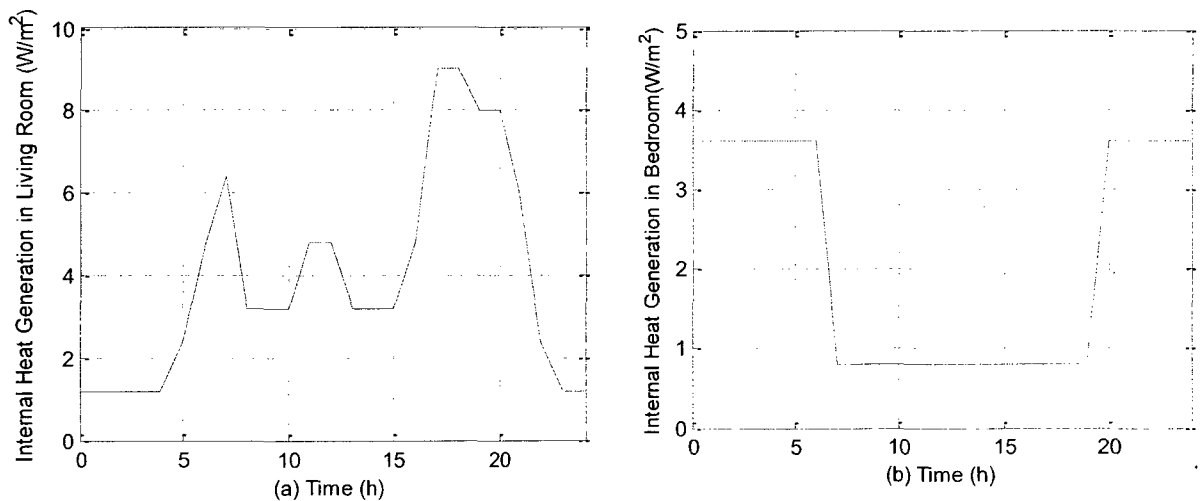
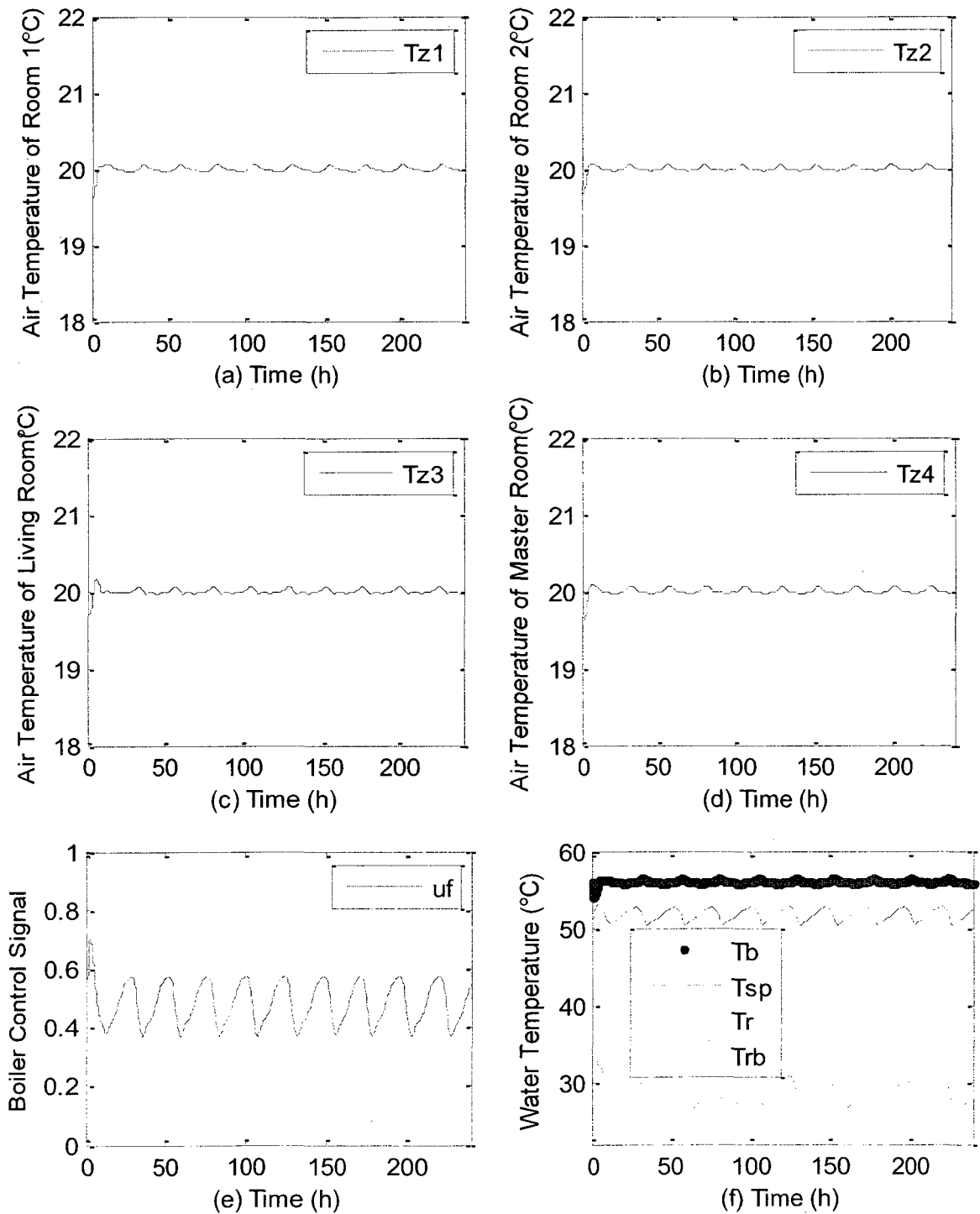


Figure 4.5.2 Internal heat gain

The simulation results with multiple disturbances acting on the multi-zone RFH system are depicted in Figure 4.5.3. Note that during these simulations, the same set of controller gains as those in Figure 4.4.2 were used.



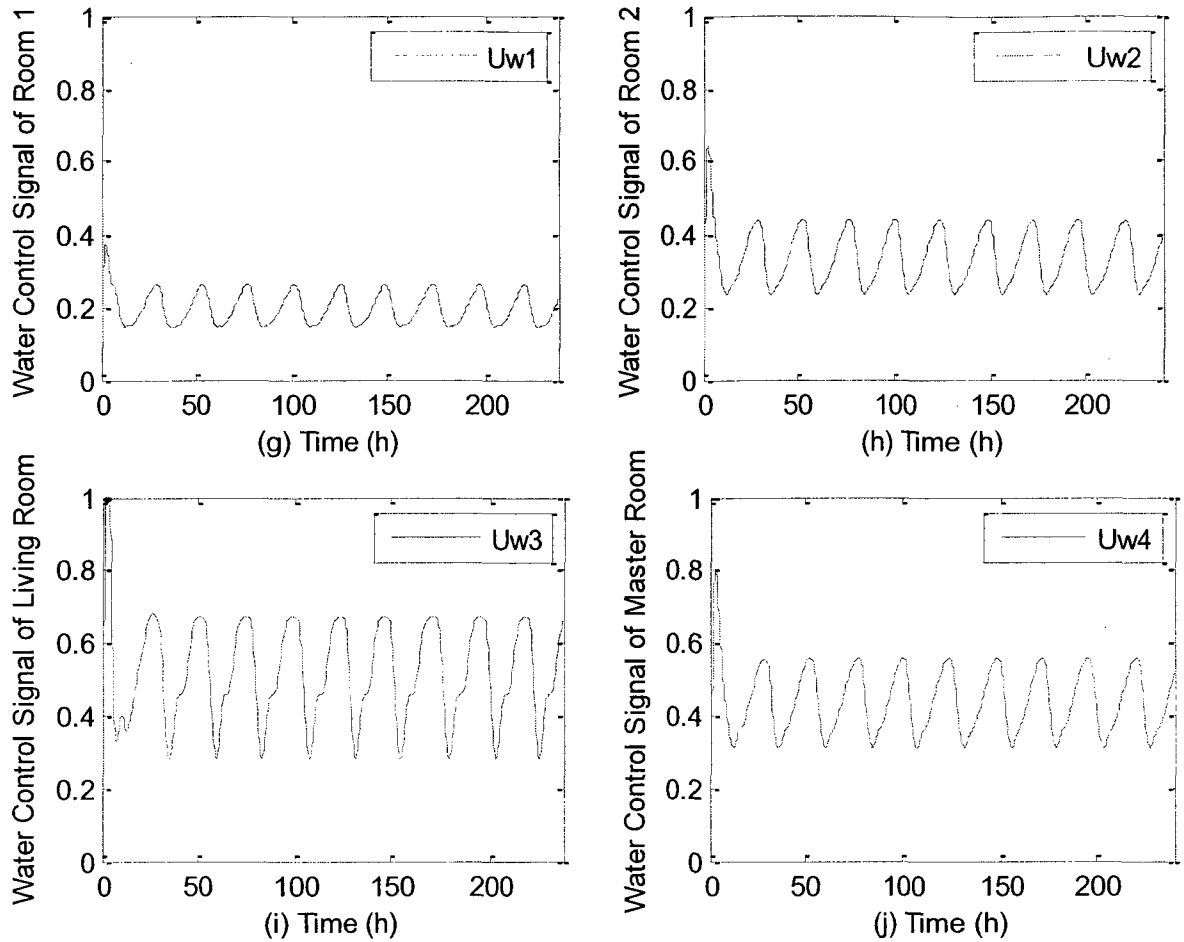


Figure 4.5.3 Simulation results of multi-zone RFH system under conventional PI control with multiple disturbances

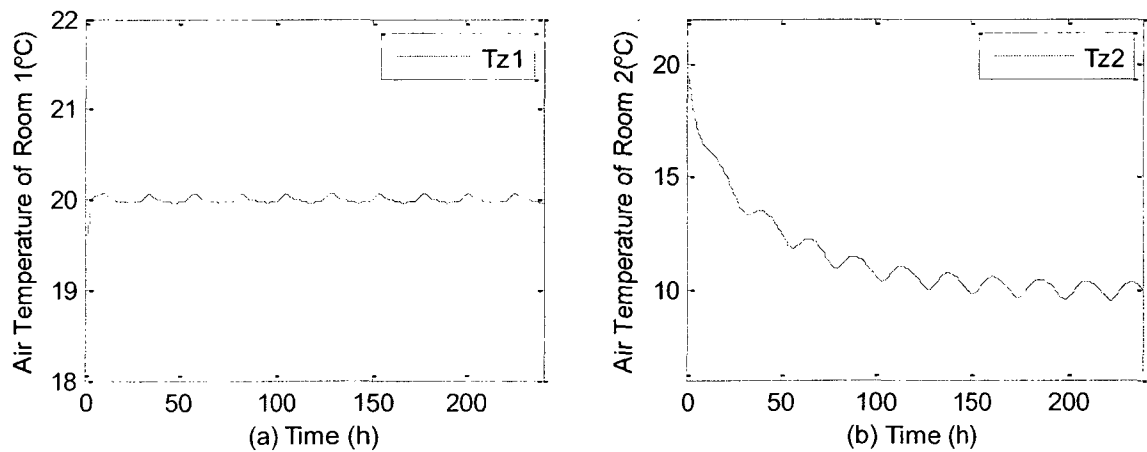
The Figure 4.5.3 shows that when all the disturbances, such as outside air temperature, solar radiation gain and internal heat gain, are acting simultaneously on the multi-zone RFH system, the controllers were able to maintain the indoor air temperature of all the 4 zone between 19.96°C and 20.07°C , which can be considered as acceptable performance. Compared to Figure 4.4.3, the only apparent difference is that the gas burning rate is a little smaller with internal heat gains and solar radiation gain than without as it should be. The energy consumption during the simulation period was $34.7444 \times 10^2 \text{ MJ}$ with internal

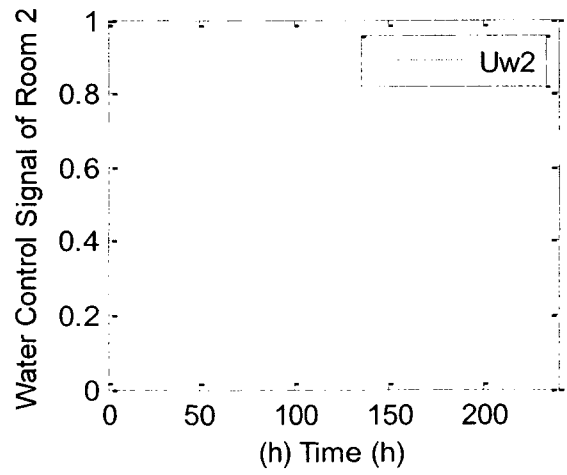
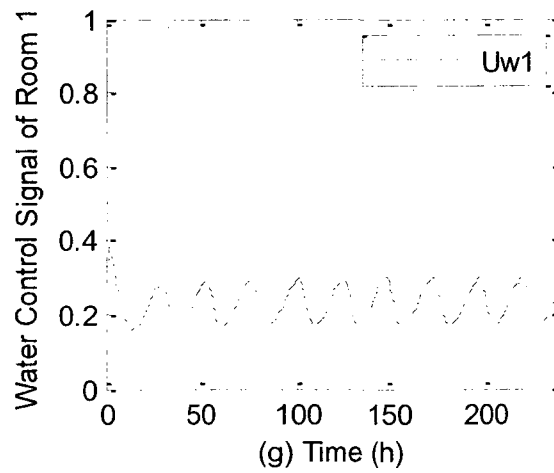
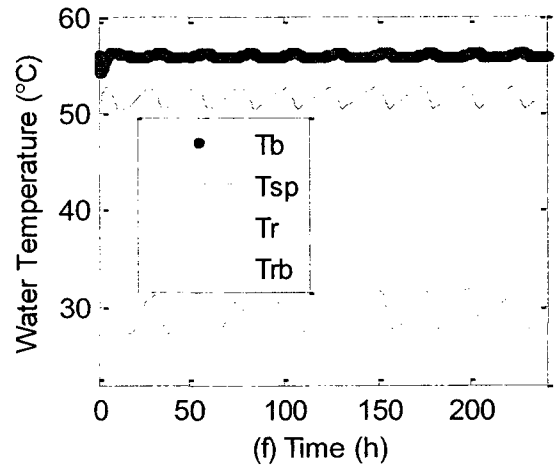
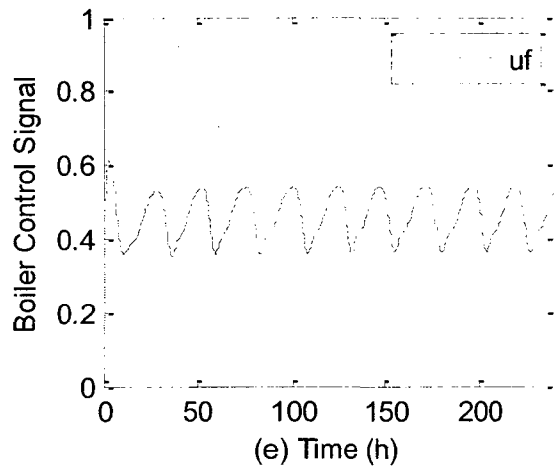
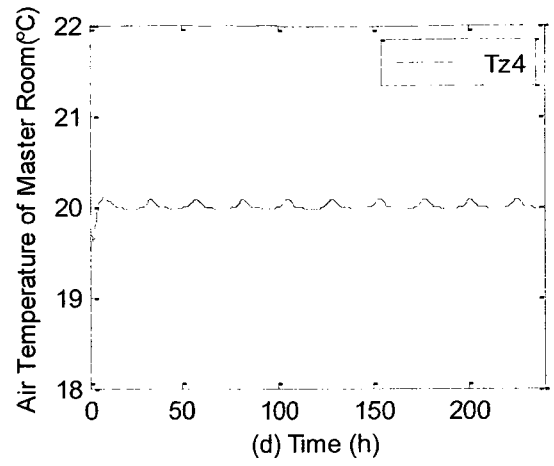
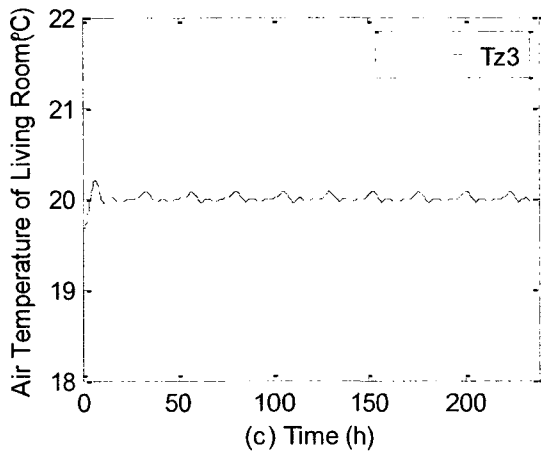
heat sources and solar radiation gains, compared to $39.0813 \times 10^2 \text{ MJ}$ without internal heat sources and solar radiation. The difference is contributed by the heat gain from solar radiation and internal heat generation.

4.6 Impact of one zone on the other zones under conventional PI control

Usually, it is a very common situation that there are no occupants in one of the rooms in an apartment. As a result, the indoor air temperature in that room is lowered to save energy. However, lowering the thermostat setting in one room could affect the temperature in the other rooms. Therefore, the objective of this section is to check whether the other zones are significantly affected or not when the indoor air temperature set-point of one zone in the apartment is reduced.

By assuming that the zone air temperature set-point of room 2 is lowered by shutting down water flow rate in closed loop 2, the simulation results corresponding to this condition are shown in Figure 4.6.1.





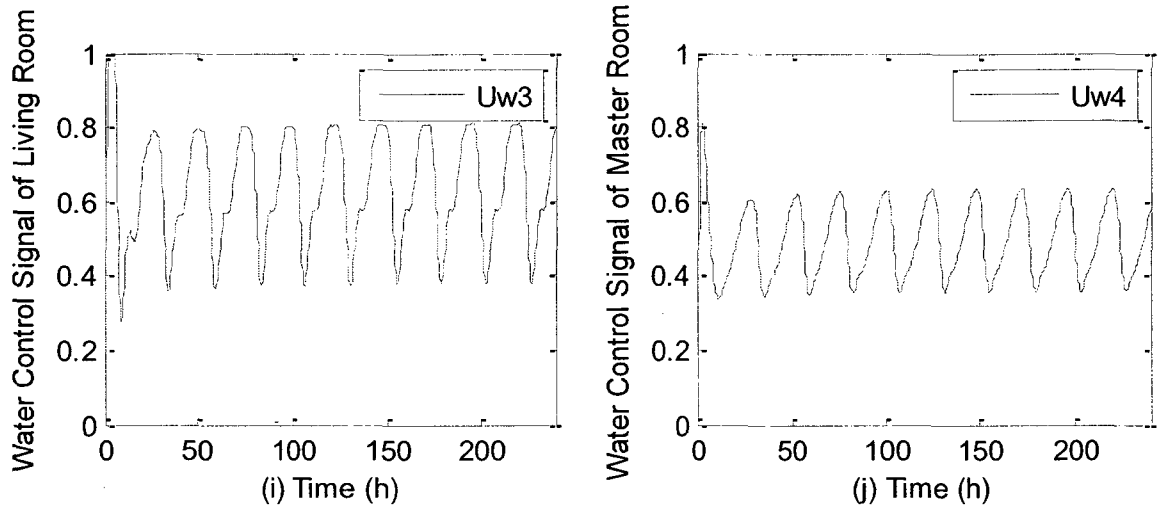


Figure 4.6.1 Simulation results of multi-zone under energy saving mode

From above figure, we can clearly see that the air temperature in room 1, living room and Master room could be maintained close to the set-point when the tube-loop 2 is shut down by PI controller because of the reduced thermostat set-point in zone 2. Since the flow rate in zone 2 is 0, the zone 2 air temperature decreases as shown in Figure 4.6.1 (b). In other words, the other zone air temperatures are not affected by stopping the circulation of water in the unoccupied zone. This resulted in an energy saving of 4.9%.

4.7 Summary

A conventional PI control strategy, which uses zone air temperature as a control signal to regulate the water mass flow rate and uses boiler water temperature as a control signal to regulate the gas-burning rate so as to maintain the boiler water temperature around the constant set-point, has been applied to the single zone RFH system and the multi-zone RFH system. The simulation results show that the zone air temperatures remain close to

the set-point (-0.05°C to 0.10°C) throughout the day. The control performance is acceptable.

Besides, when multiple disturbances, including the variation of outside air temperature, solar radiation and internal heat generation, are considered in the multi-zone RFH model, and the multi-zone RFH system is controlled by the same PI control strategy, the simulation results reveals that the temperature in all the 4 zones are maintained close to the set-point.

In addition, the base case PI control strategy has also been proved to be valid in compensating for the effects of change in thermostat set-point in one zone on the other zones. In other words, inter-zone effects are effectively compensated by the conventional PI control strategy.

From above, we could conclude that the conventional PI control strategy is a good control strategy for both single zone and multi-zone RHF system from the point of view of temperature regulation.

CHAPTER 5

Predictive PI Control strategy for RFH System

5.1 Introduction

An efficient control strategy for RFH system should include a good temperature regulation and high energy efficiency. In chapter 4, it was shown that PI control strategy is an excellent control strategy for temperature regulation in RFH system. The objective of this chapter is to seek some improvement, such as improving the energy efficiency and achieving a better temperature regulation using the PI control structure.

References [33] (2002) and reference [28] (1991) concluded that the use of variable supply water temperature as a function of outdoor air temperature instead of constant supply water temperature could achieve a good control performance. With this as a basis, a new predictive PI control strategy will be developed.

First, the predictive PI control strategy is described. The performance of zone air temperature regulation in both single zone and multi-zone zone RFH system under the predictive PI control strategy will be presented. Furthermore, the energy consumption of the predictive PI control strategy will be compared with the conventional PI control strategy.

5.2 Predictive PI control strategy

In the predictive control strategy, boiler water temperature set-point is not constant but it is predicted according to the variation of the outdoor air temperature. When the outdoor air temperature decreases, the supply water temperature will increase. In reverse, when the outdoor air temperature goes up, the supply water temperature will go down. That is where we believe the predictive control strategy will achieve a better performance. However, one area we need to figure out is how to determine the set-point scale as a function of the outdoor air temperature change. The predictive control technique is described by following steps:

1. According to the initial condition, calculate the heat transfer to the zone:

$$q_0 = U_w c_w m_w (T_{sp_0} - T_{r_0}) \quad (5.2.1)$$

Where, U_w is the average value of the signal of water flow rate, and T_{sp_0}, T_{r_0} are the initial values of water temperature being supplied to the radiant floor and water temperature return from the radiant floor respectively.

2. The heat transfer from the water to the zone at Δt seconds later is predicted as follows:

$$q_{pre} = q_0 - \theta_1 \cdot \eta \cdot q_0 \quad (5.2.2)$$

Where, θ_1 is the ratio of outdoor air temperature change during the first

Δt seconds, $\theta_1 = \frac{T_{o_1} - T_{o_0}}{\Delta t}$, and η is a weighting factor.

3. According to the predicted heat transfer obtained above, the predicted supply water temperature is computed from:

$$T_{sp_1} = T_{r_0} + \frac{q_{pre_1}}{u_w m_{wd} c_w}$$

(5.2.3)

4. Assuming the supply water temperature T_{sp} to be a linear function during the time period $[0, \Delta t]$ between T_{sp_0} and T_{sp_1} , solve the model equations for the simulation period Δt seconds and obtain the return water temperature T_{r_1} .
5. With the supply water temperature T_{sp_1} , return water temperature T_{r_1} , and outside air temperature change ratio during the second Δt time interval, predict the heat transfer and supply water temperature for the second Δt time step:

$$q_{pre_2} = q_1 - \theta_2 \cdot \eta \cdot q_1 \quad (5.2.4)$$

$$T_{sp_2} = T_{r_1} + \frac{q_{pre_2}}{U_w m_{wd} c_w} \quad (5.2.5)$$

6. Similarly, repeat the calculations to determine $T_{sp_3}, T_{sp_4}, T_{sp_5}, \dots$ as needed.
7. According to the supply water temperature series $T_{sp_0}, T_{sp_1}, T_{sp_2}, T_{sp_3}, \dots, T_{sp_n}$ and heat transfer coefficient U_p from the pipe to the ground, calculate the boiler water temperatures $T_{b_0}, T_{b_1}, T_{b_2}, T_{b_3}, \dots, T_{b_n}$ and this series of boiler water temperatures is taken as the set-point of boiler water temperature.

8. A PI controller is used to regulate the boiler water temperature towards the set-points by changing the fuel firing rate. Likewise, zone air temperature is regulated by changing water mass flow rate by the other PI control controller.

Note that by choosing a proper weighting factor η , the predictive control performance can be improved.

5.3 Predictive PI control strategy on the single zone

In order to compare the performance of predictive PI control strategy and conventional PI control strategy, multiple disturbances, such as outdoor air temperature variation and solar radiation gain, etc., were considered as those in the conventional PI control. By choosing water mass flow signal $U_w = 0.5$ and a weighting factor $\eta = 150$, the boiler water temperature set-point and outside air temperature are plotted in Figure 5.3.1.

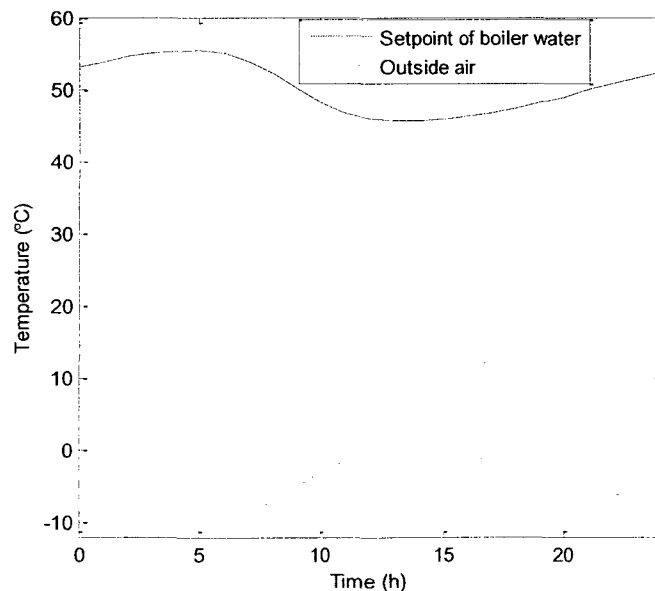


Figure 5.3.1 Predicted boiler water temperature set-point and outdoor air temperature

Figure 5.3.1 shows that when the outside air temperature reaches its lowest value of -10°C , the boiler water temperature set-point goes up to its highest value of 55°C . Likewise, when the outside air temperature reaches the highest value of 0°C , the boiler water temperature set-point reaches its lowest value of 46°C . In other words, a 9°C variation in boiler water temperature set-point occurs over a 24 hours period.

Based on the predicted set-point of boiler water temperature plotted in Figure 5.3.1 and with constant gains $k_{p1} = 1.5, k_{i1} = 0.0008, k_{p2} = 0.2, k_{i2} = 0.00001$, the simulated dynamic responses of the single zone RFH system subject to a step change in outdoor air temperature are plotted in figure 5.3.2.

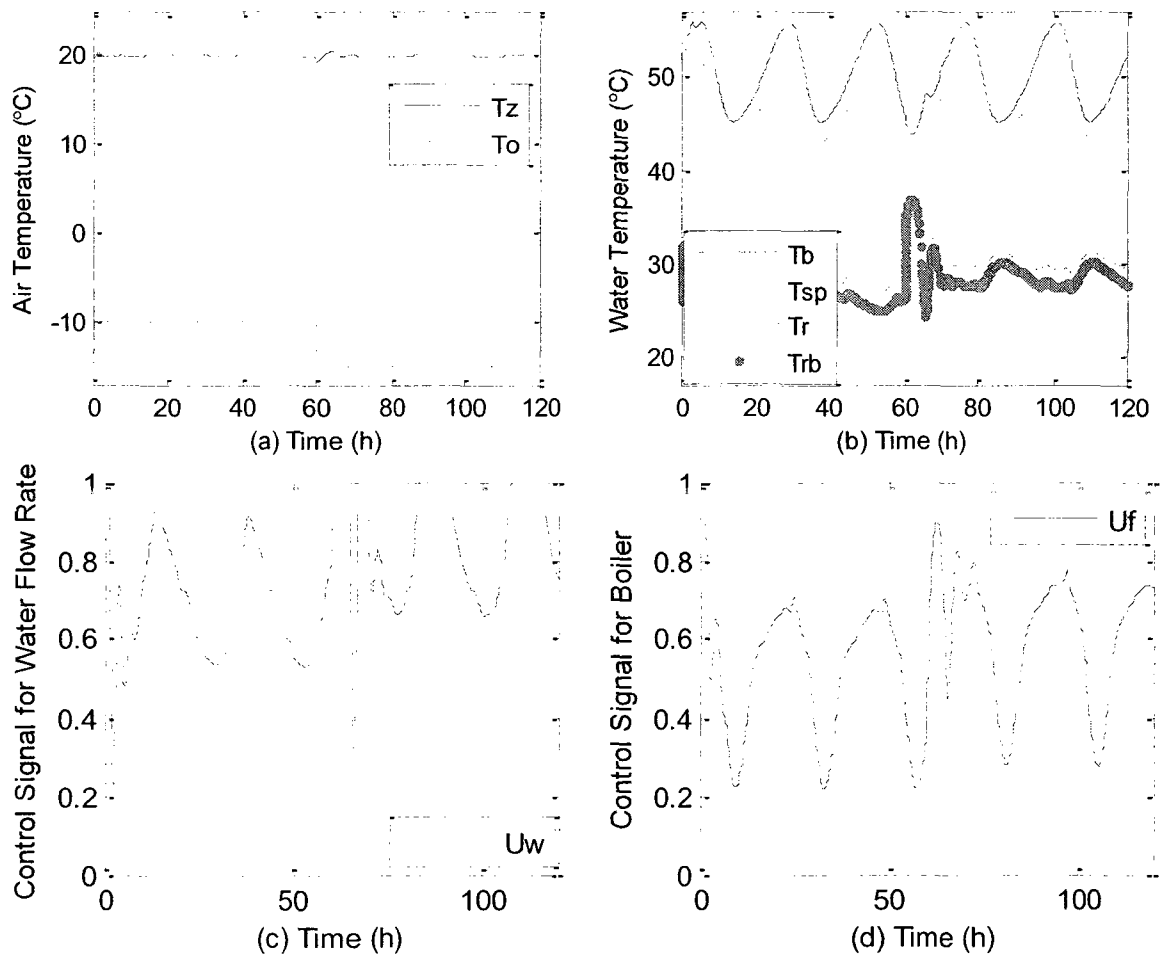
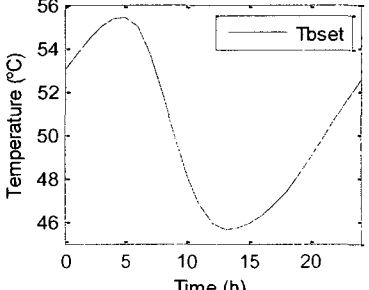
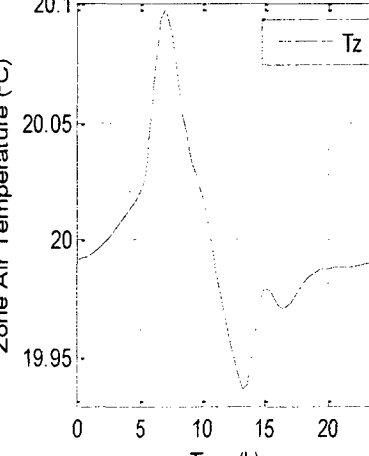
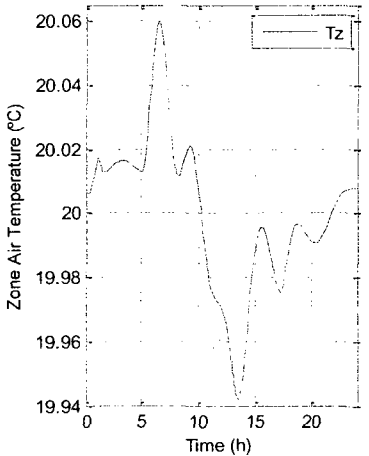


Figure 5.3.2 Predictive PI control responses of single zone RFH system

From the above figures, we can see that the single zone RFH system responses are stable in spite of sudden change in outdoor air temperature. Since the boiler water temperature is changing all the time, the water flow rate and the gas burning rate are also changing correspondingly as opposed to constant set-point of boiler water temperature as in the conventional PI control mode.

5.3.1 Comparison between the conventional PI control strategy and the predictive PI control strategy

The performance comparison between the conventional PI control strategy and the predictive PI control strategy applied to the single zone RFH system was made. The results are summarised in Table 5.3.1.

Item	Conventional PI control	Predictive PI control
Set-point of boiler water temperature	60°C constant	
Zone air temperature		

Fluctuation range (°C)	19.94~20.10	19.94~20.06
Energy consumption (MJ)	142.2732	125.0885
Energy saving	-----	12.08%

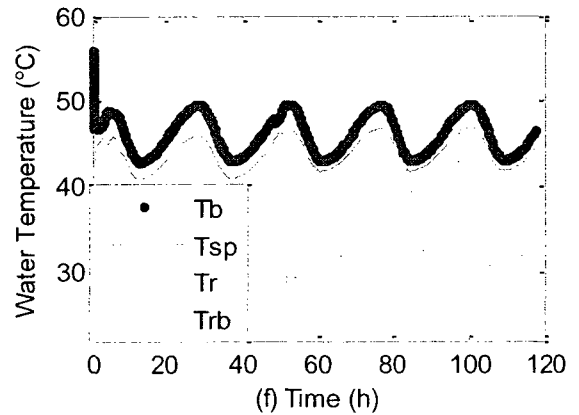
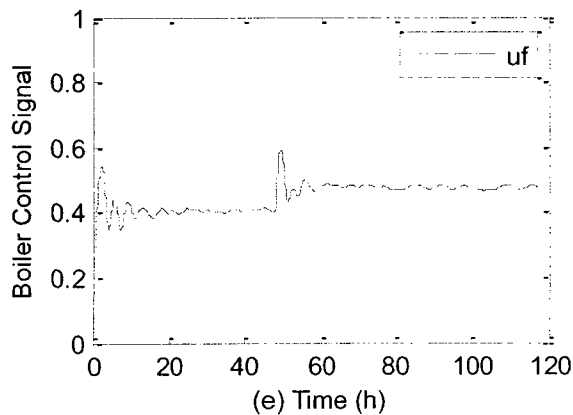
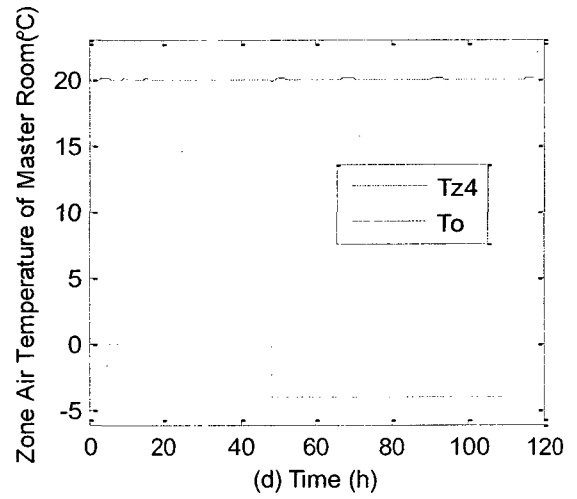
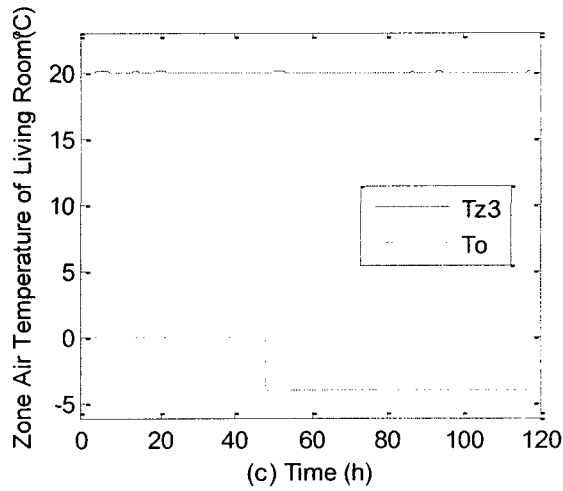
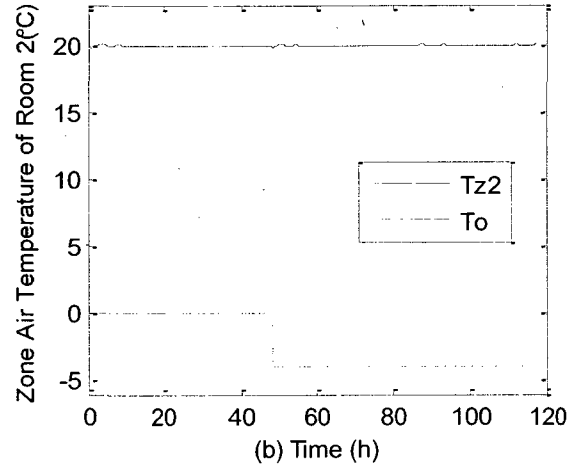
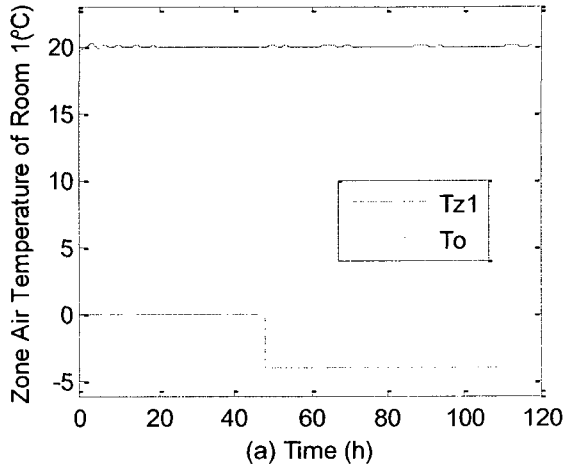
Table 5.3.1 Comparison between conventional PI control and predictive PI control for single zone RFH system

From Table 5.3.1, it can be clearly seen that the fluctuations in zone air temperature under predictive PI control mode are slightly smaller than under conventional PI control mode. Under predictive PI control, the zone air temperature is between 19.98°C and 20.02°C in most of the simulation time. In addition, the most important difference is that the predictive PI control strategy could save 12.08% of energy, compared to conventional PI control strategy. In other words, the energy performance of the single zone RFH system has been significantly improved by selecting the boiler water temperature set-point according to the variation rate of the outdoor air temperature.

5.4 Predictive PI control of multi-zone RFH system

By trying different values of the constant gains for the PI controller and weighting factor η , following set that gave good responses were obtained. These are $k_{p1} = 0.5$, $k_{i1} = 0.0006$, $k_{p2} = 1$, $k_{i2} = 0.0008$, $k_{p3} = 1$, $k_{i3} = 0.0008$, $k_{p4} = 1$, $k_{i4} = 0.0008$, $k_{p5} = 0.2$, $k_{i5} = 0.00001$, and $\eta = 200$. Simulation runs were made to study the dynamic

responses of the multi-zone RFH system for a step change in the outdoor air temperature from 0°C to -4°C . The results are plotted in Figure 5.4.2.



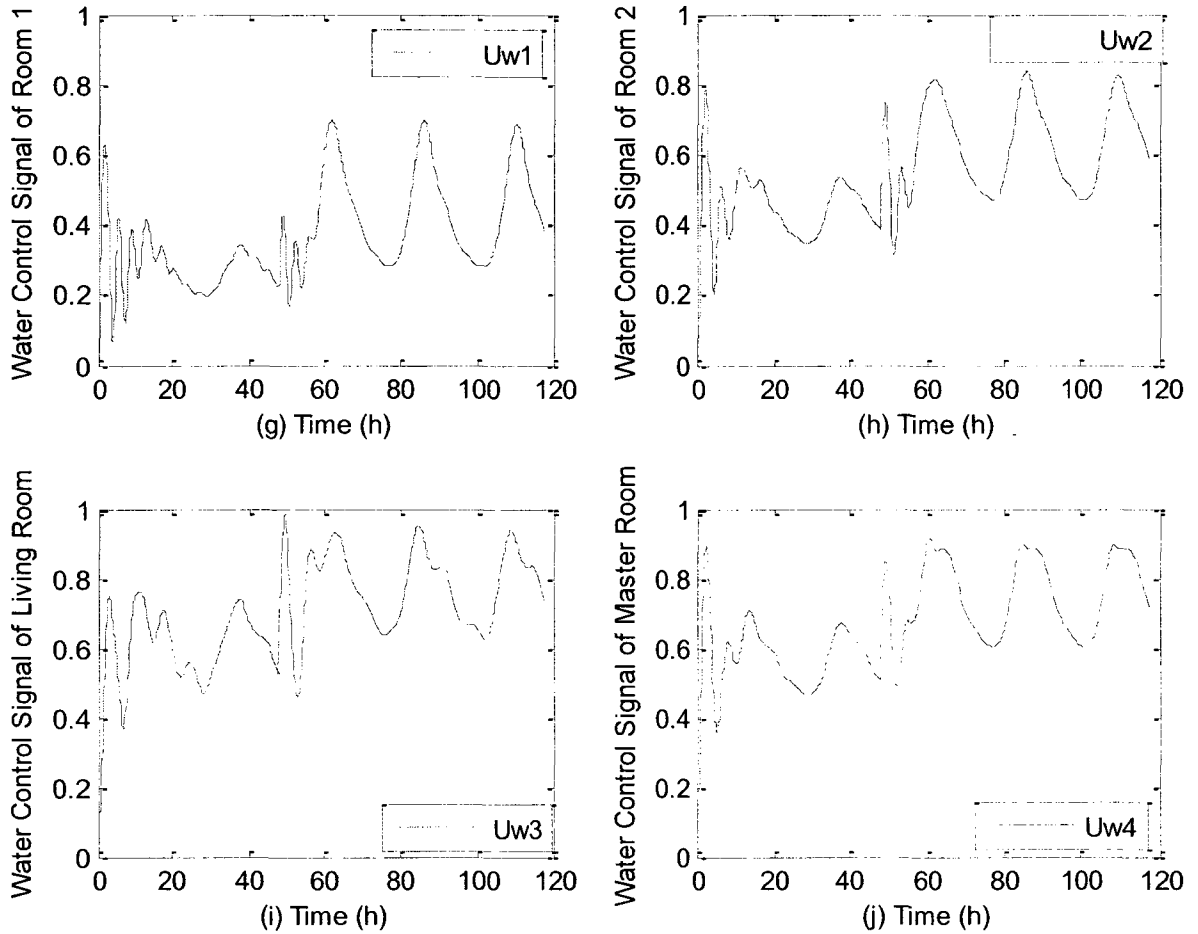
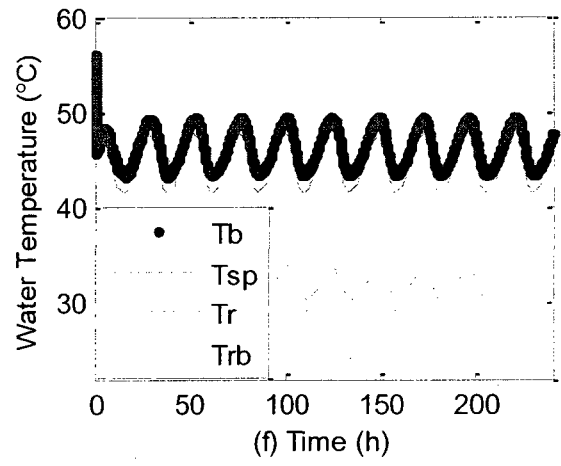
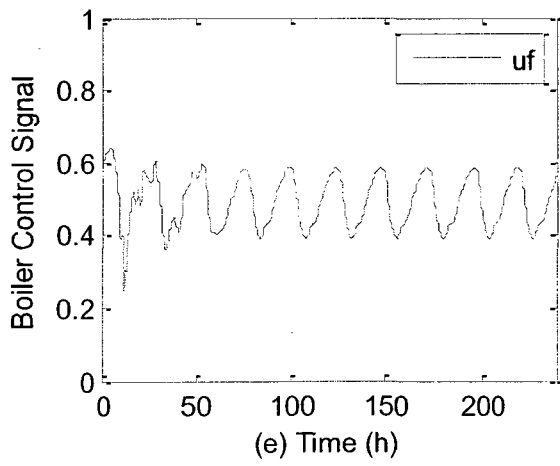
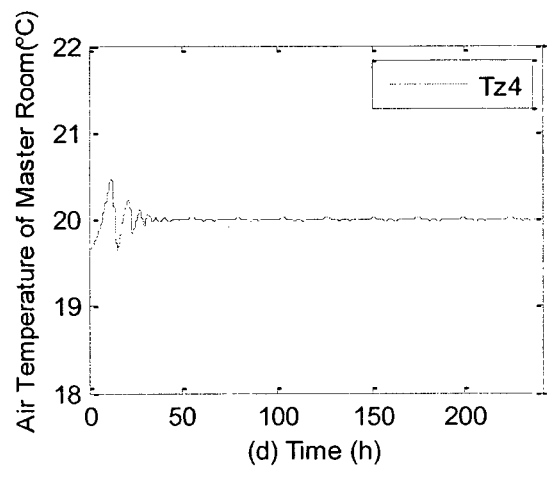
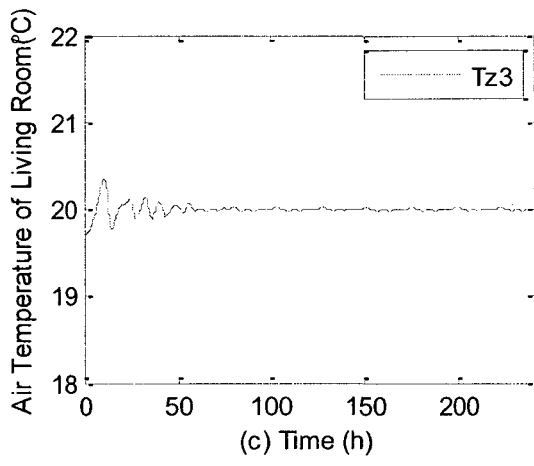
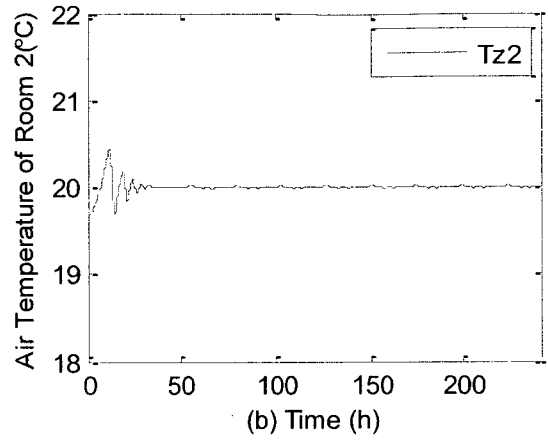
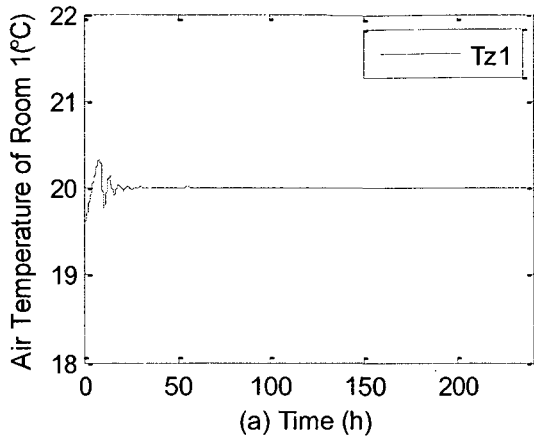


Figure 5.4.2 Validation of the constant gain values of PI controllers for multi-zone RFH system under predictive PI control strategy

From above figures, we can see that the multi-zone RFH system reaches steady state in response to step change in outdoor air temperature. The system responses are fast and stable.

Multi-zone RFH system responses to typical daily variations in outdoor air temperature were simulated. The simulation runs were made for ten consecutive days. The zone air temperatures, boiler water temperature set-point and supply/return water temperature responses are depicted in Figure 5.4.3 (a-j).



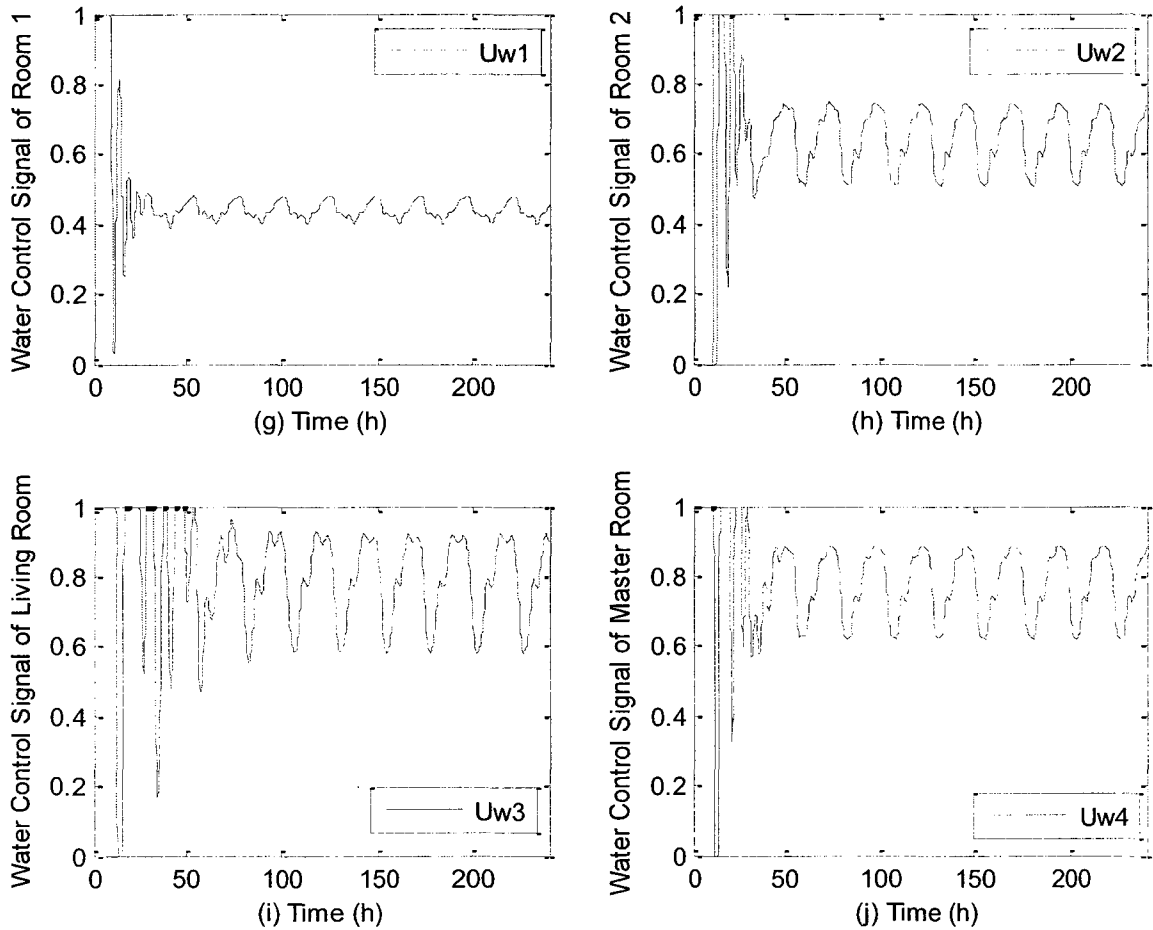


Figure 5.4.3 Simulation results of multi-zone under predictive PI control

From Figure 5.4.3, it can be clearly seen that, under the predictive PI control, the zone air temperatures in all the zones are well regulated. The zone air temperature fluctuation range is between $19.99\sim 20.01^{\circ}\text{C}$, $19.985\sim 20.02^{\circ}\text{C}$, $19.98\sim 20.025^{\circ}\text{C}$ and $19.985\sim 20.02^{\circ}\text{C}$ respectively in room 1, room 2, living room and Master Room. The energy consumption during the simulation period was $3.51510\cdot 10^3\text{MJ}$.

5.5 Comparison between the conventional PI control strategy and the predictive PI control strategy for the multi-zone RFH system

Comparisons between conventional PI performance and predictive PI control strategy performance of the multi-zone RFH system were made to compare energy consumption and fluctuations in zone air temperatures. The results are listed in Table 5.5.1.

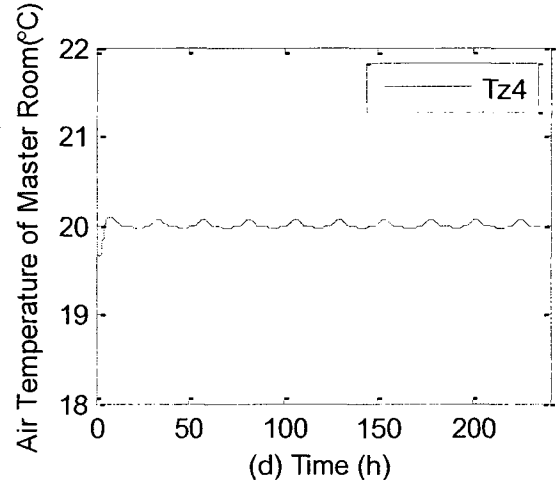
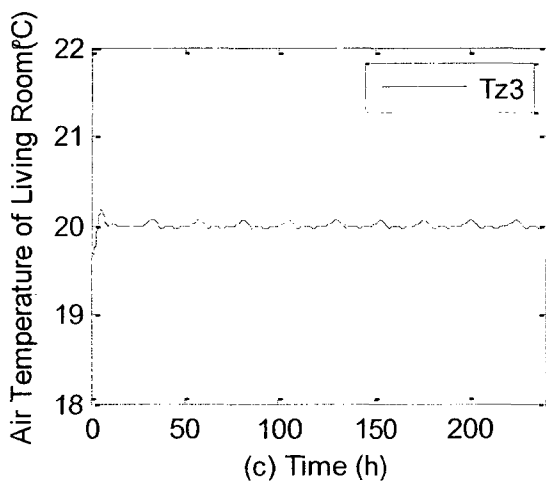
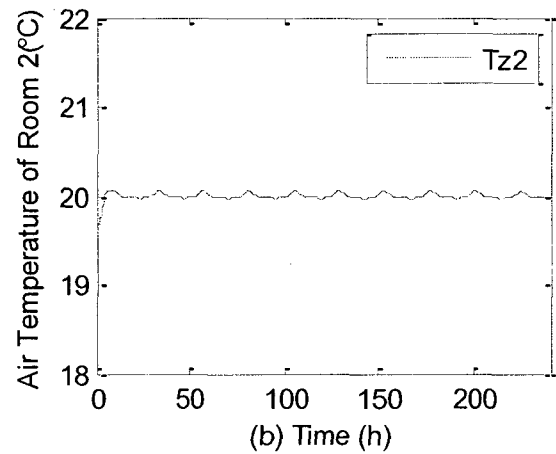
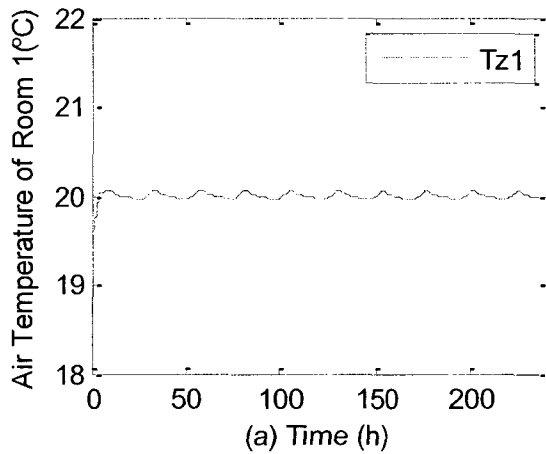
Item		Conventional PI control	Predictive PI control
Set-point of boiler water temperature (°C)		55°C constant	[41.62, 47.92]
Zone air temperature fluctuation range (°C)	Room 1	[19.97, 20.07]	[19.99, 20.01]
	Room 2	[19.97, 20.07]	[19.99, 20.02]
	Living room	[19.96, 20.07]	[19.98, 20.02]
	Master room	[19.97, 20.08]	[19.99, 20.02]
Energy consumption (MJ)		3.90813×10^3	3.51510×10^3
Energy saving		----	10.06%

Table 5.5.1 Comparisons between the conventional PI and predictive PI control for the multi-zone RFH system

Table 5.5.1 shows that, under predictive PI control, the zone air temperatures in multi-zone RFH system fluctuated between 19.98°C and 20.02°C, which can be regarded as a good performance of temperature regulation. What's more, the predictive PI control strategy could save 10.06% of energy, compared to the conventional PI control strategy.

5.6 Predictive PI control of multi-zone RFH system subject to multiple disturbances

Previous section showed that the predictive PI control strategy gives good control when there is no solar gain and no internal heat gains. Therefore, the objective of this section is to examine the performance of the multi-zone RFH system when multiple disturbances, such as variation in outdoor air temperature, solar radiation and internal heat generation, are added to the system. The simulation results are plotted in Figure 5.6.1.



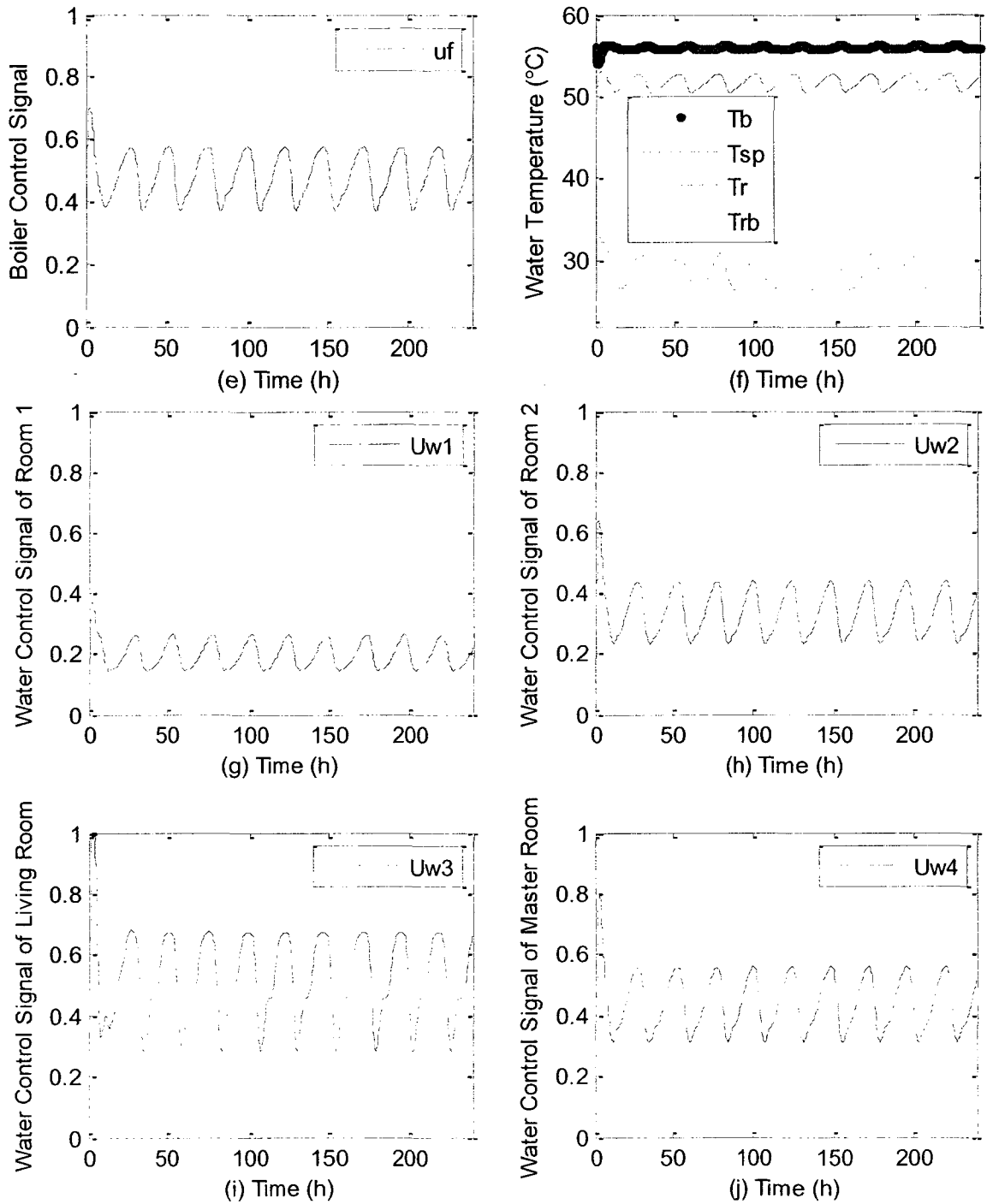
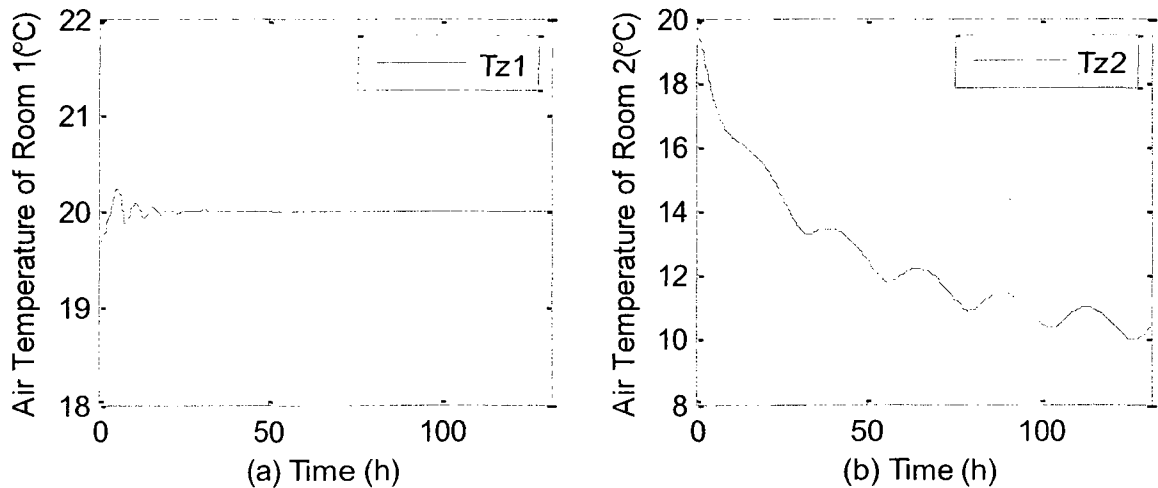


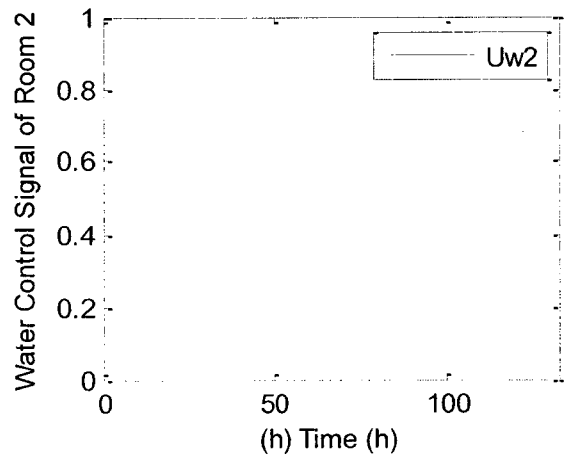
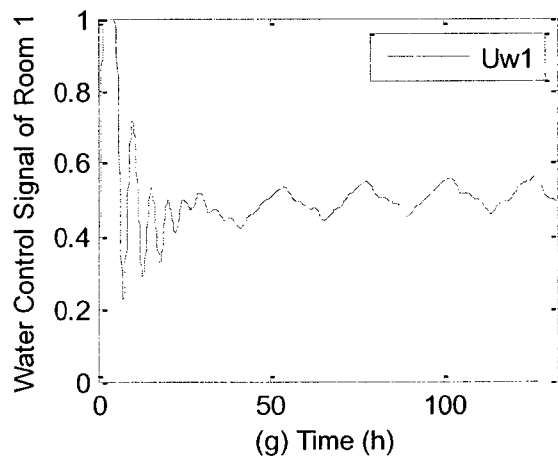
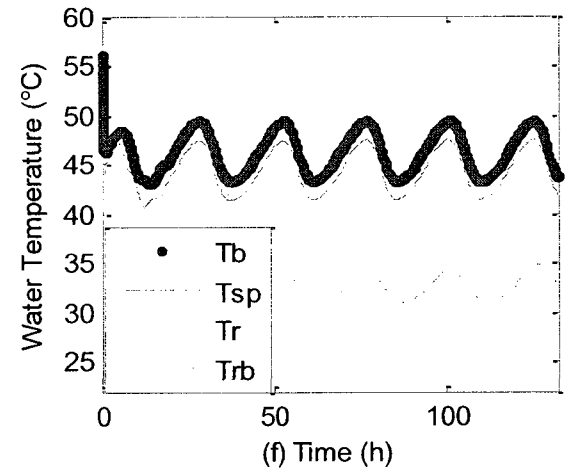
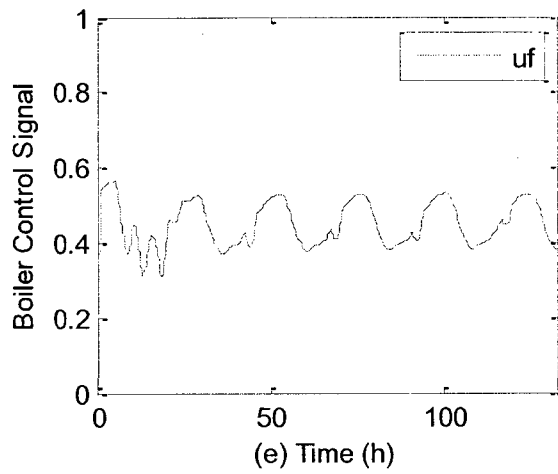
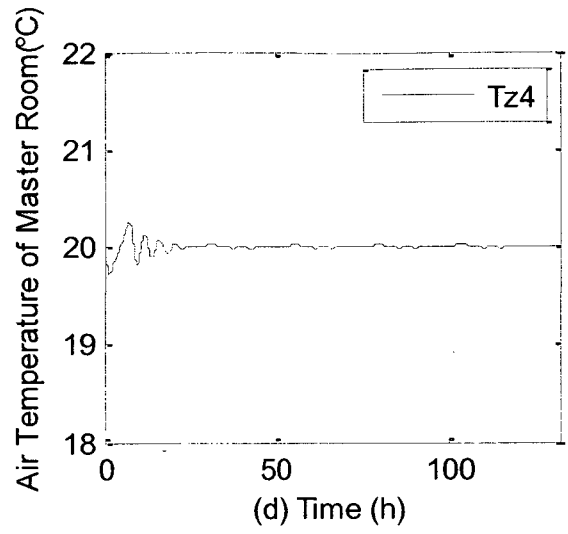
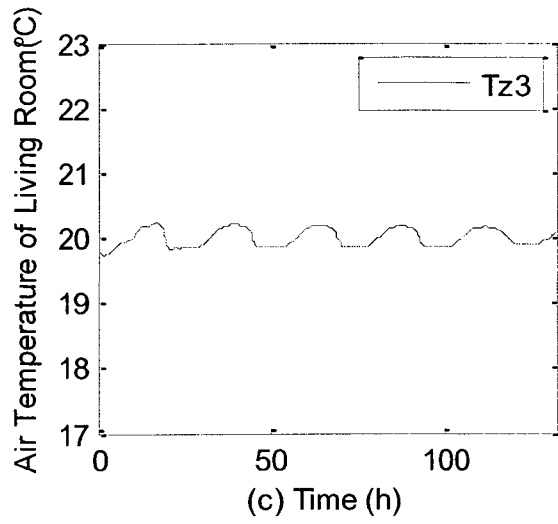
Figure 5.6.1 Simulation results of multi-zone RFH system under conventional PI control with multiple disturbances

The results depicted in Figure 5.6.1 show that the responses of multi-zone RFH system with multiple disturbances under predictive PI control are stable and a good control performance over continuous operation of the RFH system could be obtained. The zone air temperatures are maintained very close to their set-point and boiler water temperature tracks the predicted boiler water temperature set-point very well.

5.7 Predictive PI control strategy of multi-zone RFH system: the impact of one zone on the other zones

This section will discuss a very common case that one zone is unoccupied and the other zones are occupied. Thus, the multi-zone RFH system shuts down the water circulation in the zone without occupants. Assume nobody stays in room 2 and the water circulation in that room is shut down by the PI controller because of a very low zone air thermostat set-point. The performance of the system under this case is shown in Figure 5.7.1.





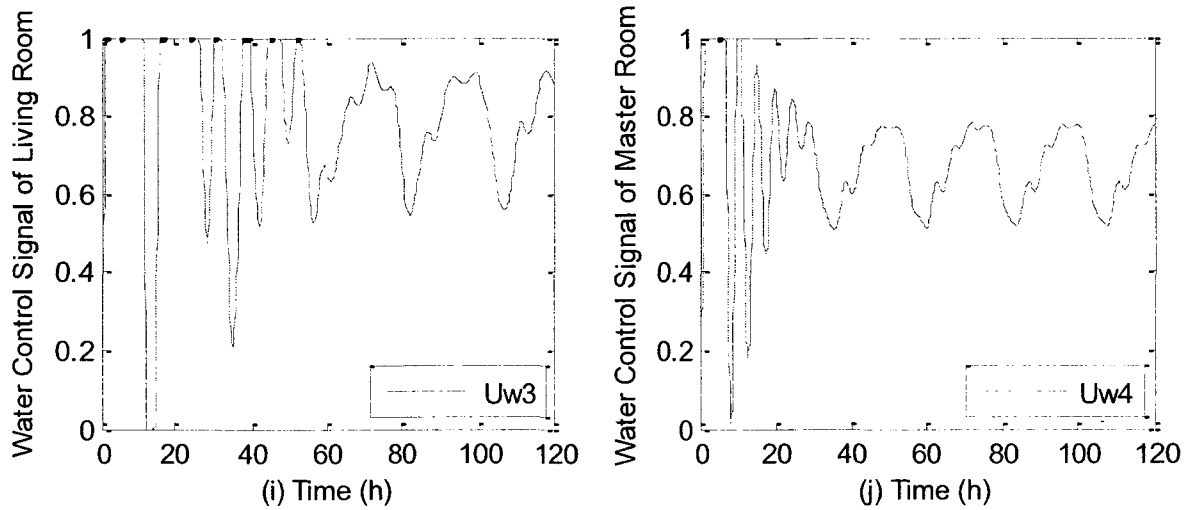


Figure 5.7.1 The performance of multi-zone RFH system with predictive PI control under energy saving mode

Although no water enters into the water-loop in room 2 (shown in Figure 5.7.1 (h)), Figure 5.7.1 (a), (c) and (d) show that the zone air temperature in room 1, living room and Master room are not affected by zone 2. From this point of view, the predictive PI control is also an effective control strategy in minimizing or eliminating the impact of one zone on the others. Furthermore, the energy consumption is 5.70% less than that of without shutting down the water circulation in room 2.

5.8 Summary

Compared to the conventional PI control strategy, the predictive PI control strategy, in which the set-point of boiler water temperature is selected according to the outdoor air temperature, is shown to be more energy efficient. By applying the new control strategy on both single zone and multi-zone RFH system, the simulation results show that the

zone air temperature fluctuation is smaller, compared to the conventional PI control. Besides, the predictive control strategy could save about 10% of energy, compared to the conventional PI control strategy.

Predictive PI control strategy works efficiently in counteracting the effects of multiple disturbances and gives stable temperature regulation in all zones.

In addition, it was shown that the predictive PI control strategy eliminates the inter-zone interactions when the water circulation in one of the zones is shut down. By doing that, a 5.70% of energy can be saved and the occupied zones are not affected.

From above, it is concluded that the performance of RFH systems could be improved significantly by the predictive PI control strategy from both aspects of temperature regulation and energy consumption.

CHAPTER 6

Optimal Operation of RFH System

6.1 Introduction

As shown in Chapter 5, the predictive PI control strategy can save over 10% energy, compared to the conventional PI control strategy. It is of interest to explore optimal control to see if further savings in energy can be obtained. To this end, in this chapter, steady state optimal set-points of boiler water temperature are determined by formulating and solving the steady state optimization problem.

6.2 Formulation of the optimization problem for RFH system

This section will discuss the optimization of the single zone RFH system under steady state. The optimization problem was formulated and the resulting equations were solved using MATLAB subroutines.

6.2.1 Determination of the optimized set-point of boiler water temperature

The single zone model of RFH system in steady state was written as:

$$f(x, U_f, U_w, T_o) = 0 \quad (6.2.1)$$

$$x_0 = x|_{t=0} \quad (6.2.2)$$

Where x is the state vector $x = [T_{wi} \ T_{mwi} \ T_{mpi} \ T_{mi} \ \dots \ T_b \ T_{sp} \ T_r \ T_{rb} \ T_z]^T$ and x_0 is the initial value of the variables.

The constraints (upper and lower bounds) of all the variables were set, as:

$$\alpha_j < x_j < \beta_j, \quad j = 1, 2, \dots, n. \quad (6.2.3)$$

The objective function to be minimized was based on three considerations: (i) the zone air temperature must be maintained close to the set-point, (ii) the energy input to the boiler should be minimized, and (iii) the variables x should not exceed its upper and lower bounds. In other words, equation 6.2.3 must be satisfied. The cost function J satisfying these conditions can be expressed as

$$J = (T_z - T_{zset})^2 + U_f m_{fmax} HVeb \quad (6.2.4)$$

The equations were solved by using the function $f_{mincon}(J)$ in MATLAB to obtain the boiler water temperature as a function of different water flow control signal U_w and outside air temperature T_o . The relationship between the optimized boiler water temperature and the outdoor air temperature based on different water flow control signal U_w is plotted in Figure 6.2.1.

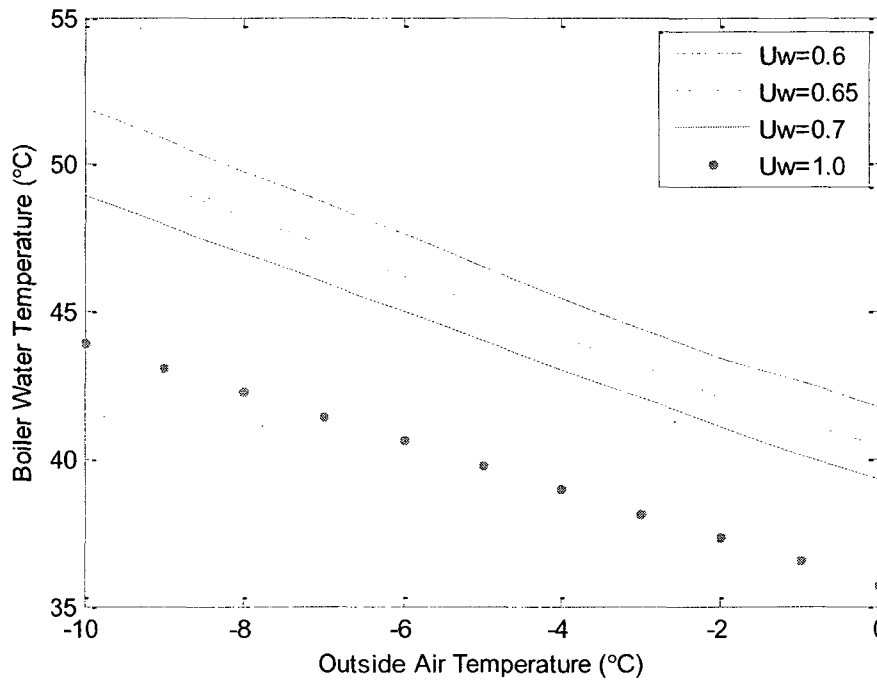
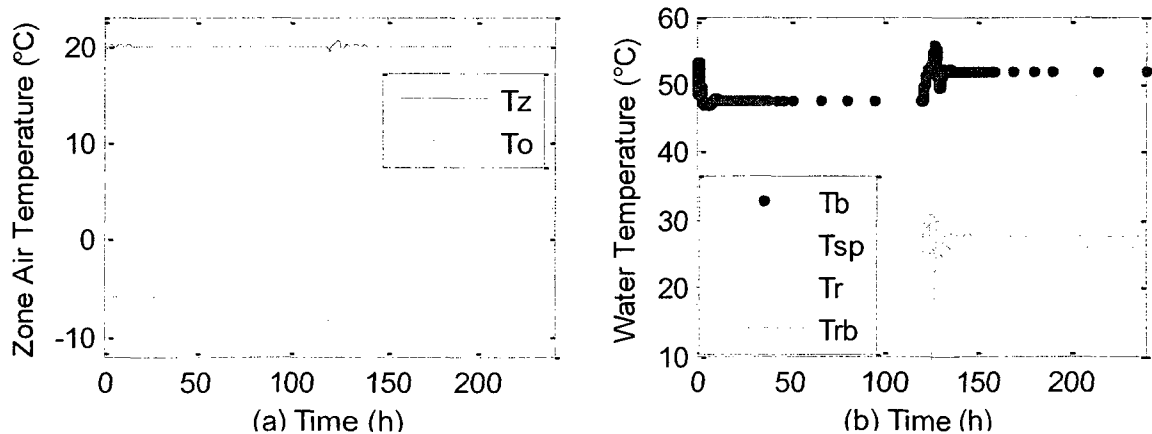


Figure 6.2.1 Optimization of the open loop test of single zone RFH system

The above figure shows that the optimized boiler water temperature decreases when outside air temperature increases. Also, the optimized boiler water temperature decreases as the water flow rate increases.

6.2.2 Performance of the single zone RFH system under optimal PI control

Dynamic responses of the single zone RFH system under optimal PI control subject to step change in outdoor air temperature from -6°C to -10°C are plotted in Figure 6.2.2.



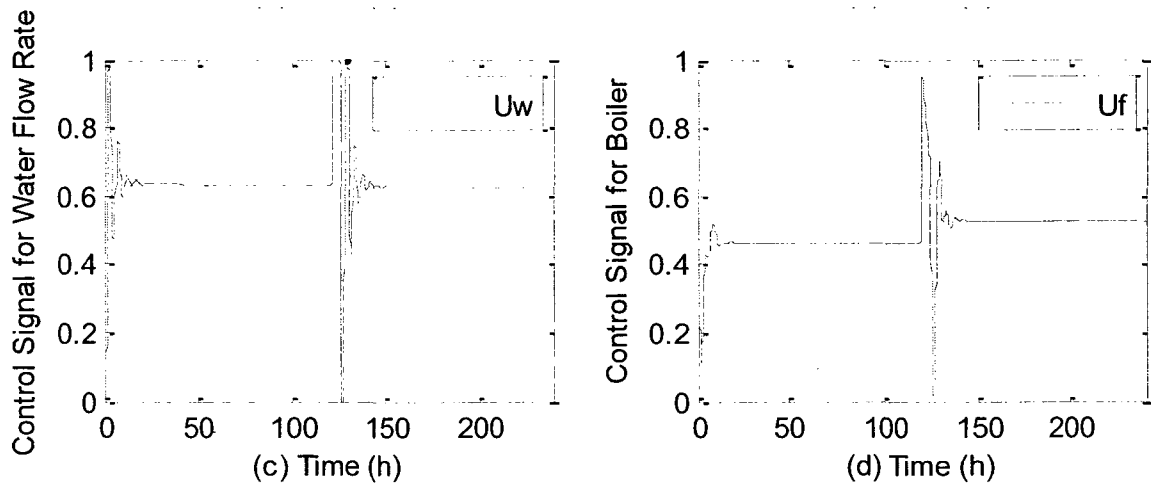
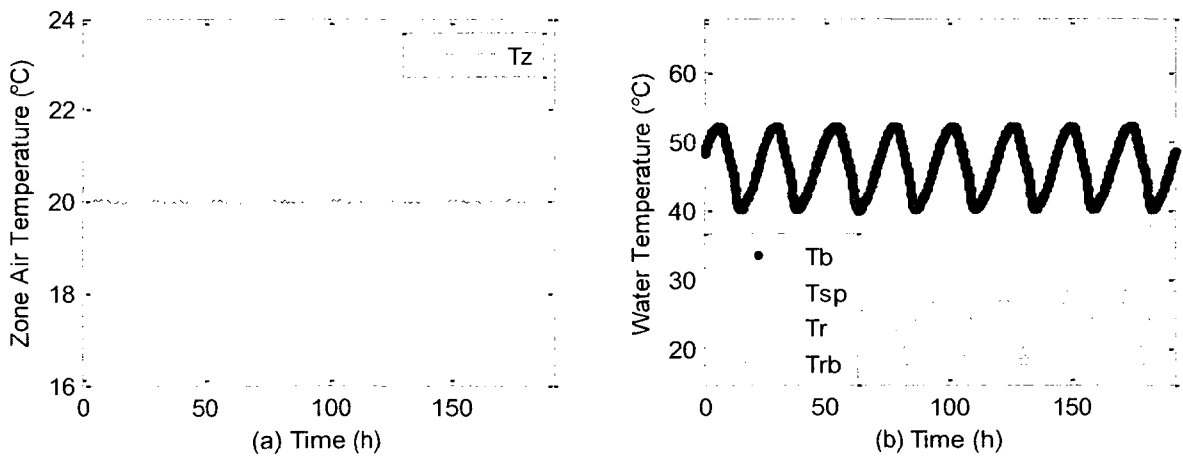


Figure 6.2.2 Validation of the constant gain values of PI controllers for single zone RFH system under optimal PI control

From Figure 6.2.2, we can see that except for a sudden change in boiler water temperature set-point, the other responses remain smooth and stable. This was verified by conducting simulation runs over continuous ten days period under the predicted outdoor air temperature as shown in Figure 6.2.3.



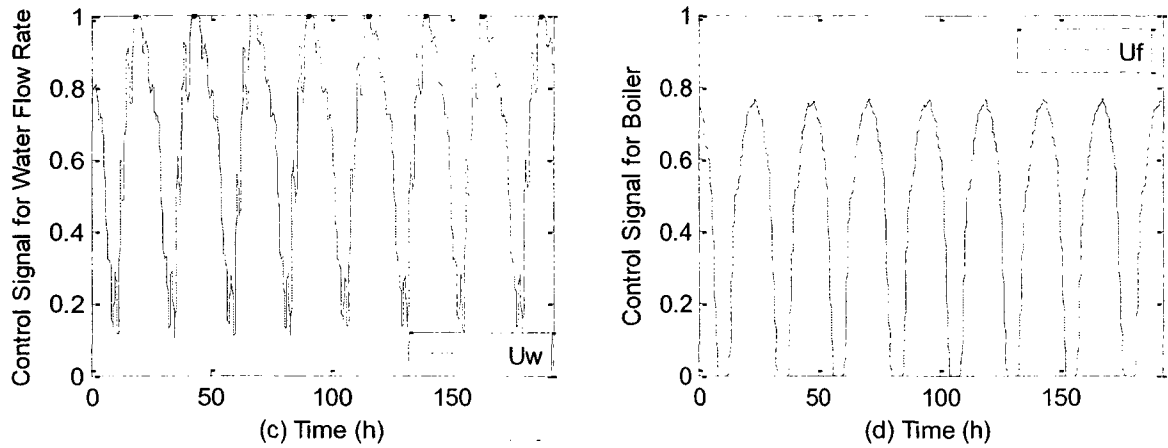


Figure 6.2.3 Responses of single zone under optimal PI control strategy

Figure 6.2.3 (a) shows that the zone air temperature fluctuates between 19.94°C and 20.03°C . Besides, Figure 6.2.3 (c) shows that the water flow rate is saturated sometimes, which should be avoided in real applications by imposing hard constraints.

6.3 Comparison between conventional, predictive and optimal control

The simulation results of the single zone RFH system under conventional PI control, predictive PI control and optimal PI control strategy were compared. The results are summarized in Table 6.3.1.

Item	Conventional PI control	Predictive PI control	Optimal PI control
Set-point of Boiler water temperature	60°C constant		

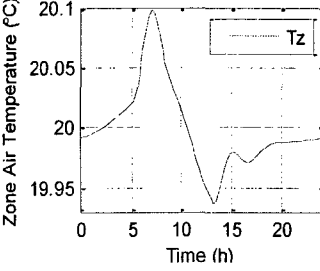
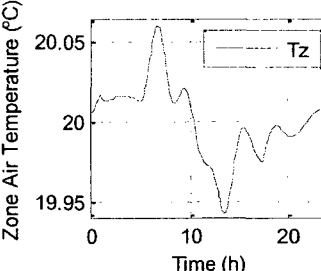
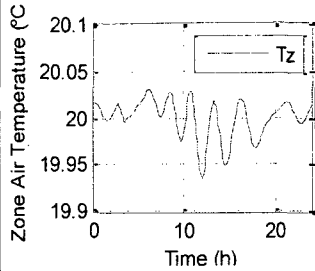
Zone air temperature			
Fluctuation range (°C)	19.94~20.1	19.94~20.06	19.94~20.03
Energy consumption (MJ)	142.2732	125.0885	121.0326
Energy saving	-----	12.08%	14.93%

Table 6.3.1 Comparison among the 3 control strategy on single zone RFH system

From Table 6.3.1, it can be clearly seen that the optimal PI control strategy not only has the best zone air temperature regulation, but also it has the greatest energy efficiency. Since the energy saving obtained by optimal PI control strategy is not too different compared to the predictive PI control, the predictive control is preferred choice as it is simple and easy to implement.

6.4 Summary

By applying the optimal control strategy to the single zone RFH system, the simulation results showed that, the zone air temperature fluctuation range is the smallest among the

3 control strategies. Also, the optimal control strategy could save about 14.93% of energy, compared to the conventional PI control strategy.

CHAPTER 7

Conclusions, contributions and Recommendations for Future Research

7.1 Conclusions and contributions

The contributions of this thesis are in the area of modelling and the study of control strategies for both single zone and multi-zone radiant floor heating (RFH) systems. These are summarized in the following.

7.1.1 Modelling of RFH systems

- (1) A dynamic model for RFH system which predicts the mean zone air temperature, the temperature distribution of flow water, the temperature distribution in floor slab and slab surface temperature under design and off design condition has been developed.
- (2) The simulation results showed that the maximum surface temperature difference in RFH system is about 4°C.
- (3) A zonal model of single zone RFH system was developed. Simulation results from the zonal model show that maximum variation in air temperature in the zone could reach as much as 1.6°C.

- (4) The simulation results from the multi-zone model showed that increasing the number of water tubes and increasing the water mass flow rate could compensate for the high heat loss rate in the zone.
- (5) The time needed for the RFH system to reach steady state depends on the initial condition and thermal capacity of the floor slab. The steady state time ranged between 10 to 15 hours.
- (6) The supply water temperature has significant impact on zone air temperature, compared to changes in water mass flow rate.

7.1.2 Control strategies for RFH system

The contributions and conclusions in the area of control strategies for RFH system are summarized as below:

- (1) The conventional PI control strategy, in which the set-point of boiler water temperature was constant, was applied to a single zone and a multi-zone RFH system. The results show good and smooth zone air temperature control.
- (2) A predictive control strategy in which the boiler water temperature set-point is predicted every 15 minute time interval is developed. The predictive set-points were tracked by PI controllers. The results showed that 10-15% energy can be saved compared to conventional constant set-point PI control strategies. The predictive control strategy was also applied to both the single and multi-zone RFH systems under multiple disturbances. The predictive control system responses were smooth and stable over the entire simulation time spanning 10 days.

- (3) A steady state optimization problem to find optimal boiler water temperature set-point was formulated and solved. The resulted optimal set-points were tracked by PI controllers. The results showed that the optimal set-point results in slightly more energy savings, compared to predictive control strategy.

7.2 Recommendations for future research

Research results conducted in the thesis present opportunities for future development in modelling RFH system and optimal operation.

- (1) Pressure balancing should be incorporated into the dynamic model for RFH system, to study the hydraulic system control responses.
- (2) Dynamic optimal control of multi-zone RFH systems should be studied to develop improved control strategies.

Reference:

- [1] Algren, A.B. Field Studies of Floor Panel Control Systems. *ASHVE Transactions* 59 part 1. pp 173-196.
- [2] ASHRAE Cooling and Heating Load Calculation Manual, 2nd ed., 1992.
- [3] Athienitis, A.K. Numerical Model of Floor Heating System. *ASHRAE Transactions*. (1994). part 1, pp: 1024-1030.
- [4] Buckley, N.A., Application of radiant heating saves energy. *ASHRAE J.* 31, 17-26 (1989).
- [5] Campo, A. & Amon, C.H. Remarkable Improvement of the Leveque Solution for Isoflux Heating with a Combination of the Transversal method of Lines (TMOL) and a Computer-extended Frobenius Power Series. *International Journal of Heat and Mass Transfer* 48 (2005) 2110-2116.
- [6] Chapman, K.S. & Zhang, P. Energy Transfer Simulation for Radiantly Heated and Cooled Enclosures. *ASHRAE Transactions* 1996, Part 1, pp 76-85.
- [7] Chen, T.Y. Application of Adaptive Predictive Control to a Floor Heating System with a Large Thermal lag. *Energy and Buildings*. 34 (2002). pp: 45-51.
- [8] Cho, S. H. & Zaheer-uddin, M. Temperature Regulation of Radiant Floor Heating Systems Using Two-Parameter On-Off Control: An Experimental Study. *ASHRAE Transactions*, 1997, pp:966-980.

- [9] Cho, S.H. & Zaheer-uddin, M.. An Experimental Study of Multiple Parameter Switching Control for Radiant Floor Heating Systems. *Energy* 24 (1999). pp: 433-444.
- [10] Cho, S.H. & Zaheer-uddin, M. Predictive Control of Intermittently Operated Radiant Floor Heating Systems. *Energy Conversion and Management* 44 (2003) 1333-1342.
- [11] Chun, W.G., Jeon, M.S., Lee, Y.S. & Lee, T.K. A Thermal Analysis of a Radiant Floor Heating System Using SERI-RES. *International Journal of Energy Research* (1999) 23, 335-343.
- [12] Gibbs, D.R. Control of Multi-zone Hydronic Radiant Floor Heating System. *ASHRAE Transactions*. 1994.part 1. pp.1003-1009.
- [13] Good, J., Ugursal, V.I. & Fung, A. Simulation Strategy and Sensitivity Analysis of an In-Floor Radiant Heating Model. *Building Simulation* (2005). Ninth International IBPSA Conference.
- [14] Hannay, J.L., Lebrun, J., Marret, D. & Nussgens, P.. Thermal Comfort and Energy Consumption in Winter Conditions-New Experimental Approach. *ASHRAE Transaction*. 84 (1978). part 1.
- [15] Ho, S.Y., Hayes, R.E., Wood, R.K., Simulation of the Dynamic Behaviours of a Hydronic Floor Heating System. *Heat Recovery System & CHP*. Vol. 15. No.6. pp. 505-519, 1995.

- [16] Hogan, R.E. & Blackwell, B.F. Comparison of Numerical Model with ASHRAE Design Procedure for Warm Water Concrete Floor Heating Panels. *ASHRAE Transactions*, (1986), no.2,vol,13.pp 589-597.
- [17] Hu, L.M., The Main Points and Development Prospect of Low Temperature Radiant Floor Heating System. *Exchange of Jiangchang Science and Technology*. Vol. 34, No.2 (2008).
- [18] Hutcheon, N.B. & Handegord, G.O.P. *Building Science for a Cold climate*.
- [19] Inard, C., Bouia, H., & Dalicieux, P., Prediction of Air Temperature Distribution in Buildings with a Zonal Model. *Energy and Buildings*. 24 (1996) 125-132.
- [20] Laouadi, A. Development of a Radiant Heating and Cooling model for Building Energy Simulation Software. *Building and Environment* 39 (2004) 421-431.
- [21] Lebrun, J. & Marret, D.J. Thermal Comfort and Energy Consumption in Winter Conditions- Continuation of the Experimental Study. *ASHRAE Transactions*. 85(1979), part 2.
- [22] Leigh, S.B. & MacCluer, C.R. A Comparative Study of Proportional Flux-Modulation and Various types of Temperature-Modulation Approaches for Radiant Floor Heating System Control. *ASHRAE Transactions*. 1994.pp.1040-1053.
- [23] Li, L.Z. Dynamic Modelling, Intelligent Control and Diagnostics of Hot Water Heating Systems. PHD thesis in department of Building, Civil and Environmental Engineering, Concordia University. 2008.

- [24] Liesen, R.J. & Pedersen, C.O. An Evaluation of Inside Surface Heat Balance Models for Cooling Load Calculations. *ASHRAE Transactions*, (1997) 103 (2).
- [25] MacCluer, C.R. Temperature Variation of Flux-modulated Radiant Slab Systems. *ASHRAE Transactions* 1989, part 1, pp:1010-1014.
- [26] MacCluer, C.R. & Miklavcic, M. The Temperature Stability of a Radiant Slab-on-grade. *ASHRAE Transaction*. 1989, pp: 1001-1009.
- [27] MacCluer, C.R. Analysis and Simulation of Outdoor Reset Control of Radiant Slab Heating Systems. *ASHRAE Transaction*. 1990. pp: 1283-1287.
- [28] MacCluer, C.R. The Response of Radiant Heating Systems Controlled by Outdoor Reset with Feedback. *ASHRAE Transactions*. 1991. part 2. pp 795-799.
- [29] Mendonsa, K.C., Inard, C & Wurtz, E. A Zonal Model for Predicting Simultaneous Heat and Moisture Transfer in Buildings. *Indoor Air 2002- The 9th International Conference on Indoor Air Quality and Climate*.
- [30] Miriel, J., Serres, L. & Trombe, A. Radiant Ceiling Panel Heating-cooling System: Experimental and Simulated Study of the Performance, Thermal Comfort and Energy Consumptions. *Applied Thermal Engineering*. 22 (2002) 1861-1873.
- [31] Olesen, B.W., Mortensen, E. Thorshauge, J. & BergMunch, B, Thermal Comfort in a Room Heated by different Methods. *ASHRAE Transactions*. 86 (1980), part 1.
- [32] Olesen, B.W. Comparative Experimental Study of Performance of Radiant Floor-heating System and a Wall Panel Heating System under Dynamic Conditions. *ASHRAE Transaction*, 1994, Vol, 13. pp,1011-1023.

- [33] Olesen, B. W., Radiant Floor Heating in Theory and practice (2002). American Society of Heating, Refrigerating and Air-Conditioning Engineers. *ASHRAE J.*
- [34] Qu, S.L., Ma, F., Liu, L. & Yu, J. Experiment System Analysis of an Indirect Expansion Solar Assisted Water Source Heat Pump Radiant Floor Heating System. *International Conference on Energy and Environment Technology*, (2009).
- [35] Rhee, K.N. Ryu, S.R. Yeo, M.S. & Kim, K.W. Simulation Study on Hydronic Balancing to Improve Individual Room Control for Radiant Floor Heating System. *Building Serv. Eng. Res. Technol.* 31, 1 (2010). pp: 57-73.
- [36] Ryu, S.R., Lim, J.H., Yeo, M.S. & Arch, K.W. A Study on the Control Methods for Radiant Floor Heating and Cooling System in Residential Building. *ASHRAE Transactions*. 2004. pp, 106-116.
- [37] Sattari, S. & Farhanieh, B. A Parametric Study on Radiant Floor Heating System Performance. *Renewable Energy* 31 (2006) 1617-1626.
- [38] Song, G.S. Buttock Responses to Contact with Finishing Materials over the ONDOL Floor Heating System in Korea. *Energy and Buildings*, 37 (2005) 65-75.
- [39] Steinman, M., Kalisperis, L.N. & Summers, L.H. The MRT-Correction Method: A new Method of Radiant Heat Exchange. *ASHRAE Transactions*, (1989) vol, 17. pp:1015-1027.
- [40] Strand, R.K. & Pedersen, C.O., Implementation of a Radiant Heating and Cooling Model into an Integrated Building Energy Analysis Program. *ASHRAE Transaction* 97 (2): 949-958.

- [41] Strand, K. & Pedersen, C.O. Modelling Radiant Systems in an Integrated Heat Balance Based Energy Simulation Program. *ASHRAE Transactions*, (2002) part 1, vol,14. pp:979-987.
- [42] Walton, G.N. A New Algorithm for Radiant Interchange in Room Load Calculations. *ASHRAE Transaction*. (1980). 86 (2). pp: 190-208.
- [43] Weitzmann, P., Kragh, J., Roots, P. & Svendsen, S.. Modelling Floor Heating Systems Using a Validated Two-dimensional Ground-coupled Numerical Model. *Building and Environment* ,40 (2005) 153-163.
- [44] Wurtz,E., Nataf, J-R. & Winkelmann, F. Two- and three-dimensional natural and mixed convection simulation using modular zonal models in buildings. *International Journal of Heat and Mass Transfer* 42 (1999) 923-940.
- [45] Zaheer-uddin, M. Zheng, G.R. & Cho, S.H. Optimal Operation of an Embedded-Piping Floor Heating System with Control Input Constraints. *Energy Conversion and Management* 38 (1997) 713-725.
- [46] Zaheer-uddin, M., Zhang, Z.L. & Cho, S.H. Augmented Control Strategies for Radiant Floor Heating Systems. *International Journal of Energy Research*. (2002). 26: 79-92.
- [47] Zhang, Z. & Pate, M. (1988). Investigation of a Residential Solar System Coupled to a Radiant Panel Ceiling. *ASME Journal. Sol. Energy Eng.* 110 (3). pp172-179.

- [48] Zhang Z.L., Temperature Control Strategies for Radiant Floor Heating Systems.
Thesis in department of Building, Civil and Environmental Engineering, Concordia
University. 2001.